UNIVERSIDAD NACIONAL AUTÓNOMA DE MÉXICO

PROGRAMA DE MAESTRÍA Y DOCTORADO EN INGENIERÍA
INGENIERÍA ELÉCTRICA – INSTRUMENTACIÓN

DEVELOPMENT OF OPTICAL POLARIMETERS USING LIQUID-CRYSTAL VARIABLE RETARDERS

TESIS
QUE PARA OPTAR POR EL GRADO DE:
DOCTOR EN INGENIERÍA

PRESENTA:
JUAN MANUEL LÓPEZ TÉLLEZ

TUTOR PRINCIPAL
DR. NEIL C. BRUCE DAVIDSON, CCADET-UNAM.
COMITÉ TUTOR
DR. JESÚS GARDUÑO MEJÍA, CCADET-UNAM.
DR. MAXIMINO AVENDAÑO ALEJO, CCADET-UNAM.

CIUDAD DE MÉXICO, JUNIO DE 2016.

JURADO ASIGNADO:

Presidente: Dr. Rafael Espinosa Luna.

Secretario: Dr. es s ardu o e ía.

1 er. Vocal: Dr. eil Charles ruce Davidson.

2 do. Vocal: Dr. a imino venda o le o.

3 er. Vocal: Dr. Oscar abriel Rodríguez errera.

Lugar donde se realizó la tesis:

CE RO DE CIE CI S PLIC D S DES RROLLO EC OL ICO, U .

TUTOR DE TESIS:

Dr. eil Charles ruce Davidson.

Dedico esta tesis a mi Mamá, a mis hermanos y a la memoria de mi Papá.

Agradecimientos

Agradezco a mi director de tesis, el Dr. Neil C. Bruce, por su apoyo, paciencia y dedicación para que yo pudiera llevar a cabo con éxito este trabajo. De igual forma a los demás miembros de mi comité tutoral, los doctores Maximino Avendaño Alejo y Jesús Garduño Mejía. También agradezco a los doctores Oscar Rodríguez Herrera y Rafael Espinosa Luna por su apoyo, por sus sugerencias y valiosas aportaciones que contribuyeron a mejorar esta tesis. Agradezco la asesoría técnica del Ing. Rigoberto Nava Sandoval.

Reconozco y agradezco de manera especial el apoyo incondicional de mis familiares y amigos.

Bebo agradecer las becas de estudios de doctorado y los apoyos económicos que recibí de la Coordinación de Estudios de Posgrado de la UNAM (CEP-UNAM), del Consejo Nacional de Ciencia y Tecnología (CONACyT), del Consejo Mexiquense de Ciencia y Tecnología (COMECyT) y de la Dirección General de Asuntos del Personal Académico de la UNAM (DGAPA-UNAM).

El presente trabajo fue financiado por CONACyT a través del proyecto No. 79814, y por DGAPA-UNAM a través de los proyectos PAPIIT Nos. IN-115209 e IT-100114.

Resumen

Este trabajo presenta la implementación experimental de un conjunto de técnicas polarimétricas que utilizan retardadores variables de cristal líquido (LCVRs, por sus siglas en inglés). Se propone un nuevo método para medir los parámetros de Stokes de la luz y, también, la matriz de Mueller de un material mediante la aplicación de voltajes continuamente variables a los LCVRs. Estos dispositivos generalmente se emplean para producir valores fijos de retardancia, a partir de la aplicación de valores fijos de voltaje, debido al comportamiento no-lineal de la retardancia respecto al voltaje aplicado que los caracteriza. En el método de medición que aquí se propone, primero se mide la relación voltaje-retardancia y después se realiza el ajuste lineal de los términos de retardancia de una función conocida a una señal de luz detectada. Ambas versiones de polarímetro, Stokes y Mueller, dan buenos resultados con este método de medición. Alternativamente, también se emplea un método para producir variaciones lineales de retardancia en los LCVRs como herramienta para medir los parámetros de Stokes. Además, se presenta un conjunto de procedimientos experimentales para caracterizar las propiedades ópticas de polarización, como función del voltaje aplicado, de este tipo de retardadores variables. Las propiedades estudiadas son: retardancia, diatenuación, transmitancia, posición de ejes ópticos y efectos de depolarización. Estas propiedades ópticas están directamente involucradas con el funcionamiento de estos retardadores y, por lo general, son las más importantes para el desarrollo de aplicaciones en óptica. La correcta caracterización de este conjunto de propiedades puede ser de utilidad para mejorar resultados, o estimar errores, en las aplicaciones que usan estos dispositivos. Los resultados obtenidos muestran buena precisión y correspondencia con los resultados esperados.

Abstract

This work presents the experimental implementation of a set of polarimetric techniques using liquid crystal variable retarders (LCVRs). A novel method for using LCVRs with continually varying voltage to measure both the Stokes parameters of a light beam and the complete Mueller matrix of a general sample is proposed. These devices are usually employed for producing fixed retardance values due to the nonlinear voltage–retardance behavior that they show. For the measurement method presented here, the nonlinear voltage–retardance relationship is first measured and then a linear fit of the known retardance terms to the detected signal is performed. Both versions of polarimeter, Stokes and Mueller, using this measurement method give good results. Alternatively, a method to produce linear variations of retardance from the LCVRs is also employed to measure Stokes parameters. In addition, a set of experimental procedures to characterize optical polarization properties as a function of the applied voltage for LCVRs is presented. The studied properties are those involved in the operation of these retarders and, generally, are the most significant for optical applications: retardance, diattenuation, transmittance, optical axes position, and output depolarization effects. The correct characterization of these properties can be useful to improve results, or estimate errors, in applications using these devices. The results obtained show good accuracy and good agreement with the expected results.

Contents

Chapter 1

Introduction

The measurement of the polarization of light is well established [1-13]. Recently, more use has been made of variable retarders, for example, liquid crystal retarders or electro-optic cells which have changes of the retardance depending on the voltage applied to the system. Typically, the use of this type of systems involves the application of harmonic variations (*i.e.* period of 2π) of voltage to give harmonic variations of the retardance, and thus harmonic variations of the signal detected after transmission in a linear polarizer. However, liquid crystal variable retarders (LCVRs) have a nonlinear voltage-retardance relationship which distorts the retardance variation if a harmonic voltage is applied, complicating the interpretation of the detected signals, so that a step-voltage method is generally used with this type of devices [6, 7].

Mueller-matrix polarimetry [1-5] has applications in many scientific and technological areas. Techniques that involve the determination of optical properties through the measurement of the polarization of light scattered by rough surfaces are found in applications such as biological tissue analysis [14] and optical characterization of advanced materials [15], among many others. A project to build a goniometric scatterometer in our laboratory at the CCADET-UNAM, [16, 17] to characterize materials with 2D surface roughness has motivated the development of a Mueller polarimeter, which must meet some specific requirements such as high-speed measurements, low-weight components, and no moving parts in order to avoid mechanical vibrations that could affect the accuracy of the measurements. The most frequent techniques found in the literature and used to measure the Mueller matrix are based on fixed linear polarizers and rotating retarders [1-5]. They normally use a Fourier analysis of the detected signal to obtain the Mueller matrix components. However, modern methods of polarimetric measurement use variable retarders such as electro-optics or liquid-crystal cells [18-23], which have a retardance which depends on the applied voltage. Mueller-matrix polarimeters using liquid crystal systems [24] have been implemented in this work because these devices meet the requirements described above and, furthermore, they are cheaper than other types of retarders such as, for example, Pockels cells. Previously, a Stokes polarimeter

is implemented as an intermediate step to producing a Mueller polarimeter. In this work, novel methods for measuring both the Stokes vector of a light beam and the Mueller matrix of a general sample, performing an analysis of the nonlinear voltage-retardance relationship for LCVRs, are presented.

In Chapter 2, a theoretical framework on polarized light and polarimetry is presented. Moreover, the derivation of the measurement methods to be used for both versions of polarimeter, Stokes and Mueller, is shown. Chapter 3 presents the analysis, experimental implementation, and obtained results of a set of experimental procedures to characterize optical polarization properties as a function of the applied voltage for liquid-crystal variable retarders (LCVRs). The experimental results of the Stokes-vector and Mueller-matrix measurements are presented in Chapters 4 and 5, respectively. Finally, Chapter 6 contains the conclusions and a recap of the ideas derived from this work that may be useful for future research.

The experimental techniques developed in this Thesis project and its main results have been reported in a series of publications in indexed journals. The first page from each paper is presented in appendix A. Furthermore, this work has been presented for discussion with the community in a number of international conferences and workshops. Comments and suggestions from our colleagues and journal reviewers were taken into account for improvement of this work.

Journal papers

1. J. M. López-Téllez, N. C. Bruce and O. G. Rodríguez-Herrera, "Characterization of optical polarization properties for liquid-crystal based retarders," paper in preparation.

2. J. M. López-Téllez, N. C. Bruce, J. Delgado-Aguillón, J. Garduño-Mejía and M. Avendaño-Alejo, "Experimental method to characterize the retardance function of optical variable retarders," American Journal of Physics 83(2), 143 (2015).

3. J. M. López-Téllez and N. C. Bruce, "Mueller-matrix polarimeter using analysis of the nonlinear voltage-retardance relationship for liquid-crystal variable retarders," Applied Optics 53(24), 5359 (2014).

4. J. Delgado-Aguillón, J. Garduño-Mejía, J. M. López-Téllez, N. C. Bruce, M. Rosete-Aguilar, C. J. Román-Moreno, and R. Ortega-Martínez, "Direct inversion methods for spectral amplitude modulation of femtosecond pulses," Review of Scientific Instruments 85(4), 043105 (2014).

5. J. M. López-Téllez and N. C. Bruce, "Stokes polarimetry using analysis of the nonlinear voltage-retardance relationship for liquid-crystal variable retarders," Review of Scientific Instruments 85(3), 033104 (2014).

Conference proceedings

1. J. M. López-Téllez, N. C. Bruce, and R. Nava-Sandoval, "Scanning Polarimetric Scatterometer for Two-Dimensional Rough Surfaces," in Frontiers in Optics 2015, OSA Technical Digest (online) (Optical Society of America, 2015), paper JTu4A.35.

2. J. M. López-Téllez and N. C. Bruce, "Polarimetry of light using analysis of the nonlinear voltage-retardance relationship for liquid-crystal variable retarders," in Latin America Optics and Photonics Conference, OSA Technical Digest (online) (Optical Society of America, 2014), paper LTh3B.2.

3. R. Nava-Sandoval, N. C. Bruce, J. M. López-Téllez, "Procedimiento de calibración y ajuste de un esparcímetro goniométrico para medición polarimétrica de la luz esparcida en superficies rugosas," Boletín Científico Técnico INIMET 1, 9 (2014).

4. J. M. López-Téllez and N. C. Bruce, "Experimental method to characterize a liquid-crystal variable retarder and its application in a Stokes polarimeter," Proceedings of SPIE 8785, 87852J (2013).

5. J. M. López-Téllez and N. C. Bruce, "The effect of alignment errors in polarimetry of light using liquid-crystal variable retarders," Proceedings of SPIE 8011, 801107 (2011).

6. C. A. Velázquez Olivera, J. M. López-Téllez and N. C. Bruce, "Stokes polarimetry using liquid-crystal variable retarders and nonlinear voltage-retardance function" Proceedings of SPIE 8011, 80110C (2011).

Science popularization

1. N. C. Bruce and J. M. López-Téllez "Medición de la polarización de la luz," Explorando en la Óptica (online) (Academia Mexicana de Óptica A.C., 2015).

Conferences and workshops

1. J. M. López-Téllez, N. C. Bruce, and R. Nava-Sandoval, "Scanning Polarimetric Scatterometer for Two-Dimensional Rough Surfaces," OSA Frontiers in Optics 2015, San José, California, USA.

2. J. M. López-Téllez and N. C. Bruce, "Polarimetry of light using analysis of the nonlinear voltage-retardance relationship for liquid-crystal variable retarders," Summer School LiSci 2015, Tequisquiapan, México.

3. J. M. López-Téllez and N. C. Bruce, "Polarimetry of light using analysis of the nonlinear voltage-retardance relationship for liquid-crystal variable retarders," FOCUS Latin America 2014, Medellín, Colombia.

4. J. M. López-Téllez and N. C. Bruce, "Polarimetry of light using analysis of the nonlinear voltage-retardance relationship for liquid-crystal variable retarders," Latin American Optics and Photonics Conference (LAOP) 2014, Cancún, México.

5. J. M. López-Téllez and N. C. Bruce, "Experimental method to characterize a liquid-crystal variable retarder and its application in a Stokes polarimeter," International OSA Network of Students (IONS) 2013, Ensenada, México.

6. J. M. López-Téllez and N. C. Bruce, "Experimental method to characterize a liquid-crystal variable retarder and its application in a Stokes polarimeter," 8th Ibero American Optics Meeting/11th Latin American Meeting on Optics, Lasers, and Applications 2013; Porto, Portugal.

7. J. M. López-Téllez and N. C. Bruce, "The effect of alignment errors in polarimetry of light using liquid-crystal variable retarders," 22nd General Congress of the International Commission for Optics (ICO) 2011, Puebla, México.

Chapter 2

Polarized light and polarimetry

Polarization is a property that is common to all types of vector waves. Electromagnetic waves also possess this property [25]. For all types of vector waves, polarization refers to the behavior with time of one of the field vectors appropriate to that wave, observed at a fixed point in space. Light waves are electromagnetic in nature and require four basic field vectors for their complete description: the electrical field strength **E**, the electric displacement density **D**, the magnetic field strength **H**, and the magnetic flux density **B** [26, 27]. Of these four vectors the electric field strength **E** is chosen to define the state of polarization of light waves [28]. This choice is based on the fact that, when light interacts with matter, the force exerted on the electrons by the electric field of the light waves is much greater than the force exerted on these electrons by the magnetic field of the wave. In general, once the polarization of **E** has been determined, the polarization of the three remaining vectors **D**, **H**, and **B** can be found, because the field vectors are interrelated by Maxwell's field equations and the associated constitutive (material) relations.

This Chapter includes text taken from references [1], [8], [12] and [13].

2.1 Stokes vectors and Mueller matrices

To describe a general radiation field, four parameters should be specified: intensity, degree of polarization, plane of polarization, and ellipticity of the radiation at each point and in any given direction [8]. However, it would be difficult to include such diverse quantities as intensity, a ratio, an angle, and a pure number in any symmetrical way in formulating the equation of propagation. A proper parametric representation of polarized light is therefore a matter of some importance. The most convenient representation of polarized light was introduced by Sir George Stokes in 1852.

The Stokes parameters, *i.e.,* the elements of the Stokes vectors, are a set of measurable quantities that describe the polarization state of a light beam for completely polarized, partially polarized, and unpolarized light. The Stokes vector, for quasi-monochromatic light,

can be defined in terms of the cartesian components of the transverse electric field [1]; or, alternatively, it can be defined in terms of measurable irradiances:

$$S = \begin{pmatrix} S0 \\ S1 \\ S2 \\ S3 \end{pmatrix} = \begin{pmatrix} \langle E_x E_x^* + E_y E_y^* \rangle \\ \langle E_x E_x^* - E_y E_y^* \rangle \\ \langle E_x E_y^* + E_y E_x^* \rangle \\ i \langle E_x E_y^* - E_y E_x^* \rangle \end{pmatrix} = \begin{pmatrix} I_H + I_V \\ I_H - I_V \\ I_{45^o} - I_{-45^o} \\ I_R - I_L \end{pmatrix}, \tag{2.1}$$

where E_x and E_y are the components of the electric field in the x- and y-direction, respectively. The symbol $\langle\rangle$ indicates that the quantities are ensemble averages but, assuming stationarity and ergodicity, they can be replaced by time averages with the same result. The first element (S0) of the Stokes vector is the total irradiance, the second one is the fraction of light linearly polarized in the horizontal (H) and/or vertical (V) direction, the third element is the fraction linearly polarized at $\pm 45°$, from the horizontal plane, and the fourth one is the fraction of light circularly polarized with right (R) and/or left (L) handedness. All these measurements, together, allow the determination of the Stokes parameters S0, S1, S2 and S3. The degree of polarization is given by comparing the total intensity with the sum of the ones measured with polarizers. The direction of the polarization ellipse can be found by analyzing the measurement with linear polarizers, carried out under different angles of the polarizer. The sense of rotation and the ellipticity is accessible when all measurements with polarizers are considered [8].

For completely polarized light, the four parameters are related by the expression:

$$S0^2 = S1^2 + S2^2 + S3^2, \tag{2.2}$$

where S0 is the intensity of the beam and S1, S2 and S3 can have any real value between -S0 and +S0. Equation 2.2 allows a representation of the polarization states on the surface of a sphere, which is called a Poincaré sphere as shown in Figure 2.1.1. Here, S1, S2 and S3 may be regarded as Cartesian coordinates of a point **P** on a sphere of radius S0. Every possible state of polarization of a monochromatic plane wave corresponds to a point on the Poincaré sphere and vice versa. The right-handed circular polarization is represented by the north pole, the left-handed polarization by the south pole, the linear polarizations by points in the equatorial plane, and the elliptical states by the points between the poles and the equatorial plane. For and observer looking to the source direction, the right-handed polarization points lie above the equatorial plane and the left-handed lie below. According to a description of the polarization by complex numbers, the ensemble of the polarization states is mapped onto the complex plane; here it is mapped onto the surface of the Poincaré sphere and it exists as a unique projection between them.

Stokes vectors can also describe partially polarized light. This can be thought of as combinations of several mutually incoherent beams of different polarizations. The combination can

be obtained by addition of the intensities, which are represented by the individual elements of the Stokes vector. These are directly related to the so-called coherency matrix [29]. For partially polarized light the condition of Equation 2.2 will no longer be fulfilled. A measure for the validity of this condition can be the parameter p, given by

$$p = \frac{\sqrt{S1^2 + S2^2 + S3^2}}{S0}, \tag{2.3}$$

which is called the degree of polarization of light. The degree of polarization p is equal to 1 for fully polarized light and equal to 0 for non-polarized light. Stokes vectors with a degree of polarization between 0 and 1 represent partially polarized light beams. Stokes vectors of partially polarized light beams can also be represented with the help of the Poincaré sphere as points inside its surface, with radius p. Values outside the surface have non-physical sense, they are originated by experimental noise or by wrong theoretical considerations.

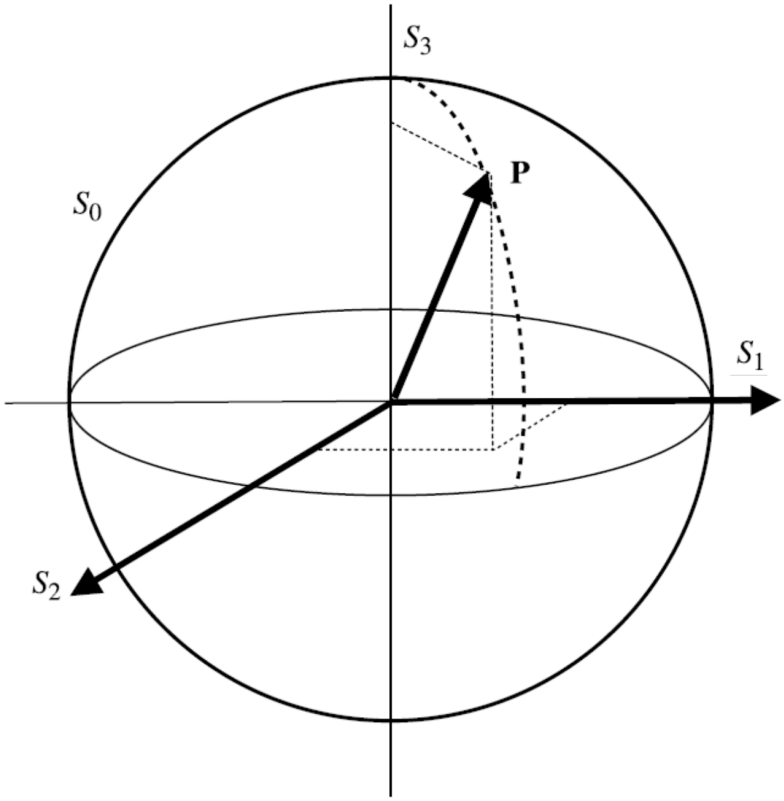

Figure 2.1.1: Poincaré sphere representation of the polarization states of a monochromatic wave. In most definitions the sphere has a radius of 1. One can introduce the parameter S_0 as the sphere radius to consider partially polarized light or different intensities. Drawing taken from Ref. [8].

We can establish a matrix formalism that relates the Stokes vector of a light beam leaving an optical device with the Stokes vector of the input beam. This matrix is called a Mueller matrix after its inventor. It is a 4×4 matrix with real elements. The Stokes vectors S are then transformed by

$$S' = \begin{pmatrix} S0'_0 \\ S1' \\ S2' \\ S3' \end{pmatrix} = \begin{pmatrix} M_{11} & M_{12} & M_{13} & M_{14} \\ M_{21} & M_{22} & M_{23} & M_{24} \\ M_{31} & M_{32} & M_{33} & M_{34} \\ M_{41} & M_{42} & M_{43} & M_{44} \end{pmatrix} \begin{pmatrix} S0 \\ S1 \\ S2 \\ S3 \end{pmatrix}. \tag{2.4}$$

The Mueller matrix contains all the information concerning the polarization properties of the object that it represents. The sample may be a surface, a polarization element, an optical system, or some other interaction which produces a reflected, refracted, diffracted, or scattered light beam [30]. Not every real 4×4 matrix can be a Mueller matrix $\mathbf{M}$. There exist conditions for testing the consistency of a matrix to be a Mueller matrix [9]. Mueller matrices can also be specified for non-depolarizing devices and then are called Mueller–Jones matrices.

Other calculi have been developed for analyzing polarization; two worth mentioning are the Jones calculus [10] and the coherence matrix calculus [31]. The Jones calculus has some unique advantages. For instance, every normalized Jones matrix that can be written down corresponds to a device that can be produced in the laboratory, and a Jones matrix can be differentiated, to yield information as the properties of the material of the optical element it represents [32]. The Jones calculus, however, is only applicable if the incident beam is completely polarized, and if the optical elements represented by the Jones matrices do not decrease the degree of polarization of light. Scattering samples cannot be represented using this formalism. The coherence matrix calculus, as well as the Mueller calculus, can account for partially polarized incident beams [33]. Nevertheless, the coherence matrix calculus is not applicable if the samples represented are of depolarizing type [10]. The propagation through depolarizing optical systems can be handled using the Mueller formalism, and it is the definition of the Stokes vector in terms of irradiances (right part of Eq. 2.1) that makes the Mueller calculus most generally suited for describing irradiance-measuring instruments [30]; for this reason, it was the formalism chosen in this Thesis.

2.2 Diattenuation and retardance

Two important concepts in polarimetry are those of diattenuation and retardance. Since these concepts are extensively used in this work, it is appropriate to present their definition.

Linear diattenuation D is a measure of the tendency of a sample to polarize linearly incident light that is unpolarized. The operational definition of the diattenuation, as given

by Chipman [34], is:

$$D \equiv \frac{\mid \tau_q - \tau_r \mid}{\tau_q + \tau_r}, \tag{2.5}$$

where τ_q and τ_r are the principal intensity transmittances (the maximum transmittance τ_q, and minimum transmittance τ_r) for orthogonal linear polarization states. For an ideal polarizer $D = 1$ and for a partial polarizer $0 < D < 1$. The diattenuation of a polarizer is related to its extinction ratio ε as follows:

$$\varepsilon \equiv \frac{\tau_q}{\tau_r} = \frac{1 + D}{1 - D}. \tag{2.6}$$

The linear retardance δ is defined as the difference between the phase change for the extraordinary wave φ_q and the phase change for the ordinary wave φ_r of the two linear eigenpolarization states after transmission through the sample. The corresponding operational definition, as given by Chipman [34], is:

$$\delta \equiv \mid \varphi_q - \varphi_r \mid . \tag{2.7}$$

The possible values for the retardance are in a range that spans more than a wavelength ($0^o - 360^o$). In a wave-plate, the direction of the polarization component that emerges with the leading phase is said to be along the direction of the fast axis, whereas the component polarized in the orthogonal direction is said to be along the direction of the slow axis. Thus, the fast axis is the direction for which the component of an incident wave polarized in this direction travels fastest within the wave-plate.

For instance, non-depolarizing objects can be represented by the combination of a linear-diattenuator and a linear-retarder. Therefore, the Mueller matrix of a linear-retarder, with its fast axis oriented in the horizontal direction, followed by a linear-diattenuator is [10]:

$$R(\tau, \Psi, \delta) = \tau \begin{pmatrix} 1 & -\cos 2\Psi & 0 & 0 \\ -\cos 2\Psi & 1 & 0 & 0 \\ 0 & 0 & \sin 2\Psi \cos\delta & \sin 2\Psi \sin\delta \\ 0 & 0 & -\sin 2\Psi \sin\delta & \sin 2\Psi \cos\delta \end{pmatrix}, \tag{2.8}$$

where τ is the transmittance for unpolarized light, δ is the retardance and Ψ, defined as:

$$\tan\Psi = \sqrt{\frac{\tau_p}{\tau_s}}, \tag{2.9}$$

for τ_p and τ_s the transmittance for p and s polarizations, is an auxiliary angle related to the diattenuation of the optical element [10].

2.3 Stokes-vector polarimetry

In this work, a Stokes polarimeter is implemented as an intermediate step to producing a Mueller matrix polarimeter. In this section, novel methods for measuring the Stokes vector of a light beam performing an analysis of the nonlinear voltage-retardance relationship for LCVRs are presented. Experimental results of measurements using all these methods will be shown in Chapter 4.

In theory [1], the measurement process can be represented as

$$I = AS, \tag{2.10}$$

where I is the vector of flux measurements as made by the detector, A is a matrix whose dimensions depend on the number of measurements and whose elements depend on the optical system, and S is the incident Stokes vector. Since we want to determine the incident Stokes vector, we must invert Eq. 2.10 so that S is given by

$$S = A^{-1}I. \tag{2.11}$$

This system of equations is generated through a set of measurements and can be solved through Fourier or non-Fourier techniques. Both solution methods will be discussed in this section.

2.3.1 Stokes polarimeter with LCVRs

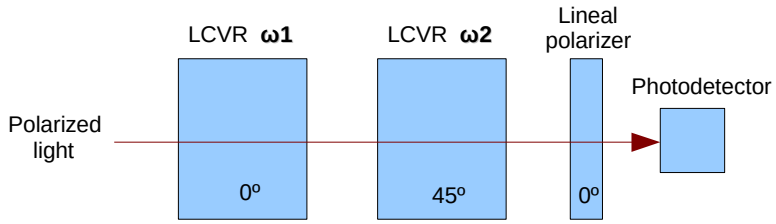

Figure 2.3.1: Block diagram of the experimental set-up used for the Stokes polarimeter. The angles associated with each component refer to the relative angle of the optical axis of that component. $\omega 1$ and $\omega 2$ are the frequencies of the variations of the retardances.

Figure 2.3.1 shows the set-up used for the Stokes polarimeter. The light to be analyzed passes through two liquid crystal variable retarders with their axes at 45º to each other and finally through a linear polarizer with its transmission axis parallel to the axis of the first retarder. The optical system affects the Stokes vector of the light following the relation,

$$S^{out} = M_{sys}S^{in}, \tag{2.12}$$

where S^{in} is the Stokes vector of the light coming from the source and S^{out} is the Stokes vector of the light at the detector. The term M_{sys} is the Mueller matrix of the system and can be written in terms of the Mueller matrices of each of the components in the system, this is

$$M_{sys} = M_P\left(0^{\text{o}}\right) M_{R2}\left(\delta_2, 45^{\text{o}}\right) M_{R1}\left(\delta_1, 0^{\text{o}}\right), \tag{2.13}$$

where $M_P\left(\alpha\right)$ is the Mueller matrix of a linear polarizer with its transmission axis at an angle $\alpha = 45^{\text{o}}$ with respect to the horizontal plane, and $M_{Ri}\left(\delta_i, \theta_i\right)$ represents the Mueller matrix of the ith retarder of retardance δ_i with its fast axis at θ_i with respect to the horizontal plane ($\theta_1 = 45^{\text{o}}$ and $\theta_2 = 0^{\text{o}}$). These matrices are given by

$$M_p\left(\alpha\right) = \frac{1}{2}\begin{pmatrix} 1 & \cos 2\alpha & \sin 2\alpha & 0 \\ \cos 2\alpha & \cos^2 2\alpha & \sin 2\alpha \cos 2\alpha & 0 \\ \sin 2\alpha & \sin 2\alpha \cos 2\alpha & \sin^2 2\alpha & 0 \\ 0 & 0 & 0 & 0 \end{pmatrix}, \tag{2.14}$$

and

$$M_{Ri}\left(\delta, \theta\right) = \begin{pmatrix} 1 & 0 & 0 & 0 \\ 0 & \cos^2 2\theta_i + \cos\delta_i \sin^2 2\theta_i & \left(1 - \cos\delta_i\right) \sin 2\theta_i \cos 2\theta_i & -\sin\delta_i \sin 2\theta_i \\ 0 & \left(1 - \cos\delta_i\right) \sin 2\theta_i \cos 2\theta_i & \sin^2 2\theta_i + \cos\delta_i \cos^2 2\theta_i & \sin\delta_i \cos 2\theta_i \\ 0 & \sin\delta_i \sin 2\theta_i & -\sin\delta_i \cos 2\theta_i & \cos\delta_i \end{pmatrix}. \tag{2.15}$$

2.3.2 Stokes polarimetry using Fourier analysis and nonlinear voltage-retardance function

Figure 2.3.2 shows the typical variation of the retardance with the voltage applied to an LCVR (the process of characterization of this device will be shown in Chapter 3). It can be seen that the curve is not linear, especially for high values of voltage which give low values of retardance. If the retardance does not depend linearly on the voltage then the voltage variations (which are usually sinusoidal) cannot be related directly to the retardance variations, and the analysis of the signals becomes very complicated. To avoid these problems, the approximately linear region of retardance between λ and $\lambda/2$ for a wavelength of 633 nm (corresponding to voltage values between approximately 1500 mV and 2500 mV) could be used. Following this idea, the development of the measurement method is as follows:

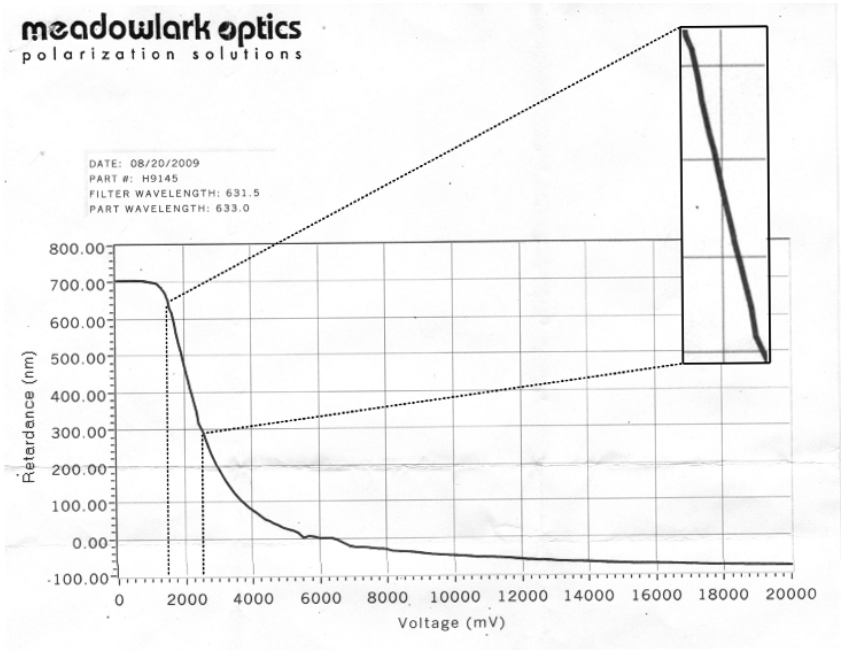

Figure 2.3.2: Retardance vs voltage for a typical liquid crystal retarder for a wavelength of 633 nm.

Let us suppose that the LCVRs give sinusoidal variations of the retardance, from a sinusoidal voltage applied over a range giving retardance from $\lambda/2$ to λ (the part of the voltage-retardance curve which is closest to linear). This is

$$\delta = \frac{3\pi}{2} + \frac{\pi}{2}\sin\omega t, \tag{2.16}$$

for both retarders in the Stokes polarimeter (Fig. 2.3.1), with ω being the frequency of oscillation of the applied voltage, for each LCVR respectively. This gives

$$\begin{aligned} \sin\delta &= -\cos\left(\tfrac{\pi}{2}\sin\omega t\right), \\ \cos\delta &= \sin\left(\tfrac{\pi}{2}\sin\omega t\right). \end{aligned} \tag{2.17}$$

By substituting the above equations in the Mueller matrix for a variable retarder (Eq. 2.15) we found that the Mueller matrix for the system (Eq. 2.13) becomes

$$M_{sys} = \frac{1}{2}\begin{pmatrix} 1 & \sin\left(\frac{\pi}{2}\sin\omega_2 t\right) & \cos\left(\frac{\pi}{2}\sin\omega_1 t\right)\cos\left(\frac{\pi}{2}\sin\omega_2 t\right) & \sin\left(\frac{\pi}{2}\sin\omega_1 t\right)\cos\left(\frac{\pi}{2}\sin\omega_2 t\right) \\ 1 & \sin\left(\frac{\pi}{2}\sin\omega_2 t\right) & \cos\left(\frac{\pi}{2}\sin\omega_1 t\right)\cos\left(\frac{\pi}{2}\sin\omega_2 t\right) & \sin\left(\frac{\pi}{2}\sin\omega_1 t\right)\cos\left(\frac{\pi}{2}\sin\omega_2 t\right) \\ 0 & 0 & 0 & 0 \\ 0 & 0 & 0 & 0 \end{pmatrix}. \tag{2.18}$$

The detected intensity is the first element of the detected Stokes vector:

$$\begin{aligned} S0^{out} = \tfrac{1}{2}\Big\{ & S0^{in} + \sin\left(\tfrac{\pi}{2}\sin\omega_2 t\right) S1^{in} + \cos\left(\tfrac{\pi}{2}\sin\omega_1 t\right)\cos\left(\tfrac{\pi}{2}\sin\omega_2 t\right) S2^{in} \\ & + \sin\left(\tfrac{\pi}{2}\sin\omega_1 t\right)\cos\left(\tfrac{\pi}{2}\sin\omega_2 t\right) S3^{in}\Big\}. \end{aligned} \tag{2.19}$$

Now, using the expansions [1]:

$$\begin{aligned} \sin(\gamma\sin\omega t) &= 2\sum_{n=0}^{\infty} J_{2n+1}(\gamma)\sin[(2n+1)\omega t] = 2J_1(\gamma)\sin(\omega t), \\ \cos(\gamma\sin\omega t) &= J_0(\gamma) + 2\sum_{n=0}^{\infty} J_{2n}(\gamma)\cos[(2n+1)\omega t] = J_0(\gamma) + 2J_2(\gamma)\cos(\omega t); \end{aligned} \tag{2.20}$$

where J_i is the Bessel function of order i and frequencies up to the double of the original frequency have been taken.

Substituting Eq. 2.20 in Eq. 2.19 gives

$$\begin{aligned} S0^{out} = \tfrac{1}{2}\Big\{ & S0^{in} + 2J_1\left(\tfrac{\pi}{2}\right)\sin(\omega_2 t)\, S1^{in} + \left[J_0\left(\tfrac{\pi}{2}\right) + 2J_2\left(\tfrac{\pi}{2}\right)\cos(2\omega_1 t)\right] \\ & \times\left[J_0\left(\tfrac{\pi}{2}\right) + 2J_2\left(\tfrac{\pi}{2}\right)\cos(2\omega_2 t)\right] S2^{in} \\ & + 2J_1\left(\tfrac{\pi}{2}\right)\sin(\omega_1 t)\left[J_0\left(\tfrac{\pi}{2}\right) + 2J_2\left(\tfrac{\pi}{2}\right)\cos(2\omega_2 t)\right] S3^{in}\Big\}. \end{aligned} \tag{2.21}$$

Combining the trigonometric terms, the measured signal can be written in terms of the frequencies of the variations of the retardances

$$\begin{aligned} S0^{out} = \tfrac{1}{2}\left[S0^{in} + J_0^2\left(\tfrac{\pi}{2}\right) S2^{in}\right] & + J_1\left(\tfrac{\pi}{2}\right) S1^{in}\sin(\omega_2 t) \\ + J_0\left(\tfrac{\pi}{2}\right) J_1\left(\tfrac{\pi}{2}\right) S3^{in}\sin(\omega_1 t) + J_0\left(\tfrac{\pi}{2}\right) J_2\left(\tfrac{\pi}{2}\right) & S2^{in}\left[\cos(2\omega_1 t) + \cos(2\omega_2 t)\right] \\ + J_1\left(\tfrac{\pi}{2}\right) J_2\left(\tfrac{\pi}{2}\right) S3^{in} & \left\{\sin\left[(\omega_1 - 2\omega_2)t\right] + \sin\left[(\omega_1 + 2\omega_2)t\right]\right\} \\ + J_2^2\left(\tfrac{\pi}{2}\right) S2^{in} & \left\{\cos\left[(2\omega_1 - 2\omega_2)t\right] + \cos\left[(2\omega_1 + 2\omega_2)t\right]\right\}. \end{aligned} \tag{2.22}$$

Resolving this equation for the components of the unknown Stokes vector, in terms of the frequency components of the detected signal, we have

$$\begin{cases} S0^{in} = 2\, S0^{out}\{0\} - J_0^2\left(\tfrac{\pi}{2}\right) S2^{in}, \\ S1^{in} = \frac{S0^{out}\{\sin[(\omega_2)t]\}}{J_1\left(\frac{\pi}{2}\right)}, \\ S2^{in} = \frac{S0^{out}\{\cos[(2\omega_1)t]\}}{J_0\left(\frac{\pi}{2}\right)J_2\left(\frac{\pi}{2}\right)} = \frac{S0^{out}\{\cos[(2\omega_2)t]\}}{J_0\left(\frac{\pi}{2}\right)J_2\left(\frac{\pi}{2}\right)} = \frac{S0^{out}\{\cos[(2\omega_1+2\omega_2)t]\}}{J_2^2\left(\frac{\pi}{2}\right)}, \\ S3^{in} = \frac{S0^{out}\{\sin[(\omega_1+2\omega_2)t]\}}{J_1\left(\frac{\pi}{2}\right)J_2\left(\frac{\pi}{2}\right)} = \frac{S0^{out}\{\sin[(\omega_1)t]\}}{J_0\left(\frac{\pi}{2}\right)J_1\left(\frac{\pi}{2}\right)}. \end{cases} \tag{2.23}$$

Finally, the above equations can be written, also, in terms of the complex components of the Fast Fourier Transform (FFT) of the detected signal

$$\begin{cases} S0^{in} = 2\,\mathrm{Re}\,S\{0\} - J_0^2\left(\frac{\pi}{2}\right) S2^{in}, \\ S1^{in} = \frac{\mathrm{Im}\,S\{\omega_2\}}{J_1\left(\frac{\pi}{2}\right)}, \\ S2^{in} = \frac{\mathrm{Re}\,S\{2\omega_1\}}{J_0\left(\frac{\pi}{2}\right)J_2\left(\frac{\pi}{2}\right)} = \frac{\mathrm{Re}\,S\{2\omega_2\}}{J_0\left(\frac{\pi}{2}\right)J_2\left(\frac{\pi}{2}\right)} = \frac{\mathrm{Re}\,S\{2\omega_1+2\omega_2\}}{J_2^2\left(\frac{\pi}{2}\right)}, \\ S3^{in} = \frac{\mathrm{Im}\,S\{\omega_1+2\omega_2\}}{J_1\left(\frac{\pi}{2}\right)J_2\left(\frac{\pi}{2}\right)} = \frac{\mathrm{Im}\,S\{\omega_1\}}{J_0\left(\frac{\pi}{2}\right)J_1\left(\frac{\pi}{2}\right)}; \end{cases} \tag{2.24}$$

where $\mathrm{Re}\,S\{\,\}$ is the real component of the FFT and $\mathrm{Im}\,S\{\,\}$ is the imaginary component of the FFT of the detected signal (S0).

From the above system of equations we can extract seven different equations to measure the Stokes parameters in terms of the frequency components of the detected signal,

$$\begin{cases} S0 = 2\,\mathrm{Re}\,S\{0\} - J_0^2\left(\frac{\pi}{2}\right) S_2, \\ S1\left(\omega_2\right) = \frac{\mathrm{Im}\,S\{\omega_2\}}{J_1\left(\frac{\pi}{2}\right)}, \\ S2\left(2\omega_1\right) = \frac{\mathrm{Re}\,S\{2\omega_1\}}{J_0\left(\frac{\pi}{2}\right)J_2\left(\frac{\pi}{2}\right)}, \\ S2\left(2\omega_2\right) = \frac{\mathrm{Re}\,S\{2\omega_2\}}{J_0\left(\frac{\pi}{2}\right)J_2\left(\frac{\pi}{2}\right)}, \\ S2\left(2\omega_1+2\omega_2\right) = \frac{\mathrm{Re}\,S\{2\omega_1+2\omega_2\}}{J_2^2\left(\frac{\pi}{2}\right)}, \\ S3\left(\omega_1\right) = \frac{\mathrm{Im}\,S\{\omega_1\}}{J_0\left(\frac{\pi}{2}\right)J_1\left(\frac{\pi}{2}\right)}, \\ S3\left(\omega_1+2\omega_2\right) = \frac{\mathrm{Im}\,S\{\omega_1+2\omega_2\}}{J_1\left(\frac{\pi}{2}\right)J_2\left(\frac{\pi}{2}\right)}. \end{cases} \tag{2.25}$$

2.3.3 Stokes polarimetry using Fourier analysis and linearized retardance

The use of a full wavelength range of retardance should give a more stable result as more polarization states are being used to find the unknown Stokes vector. For this case, in contrast with the previous case, an experimental linearization method of the retardance variation of the LCVRs has been performed (the procedure and results are presented in Chapter 4) to give a retardance variation which has the form of a linear ramp (sawtooth function). Using this procedure, the development of the measurement method is as follows:

From Eq. 2.14, we know that the Mueller matrix of a linear polarizer with its transmission axis at 0^o, $M_p\left(0^o\right)$, is given by

$$M_P\left(0^{\circ}\right)=\frac{1}{2}\begin{pmatrix}1&1&0&0\\1&1&0&0\\0&0&0&0\\0&0&0&0\end{pmatrix}, \tag{2.26}$$

and the Mueller matrix of a retarder of retardance δ with its fast axis at an angle θ, $M_R\left(\delta,\theta\right)$, is given by Eq. 2.15.

If the retardance variation is a sawtooth function, we have

$$\delta=2\pi mod\left(\frac{t}{t_i}\right), \tag{2.27}$$

where $mod\left(\frac{t}{t_i}\right)$ is the remainder of the division of the real time, t, by the period of the retarder, t_i.

Substituting the above equations in Eq. 2.13 and then this result in Eq. 2.12 the detected intensity becomes

$$\begin{aligned}S0^{out}=\tfrac{1}{2}\Big\{&S0^{in}-\cos\left(2\pi mod\left(\tfrac{t}{t_i}\right)\right)S1^{in}+\sin\left(2\pi mod\left(\tfrac{t}{t_i}\right)\right)\sin\left(2\pi mod\left(\tfrac{t}{t_i}\right)\right)S2^{in}\\&+\cos\left(2\pi mod\left(\tfrac{t}{t_i}\right)\right)\sin\left(2\pi mod\left(\tfrac{t}{t_i}\right)\right)S3^{in}\Big\}\end{aligned} \tag{2.28}$$

We can write the last equation in terms of the oscillation frequencies (ω) of the voltages applied to the variable retarders

$$S0^{out}=\frac{1}{2}\left\{S0^{in}-\cos\left(\omega_2 t\right)S1^{in}+\sin\left(\omega_1 t\right)\sin\left(\omega_2 t\right)S2^{in}+\cos\left(\omega_1 t\right)\sin\left(\omega_2 t\right)S3^{in}\right\}. \tag{2.29}$$

By expanding the products of the trigonometric terms, we have

$$\begin{aligned}S0^{out}=\tfrac{1}{2}\Big\{&S0^{in}-\cos\left(\omega_2 t\right)S1^{in}-\tfrac{1}{2}\cos\left(\left(\omega_1+\omega_2\right)t\right)S2^{in}+\tfrac{1}{2}\cos\left(\left(\omega_1-\omega_2\right)t\right)S2^{in}\\&+\tfrac{1}{2}\sin\left(\left(\omega_1+\omega_2\right)t\right)S3^{in}-\tfrac{1}{2}\sin\left(\left(\omega_1-\omega_2\right)t\right)S3^{in}\Big\}.\end{aligned} \tag{2.30}$$

We can write the components of the incident Stokes vector as

$$\begin{cases}S0^{in}=2\,S0^{out}\left\{0\right\},\\S1^{in}=-2\,S0^{out}\left\{\cos\left[\omega_2 t\right]\right\},\\S2^{in}=-4\,S0^{out}\left\{\cos\left[\left(\omega_1+\omega_2\right)t\right]\right\}=4\,S0^{out}\left(\cos\left\{\left(\omega_1-\omega_2\right)t\right\}\right),\\S3^{in}=4\,S0^{out}\left(\sin\left\{\left(\omega_1+\omega_2\right)t\right\}\right)=-4\,S0^{out}\left(\sin\left\{\left(\omega_1-\omega_2\right)t\right\}\right).\end{cases} \tag{2.31}$$

where, for instance, $2\,S0^{out}\left\{\cos\left[\omega_2 t\right]\right\}$ is the term corresponding to $\cos\left[\omega_2 t\right]$ in the Fourier expansion of the detected signal $S0^{out}$.

Finally, by using the Fourier transform of the detected signal, the components of the Stokes vector are:

$$\begin{cases} S0^{in} = 2\,\mathrm{Re}\,S\left\{0\right\}, \\ S1^{in} = -2\,\mathrm{Re}\,S\left\{\omega_2\right\}, \\ S2^{in} = -4\,\mathrm{Re}\,S\left\{\omega_1+\omega_2\right\} = 4\,\mathrm{Re}\,S\left\{\omega_1-\omega_2\right\}, \\ S3^{in} = 4\,\mathrm{Im}\,S\left\{\omega_1+\omega_2\right\} = -4\,\mathrm{Im}\,S\left\{\omega_1-\omega_2\right\}, \end{cases} \tag{2.32}$$

where, in a similar way as the previous case, $\mathrm{Re}\,S\left\{\ \right\}$ is the real component of the FFT and $\mathrm{Im}\,S\left\{\ \right\}$ is the imaginary component of the FFT of the detected signal ($S0$).

From the system of equations 2.32 we can extract six different equations to measure the Stokes parameters in terms of the frequency components of the detected signal,

$$\begin{cases} S0 = 2\,\mathrm{Re}\,S\left\{0\right\}, \\ S1 = -2\,\mathrm{Re}\,S\left\{\omega_2\right\}, \\ S2 = -4\,\mathrm{Re}\,S\left\{\omega_1+\omega_2\right\}, \\ S2 = 4\,\mathrm{Re}\,S\left\{\omega_1-\omega_2\right\}, \\ S3 = 4\,\mathrm{Im}\,S\left\{\omega_1+\omega_2\right\}, \\ S3 = -4\,\mathrm{Im}\,S\left\{\omega_1-\omega_2\right\}. \end{cases} \tag{2.33}$$

2.3.4 Stokes polarimetry using a fitting procedure

Following the basic analysis for a Stokes polarimeter presented in Sec. 2.3.1, we found that the detected intensity, the first term of the Stokes vector S^{out}, given by Eqs. 2.12 and 2.13 is

$$I = S0^{out} = \frac{1}{2}\left\{S0^{in} - \cos\left(\delta_2\right) S1^{in} + \sin\left(\delta_1\right)\sin\left(\delta_2\right) S2^{in} + \cos\left(\delta_1\right)\sin\left(\delta_2\right) S3^{in}\right\}. \tag{2.34}$$

In this case, a voltage signal which has the form of a linear ramp (sawtooth function) is applied, this is

$$V = V_{min} + \left(V_{max} - V_{min}\right) mod\left(\frac{t}{t_i}\right), \tag{2.35}$$

and the retardance is given by the nonlinear relationship of Fig. 2.3.2. Using the results of the characterization procedure of the voltage-retardance relationship for the LCVRs, which will be shown in Chapter 3, it is possible to find all the retardance values employed during the measurements. The idea of this method is to fit the detected intensity, I, to a linear

combination

$$I = A + B\cos(\delta_2) + C\sin(\delta_1)\sin(\delta_2) + D\cos(\delta_1)\sin(\delta_2)\,. \tag{2.36}$$

Then, we have

$$\begin{cases} A = \frac{1}{2}S0^{in} \\ B = -\frac{1}{2}S1^{in} \\ C = \frac{1}{2}S2^{in} \\ D = \frac{1}{2}S3^{in} \end{cases} \tag{2.37}$$

2.4 Mueller-matrix polarimetry

In this section details of the setup of the Mueller-matrix polarimeter and a brief description about how it works are presented. Also, details of two methods to measure the Mueller matrix of a general sample are described. Experimental results, for each case, will be shown in Chapter 5. The first method presented here, in a similar way as the case of the Stokes polarimeter, is a fitting algorithm in which the fitting functions take into account the nonlinear voltage–retardance relationship of the LCVRs. This method uses a saw-tooth voltage oscillation giving a range of retardance from 0 to λ. The second method is a typical step-voltage method to measure the Mueller matrix, for comparison with the experimental results of the previous case.

2.4.1 Mueller polarimeter with LCVRs

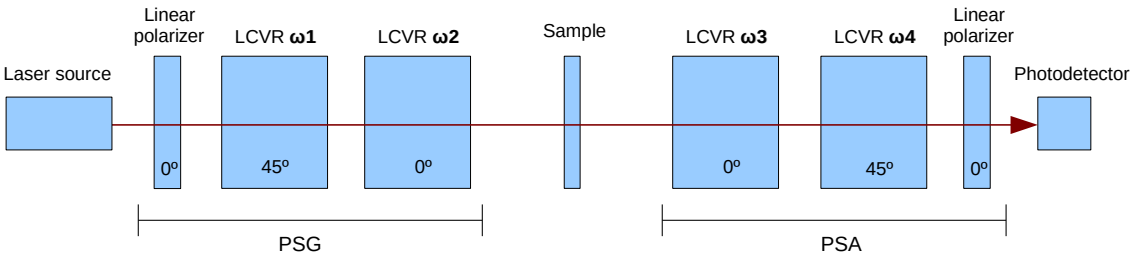

Figure 2.4.1: Block diagram of the experimental set-up used for the Mueller polarimeter. The angles associated with each component refer to the relative angle of the optical axis of that component. $\omega 1$, $\omega 2$, $\omega 3$, and $\omega 4$ are the frequencies of the variations of the retardances.

A Mueller polarimeter is an instrument designed and built to measure the 16 elements of the Mueller matrix. Figure 2.4.1 shows the setup for the Mueller polarimeter using LCVRs. This device consists of two modules: a polarization state generator (PSG) and a polarization state

analyzer (PSA). The sample under test is analyzed between those two modules. The PSG determines the polarization state of the incident light, whereas the PSA measures the change in this state after interaction with the sample. A photodetector measures the intensity of the light transmitted by the optical system.

The measurement of the Mueller matrix of the sample is as follows: the sample under test affects the Stokes vector of the light following the relation

$$S^{out} = M_S S^{in}, \tag{2.38}$$

where S^{in} is the Stokes vector of the light coming from the PSG, the term M_S is the Mueller matrix of the sample, and S^{out} is the resultant Stokes vector of the light to be analyzed in the PSA. At least four independent incident polarization states and four independent detected states are needed to determine the complete Mueller matrix of the sample. In this Thesis, two different methods to measure the Mueller matrix using the same experimental setup are presented. The development is given below.

2.4.2 Mueller polarimetry using a continually varying voltage

We can write the Mueller matrix of the PSG and the PSA in terms of the Mueller matrices of their components. This is

$$M_{PSG} = M_{R2}\left(\delta_2, 0^{\mathrm{o}}\right) M_{R1}\left(\delta_1, 45^{\mathrm{o}}\right) M_{P1}\left(0^{\mathrm{o}}\right), \tag{2.39}$$

and

$$M_{PSA} = M_{P2}\left(0^{\mathrm{o}}\right) M_{R4}\left(\delta_4, 45^{\mathrm{o}}\right) M_{R3}\left(\delta_3, 0^{\mathrm{o}}\right), \tag{2.40}$$

where $M_{Pi}\left(\alpha_i\right)$ is the Mueller matrix of the ith linear polarizer with its transmission axis at an angle α_i ($\alpha_{1,2} = 0^{\mathrm{o}}$), and $M_{Ri}\left(\delta_i, \theta_i\right)$ is the Mueller matrix of the ith retarder of retardance δ_i with its fast axis at an angle θ_i ($\theta_{1,4} = 45^{\mathrm{o}}$ and $\theta_{2,3} = 0^{\mathrm{o}}$).

Solving Eqs. 2.39 and 2.40, we get

$$M_{PSG} = \frac{1}{2}\begin{pmatrix} 1 & -1 & 0 & 0 \\ -\cos\left(\delta_1\right) & \cos\left(\delta_1\right) & 0 & 0 \\ -\sin\left(\delta_1\right)\sin\left(\delta_2\right) & \sin\left(\delta_1\right)\sin\left(\delta_2\right) & 0 & 0 \\ -\sin\left(\delta_1\right)\cos\left(\delta_2\right) & \sin\left(\delta_1\right)\cos\left(\delta_2\right) & 0 & 0 \end{pmatrix}, \tag{2.41}$$

and

$$M_{PSA} = \frac{1}{2}\begin{pmatrix} 1 & -\cos(\delta_4) & \sin(\delta_3)\sin(\delta_4) & \cos(\delta_3)\sin(\delta_4) \\ -1 & \cos(\delta_4) & -\sin(\delta_3)\sin(\delta_4) & -\cos(\delta_3)\sin(\delta_4) \\ 0 & 0 & 0 & 0 \\ 0 & 0 & 0 & 0 \end{pmatrix}. \tag{2.42}$$

Writing the Mueller matrix of the sample as

$$M_S = \begin{pmatrix} M_{11} & M_{12} & M_{13} & M_{14} \\ M_{21} & M_{22} & M_{23} & M_{24} \\ M_{31} & M_{32} & M_{33} & M_{34} \\ M_{41} & M_{42} & M_{43} & M_{44} \end{pmatrix}, \tag{2.43}$$

the total Mueller matrix of the system is

$$M_T = M_{PSA} M_S M_{PSG}. \tag{2.44}$$

Now, let us assume that the incident light is not polarized. This is, the Stokes vector of the incident light is

$$S^{in} = \begin{pmatrix} 1 \\ 0 \\ 0 \\ 0 \end{pmatrix}. \tag{2.45}$$

In this case the Stokes vector of the light coming out from the system is

$$S^{out} = M_T S^{in}, \tag{2.46}$$

and the detected intensity of light, I, is the first component of that Stokes vector. This gives

$$\begin{aligned} I = S0^{out} = \tfrac{1}{4}\{ & M_{11} - M_{12}\cos(\delta_1) - M_{13}\sin(\delta_1)\sin(\delta_2) \\ & - M_{14}\sin(\delta_1)\cos(\delta_2) - M_{21}\cos(\delta_4) + M_{22}\cos(\delta_1)\cos(\delta_4) \\ & + M_{23}\sin(\delta_1)\sin(\delta_2)\cos(\delta_4) + M_{24}\sin(\delta_1)\cos(\delta_2)\cos(\delta_4) \\ & + M_{31}\sin(\delta_3)\sin(\delta_4) - M_{32}\cos(\delta_1)\sin(\delta_3)\sin(\delta_4) \\ & - M_{33}\sin(\delta_1)\sin(\delta_2)\sin(\delta_3)\sin(\delta_4) \\ & - M_{34}\sin(\delta_1)\cos(\delta_2)\sin(\delta_3)\sin(\delta_4) \\ & + M_{41}\cos(\delta_3)\sin(\delta_4) - M_{42}\cos(\delta_1)\cos(\delta_3)\sin(\delta_4) \\ & - M_{43}\sin(\delta_1)\sin(\delta_2)\cos(\delta_3)\sin(\delta_4) \\ & - M_{44}\sin(\delta_1)\cos(\delta_2)\cos(\delta_3)\sin(\delta_4)\}. \end{aligned} \tag{2.47}$$

Then, we can find all the components of the Mueller matrix, M_S, by fitting the detected signal to a linear combination:

$$
\begin{aligned}
I = A &+ B\cos(\delta_1) + C\sin(\delta_1)\sin(\delta_2) \\
&+ D\sin(\delta_1)\cos(\delta_2) + E\cos(\delta_4) + F\cos(\delta_1)\cos(\delta_4) \\
&+ G\sin(\delta_1)\sin(\delta_2)\cos(\delta_4) + H\sin(\delta_1)\cos(\delta_2)\cos(\delta_4) \\
&+ J\sin(\delta_3)\sin(\delta_4) + K\cos(\delta_1)\sin(\delta_3)\sin(\delta_4) \\
&+ L\sin(\delta_1)\sin(\delta_2)\sin(\delta_3)\sin(\delta_4) \\
&+ M\sin(\delta_1)\cos(\delta_2)\sin(\delta_3)\sin(\delta_4) \\
&+ N\cos(\delta_3)\sin(\delta_4) + P\cos(\delta_1)\cos(\delta_3)\sin(\delta_4) \\
&+ Q\sin(\delta_1)\sin(\delta_2)\cos(\delta_3)\sin(\delta_4) \\
&+ R\sin(\delta_1)\cos(\delta_2)\cos(\delta_3)\sin(\delta_4)\,,
\end{aligned}
\tag{2.48}
$$

where

$$
\begin{array}{cccc}
A = \frac{1}{4}M_{11}, & B = -\frac{1}{4}M_{12}, & C = \frac{1}{4}M_{13}, & D = -\frac{1}{4}M_{14}, \\
E = -\frac{1}{4}M_{21}, & F = \frac{1}{4}M_{22}, & G = \frac{1}{4}M_{23}, & H = \frac{1}{4}M_{24}, \\
J = \frac{1}{4}M_{31}, & K = -\frac{1}{4}M_{32}, & L = -\frac{1}{4}M_{33}, & M = -\frac{1}{4}M_{34}, \\
N = \frac{1}{4}M_{41}, & P = -\frac{1}{4}M_{42}, & Q = -\frac{1}{4}M_{43}, & R = -\frac{1}{4}M_{44}.
\end{array}
\tag{2.49}
$$

In a similar way as the case of the Stokes polarimeter, a sawtooth voltage signal (Eq. 2.35) is applied to the LCVRs and the retardance is given by the nonlinear relationship of Fig. 2.3.2. The characterization procedure of the LCVRs will be shown in Chapter 3 and the results will be used to find all the retardance values employed during the measurements.

2.4.3 Mueller polarimetry using a step-voltage method

Measurement	Detected Intensity	Measurement	Detected Intensity
1	I(V, V)	9	I(H, V)
2	I(V, L)	10	I(H, L)
3	I(V, H)	11	I(H, H)
4	I(V, +)	12	I(H, +)
5	I(L, V)	13	I(-, V)
6	I(L, L)	14	I(-, L)
7	I(L, H)	15	I(-, H)
8	I(L, +)	16	I(-, +)

Table 2.4.1: Sixteen measurements required to obtain the complete Mueller matrix of a general sample. I(P,Q) is the detected intensity of light with incident polarization state P on the sample and analyzed polarization state Q. The used polarization states are as follows: V, linear vertical; H, linear horizontal; L, left circular; +, linear at 45°; -, linear at −45°.

In contrast with the previous case, this method analyzes the optical signal resulting from the application of a few specific retardation values, for each retarder, which are changing

in time. Nevertheless, the experimental setup used is the same as that in the previous case (Fig. 2.4.1). Following the theory developed by Bickel and Bailey [36], this method requires four independent incident polarization states and four independent polarization state measurements to yield the 16 measurements required to obtain the complete Mueller matrix of a general sample, as shown in Table 2.4.1. In contrast with the experimental procedure used by Bickel and Bailey, different polarization states for incident and analyzed light can be used. For example, in the measurements presented in this Thesis, linear polarization at 45° was analyzed instead of linear polarization at −45° because, experimentally, the polarimeter works with smaller changes of voltage, and retardance. In this way, a fast response of the variable retarders is achieved. This is a way to improve the speed and quality of the measurements.

The relationship between the detected intensities of light and the Mueller-matrix components was described by Bickel and Bailey [36]. The results are as follows:

$$
\begin{cases}
M_{11} = I(H,H) + I(H,V) + I(V,V) + I(V,H), \\
M_{12} = I(H,H) + I(H,V) - I(V,V) - I(V,H), \\
M_{13} = 2\left\{\frac{1}{2}M_{11} - I(-,H) - I(-,V)\right\}, \\
M_{14} = 2\left\{\frac{1}{2}M_{11} - I(L,H) - I(L,V)\right\}, \\
M_{21} = I(H,H) - I(H,V) + I(V,V) - I(V,H), \\
M_{22} = I(H,H) - I(H,V) - I(V,V) + I(V,H), \\
M_{23} = 2\left\{\frac{1}{2}M_{21} - I(-,H) + I(-,V)\right\}, \\
M_{24} = 2\left\{\frac{1}{2}M_{21} - I(L,H) + I(L,V)\right\}, \\
M_{31} = 2\left\{I(H,+) + I(V,+) - \frac{1}{2}M_{11}\right\}, \\
M_{32} = 2\left\{I(H,+) - I(V,+) - \frac{1}{2}M_{12}\right\}, \\
M_{33} = M_{11}\text{–}M_{13} + M_{31} - 4I(-,+), \\
M_{34} = M_{11}\text{–}M_{14} + M_{31}\text{–}4I(L,+), \\
M_{41} = 2\left\{\frac{1}{2}M_{11} - I(H,L) - I(V,L)\right\}, \\
M_{42} = 2\left\{\frac{1}{2}M_{12} - I(H,L) + I(V,L)\right\}, \\
M_{43} = 4I(-,L) - M_{11} + M_{13} + M_{41}, \\
M_{44} = 4I(L,L) - M_{11} + M_{14} + M_{41}.
\end{cases}
\tag{2.50}
$$

Chapter 3

Characterization of optical properties for LCVRs

Nowadays, liquid crystal cells, which have a birefringence that depends on an applied voltage, are finding increased use in research labs as modulators or retarders [7, 23, 37]. Modern methods of polarization measurement use variable retarders such as electro-optics or liquid-crystal variable retarders (LCVRs) [6, 18, 19, 38]. To obtain the best results using these devices, accurate knowledge of the polarization properties is required. For instance, it is important to characterize the relationship between the observed retardance and the applied voltage in order to verify the manufacturer's characterization and to be able to produce a set of polarization states with high precision. The most significant properties involved in the operation of the LCVRs for optical applications are: retardance, diattenuation, transmittance, degree of polarization of light at the output of the device (depolarization effects), and the optical axes position. In this Chapter, a set of experimental procedures to characterize these properties as a function of the applied voltage for liquid-crystal retarders, in transmission mode, is proposed.

3.1 Descritpion of the LCVRs

Nematic Liquid Crystal Variable Retarders (LCVRs) [24] are constructed using optically flat fused silica windows coated with transparent conductive indium tin oxide (ITO). These devices work in transmission mode. Two windows are aligned and spaced a few microns apart, and the cavity is filled with birefringent nematic liquid crystal material. Electrical contacts are attached, and the device is environmentally sealed. Anisotropic nematic liquid crystal molecules form uniaxial birefringent layers in the liquid crystal cell. On average, the molecules are aligned with their long axes parallel, but with their centers randomly distributed, as shown in Fig. 3.1.1. With no voltage applied, the liquid crystal molecules lie parallel to the glass

substrates and maximum retardation is achieved. When voltage is applied, the liquid crystal molecules begin to tip perpendicular to the fused silica windows. As the voltage increases, the molecules tip further causing a reduction in the effective birefringence and hence the retardance.

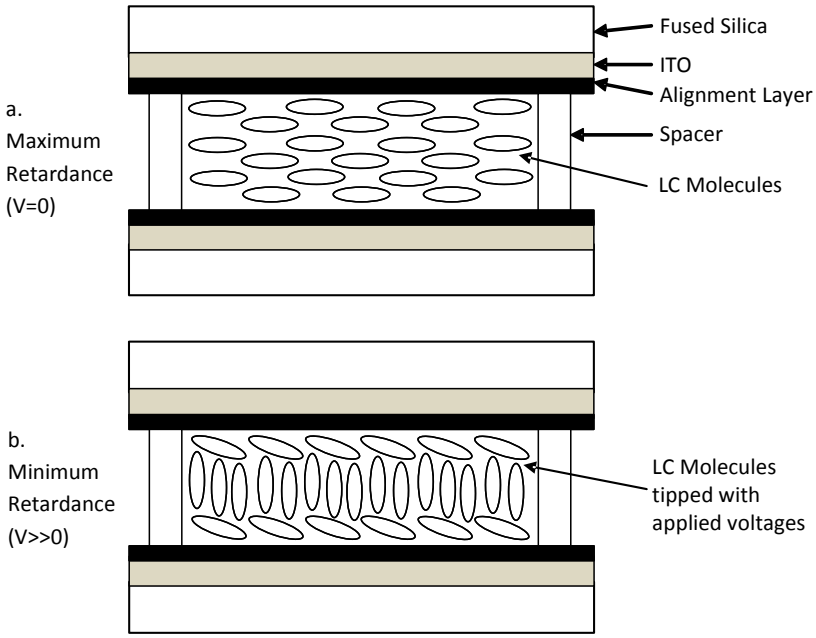

Figure 3.1.1: Schematic diagram of an LCVR showing molecular alignment without (a) and with (b) applied voltage (drawing not to scale) [24]. The horizontal layers form the optical windows of the device.

The response time of these devices depends on several parameters, including layer thickness, viscosity, temperature, variations in drive voltage, and surface treatment. Response time also depends upon direction of the retardance change. Typical response time for a standard visible LCVR is about 5 ms to switch from one-half to zero waves (low to high voltage) and about 20 ms to switch from zero to one-half wave (high to low voltage).

The LCVRs used in this work were manufactured by Meadowlark Optics [24]. The data sheet containing the most relevant technical information about these components is presented in Appendix B.

For all experiments presented in this work, the entire optical window of the LCVRs (about 1 cm diameter) was used for the measurements; uniform illumination was applied by expanding the light beam at the output of the source with a spatial filter, which includes a microscope objective and a pinhole, followed by a lens that selects and collimates only the central and homogeneous intensity region of the expanded laser beam.

3.2 Measuring the retardance-voltage relationship

Figure 3.2.1 shows a schematic diagram of the typical set-up used to characterize the retardance function of the variable retarders. The light to be analyzed passes through a linear polarizer [39], then through a variable retarder with its optical fast axis at 45° to the linear polarizer axis. Finally, the light passes through a linear polarizer with its transmission axis perpendicular to the axis of the first polarizer. For this work, we used a Hamamatsu photomultiplier tube, Model: H7468-20 (See Appendix B for more information about this device), to measure the intensity of the light transmitted by the optical system. The detected light intensity depends on the retardance, which also depends on the birefringence of the variable retarder.

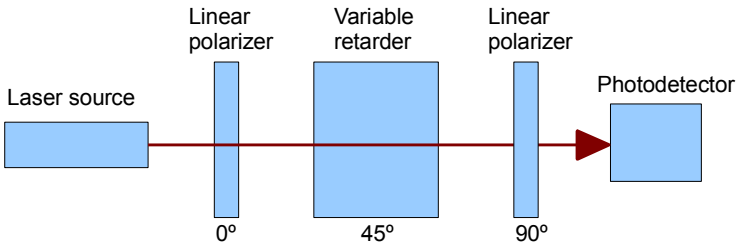

Figure 3.2.1: Block diagram of the set-up used to characterize a variable retarder. The angles associated with each component refer to the relative angle of the optical axis of that component with respect the horizontal plane.

A laser source with a wavelength of 633 nm was used to perform the experiments presented in this work (the data sheet of this device is presented in Appendix B). The stability of the source was studied in order to ensure the quality of our measurements. Also, a beam splitter after the source was used to monitor the laser intensity during experiments.

3.2.1 Theoretical analysis of the experimental set-up

Performing a theoretical analysis in a similar way as for the previous cases shown in Chapter 2, by using a combination of Stokes vectors and Mueller matrices, the optical system affects the Stokes vector of the light through the following relation:

$$S^{out} = M_{sys} S^{in}, \tag{3.1}$$

where S^{in} is the Stokes vector of the light coming from the source, and S^{out} is the Stokes vector of the light at the detector. The detected intensity I is the first term of the Stokes vector S^{out}, which is

$$I = S0. \tag{3.2}$$

The term M_{sys} in Eq. 3.1 is the Mueller matrix of the system and can be written in terms of the Mueller matrices of each of the components in the system; namely,

$$M_{sys} = M_{P2}\left(90^{o}\right) M_{R}\left(\delta, 45^{o}\right) M_{P1}\left(0^{o}\right), \tag{3.3}$$

where $M_{Pi}\left(\alpha_i\right)$ is the Mueller matrix of the ith linear polarizer with its transmission axis at an angle α_i ($\alpha_1 = 0^{o}$ and $\alpha_2 = 45^{o}$) defined in Eq. 2.14), and $M_R\left(\delta, \theta\right)$ is the Mueller matrix of a retarder of retardance δ with its fast axis at $\theta = 45^{o}$ defined in Eq. 2.15.

Thus, the Mueller matrix for the system becomes

$$M_{sys} = \frac{1}{4}\begin{pmatrix} 1-\cos\delta & -1+\cos\delta & 0 & 0 \\ 1-\cos\delta & -1+\cos\delta & 0 & 0 \\ 0 & 0 & 0 & 0 \\ 0 & 0 & 0 & 0 \end{pmatrix}. \tag{3.4}$$

To perform the calculation of the output Stokes vector of the light after the polarizer in the detector arm, a particular value of the input Stokes vector (for the light arriving at the first polarizer) is required. This incident Stokes vector can be in any polarization state, since the first polarizer will always cause it to become linearly polarized. For simplicity here, we assume the incident light to be unpolarized. Substituting Eq. 3.4 into Eq. 3.1 with the Stokes vector of the incident light given by

$$S^{in} = \begin{pmatrix} 1 \\ 0 \\ 0 \\ 0 \end{pmatrix}, \tag{3.5}$$

the detected intensity I becomes

$$I = A(1-\cos\delta), \tag{3.6}$$

where δ is the retardance of the liquid-crystal cell and A is a constant that depends on the experimental parameters such as the absorption and extinction ratio of the polarizers. The maximum intensity I_{max}, is achieved when $\cos\delta = -1$. Thus, substituting this value in Eq. 3.6 we have

$$I_{max} = A(1+1) = 2A, \tag{3.7}$$

so that in this case

$$A = \frac{I_{max}}{2}, \tag{3.8}$$

and, Eq. 3.6 becomes

$$I = \frac{I_{max}}{2}(1 - \cos\delta). \tag{3.9}$$

Therefore,

$$\delta = \cos^{-1}\left(1 - \frac{2I}{I_{max}}\right). \tag{3.10}$$

The retardance of an LCVR as function of the detected intensity is given by Eq. 3.10.

3.2.2 Experimental results

Figure 3.2.2 shows the light intensity variation with the voltage applied to the LCVR, for a wavelength of 633 nm. The error associated to each measurement in Fig. 3.2.2 is about ±0.01 and represents the standard deviation of a set of 500 intensity measurements performed for each applied voltage value. The measurement time was 0.004 seconds. Applying Eq. 3.10 to the measured values of light intensity shown in Fig. 3.2.2, we get the retardance as a function of the voltage applied to a liquid crystal retarder as seen in Fig. 3.2.3. This figure shows the curve of the retardance variations (in degrees) with the applied voltage, but its phase is "wrapped" into a range from 0° to 180°. The origin of this range is due to the application of Eq. 3.10, where the phase is limited to values between 0 and π. Because actual retardance values cannot be extracted directly from the physical signal, it is necessary to perform a phase unwrapping. The procedure is given below.

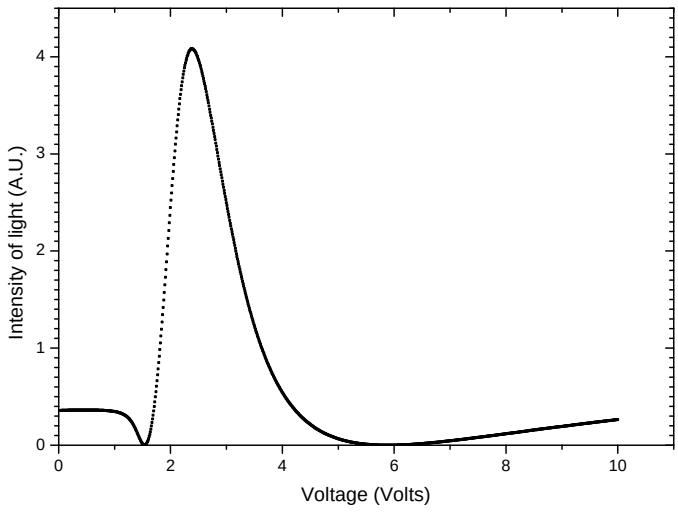

Figure 3.2.2: Intensity of light as a function of the voltage applied to a liquid crystal retarder. Measurements were made in steps of 0.01V, from 0 to 10V. The resultant error bar for each measurement is smaller than its distinctive symbol (±0.01).

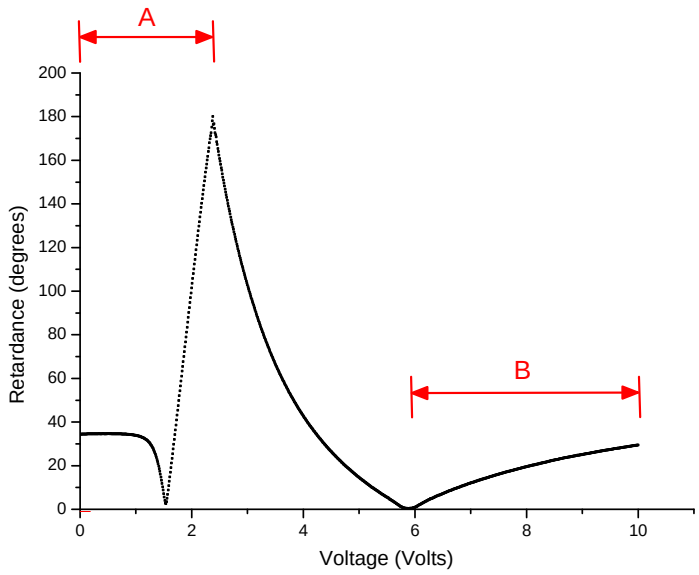

Figure 3.2.3: Optical retardance as a function of the voltage applied to a liquid crystal retarder for a wavelength of 633 nm. The sections labeled A and B need to be corrected using the phase unwrapping procedure discussed in Sec 3.2.3.

3.2.3 Phase unwrapping procedure

The experimental procedure described above generates data in the range between 0° and 180°. Because of the trigonometric functions that are used in the analysis procedure, an analysis known as "phase unwrapping" must be performed on the experimental data to indirectly obtain the original, continuous function of the applied-voltage-to-retardance relationship by removing discontinuities known as "phase jumps" (see Figs. 3.2.3 and 3.2.4). This problem can be solved for low-noise data by integrating the wrapped phase over the full domain of voltage values [40, 41]. The final result is a continuous curve that shows the full range of variation of the optical retardance with applied voltage, which usually spans more than a wavelength (0°-360°). The problem described here corresponds to the simplest case of one-dimensional phase unwrapping.

To perform the phase unwrapping of our experimental results, the following steps are used. First, it is necessary that the final shape of the experimental curve be smooth, with no discontinuities or sudden changes in the slope. Second, sections of the curve that need to be corrected (for phase jumps) must be identified. For example, Fig. 3.2.3 shows two sections (A and B) on the curve of the experimental results that need to be corrected. Third, one must identify sections of the curve where the phase can be smoothed by multiplying the values of the phase by -1 (e.g., section B in Fig. 3.2.3). Fourth, in the sections where the phase exceeds the value of 180° (e.g., section A of Fig. 3.2.3), the curve can be corrected by correcting the phase using

$$\delta' = 2\delta_{max} - \delta, \tag{3.11}$$

where δ_{max} is the largest value of the retardance on the current version of the curve. For example, in Fig. 3.2.3 the highest value is seen to be $\delta_{max} = 180^{o}$. Here, δ is the value of retardance that needs to be corrected and δ' is the corrected retardance value. The sections A and B of Fig. 3.2.3 were corrected following steps 3 and 4, respectively, and the result is shown in Fig. 3.2.4. As can be seen, there is another section that needs to be corrected (section C). Thus, it is necessary to repeat step 4 (now with δ_{max} equal to 360^{o}) to obtain the experimental curve given by Fig. 3.2.5. Each time the fourth step is repeated the value of δ_{max} is readjusted.

Hence, by solving the phase unwrapping problem, we get a continuous curve that shows the full range of variation of the optical retardance with the applied voltage, as seen in Fig. 3.2.5. In this figure, there are no significant differences between the curve obtained with our procedure and that provided by the manufacturer. The error associated to measurements presented in Fig. 3.2.5 was derived from the propagation of the error of the intensity measurements in Fig. 3.2.2 in Eq. 3.10 using the *general method for uncertainty in functions* described in Ref. [45].

The experimental procedure shown here was used to characterize the retardance function of the four LCVRs used in this Thesis for the polarimetric measurements [42, 43].

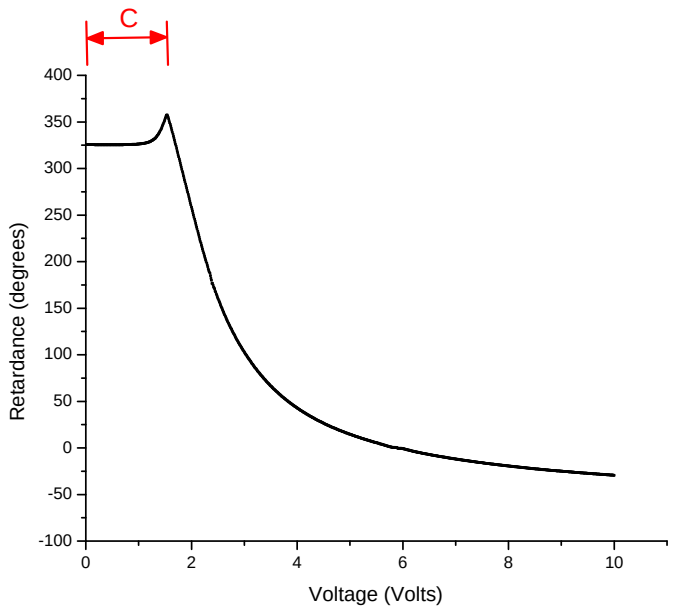

Figure 3.2.4: Curve resulting from the phase unwrapping procedure. By comparison with the Fig. 2.3.2, it can be seen that there is another section that needs to be corrected (section C).

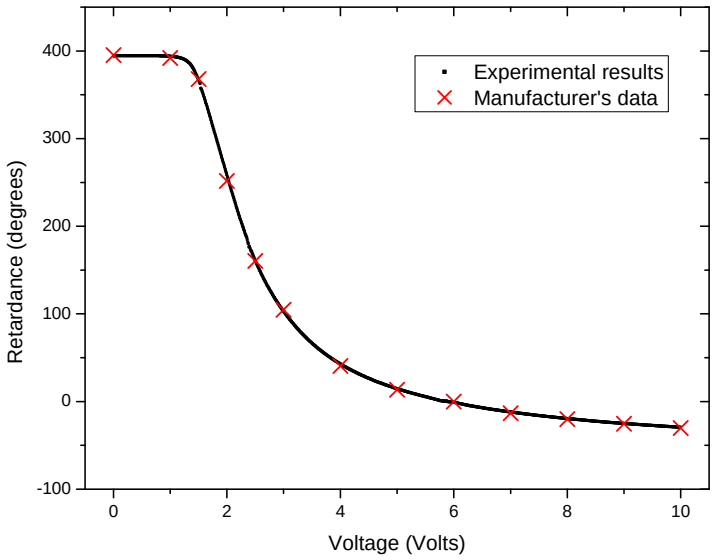

Figure 3.2.5: The experimental results match with the data provided by the manufacturer of the LCVR. The resultant error bar for each measurement has the same size as its distinctive symbol.

3.3 Location of the retardation-axes position

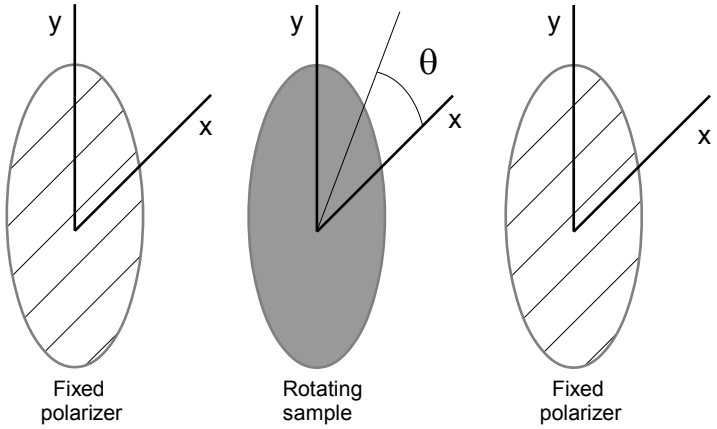

Figure 3.3.1: Diagram of the experimental set-up used to locate the optical axes position and to perform the Chenault-Chipman characterization procedure [44]. The sample (LCVR) rotates between the two fixed linear polarizers.

To study the behavior of the optical axes position with the applied voltage for the LCVRs, as a first experiment, we performed a very simple procedure: for any retarder between two fixed linear polarizers, with perpendicular transmission axes, the minimum intensity transmitted by the system is obtained when one of the axes of the retarder is parallel to the transmission axis of the polarizer located between the light source and the LCVR. Therefore, for each

applied voltage, the LCVR is rotated to obtain the minimum intensity, thus giving the direction of one of the axes of the retarder. In theory, the optical axes of the retarder are perpendicular to each other. Figure 3.3.1 shows the diagram of the experimental set-up configuration.

3.3.1 Experimental results

Figure 3.3.2 shows the typical results for an LCVR using the procedure described above. For each applied voltage value, measurements were repeated five times. It can be seen that there is a wide range of variation of the axes position from 0V to 10V. For voltages giving values of retardance close to 0λ and 1λ (5.89V and 1.53V, respectively) the minimum intensity is not found, or it cannot be clearly distinguished. Hence, the measurements corresponding to 1.5V, 5.5V, and 5.75V were not considered in Fig. 3.3.2. However, the results presented here show a similar behavior to those presented by Terrier *et al.* [7].

Figure 3.3.3 shows the repeatability of measurements when, first, an ascending and, then, a descending sequence of voltage values is used in a range of variation from 2V to 5V (corresponding to a variation of retardance from 0.72λ to 0.04λ). It can be seen that, for these two cases, the results match each other within the accuracy of our measurements. The resulting change of the axes position is 9.83° ±0.01° using an ascending voltage signal, and 9.25° ±0.01° using a descending voltage signal.

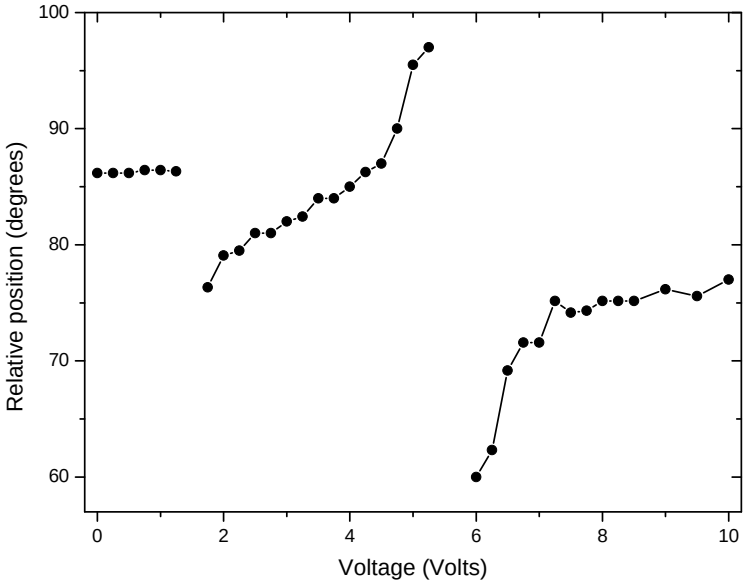

Figure 3.3.2: Optical axes location for an LCVR using this analysis procedure. The resultant error bar for each measurement is smaller than its distinctive symbol. The error associated to each measurement represents the accuracy of the measuring scale (±0.01°).

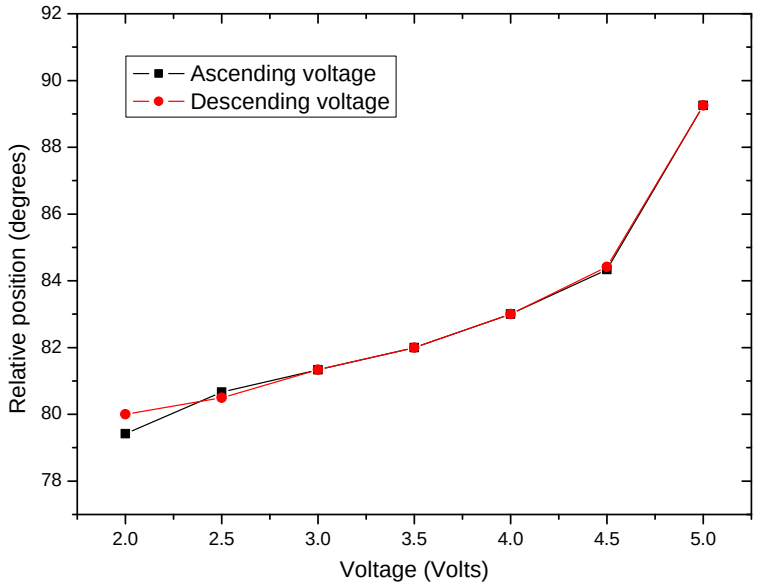

Figure 3.3.3: Relative position of the optical axes when ascending and descending sequences of voltage values are used to drive the LCVR.

3.4 Measuring diattenuation, retardance and location of the retardation-axes position: the Chenault–Chipman procedure

To measure the linear diattenuation and the retardation-axes position, as a function of the applied voltage, an experimental method developed by Chenault and Chipman [44] was used. This method consists of analyzing the light intensity modulation that results from the rotation of the LCVR between two fixed linear polarizers with transmission axes parallel to each other. The experimental set-up configuration is shown in Fig. 3.3.1.

This procedure was performed to study the relationship of the above cited parameters with the voltage applied to the LCVRs, and to know how it could affect the results obtained with the polarimetric measurement methods presented in this Thesis.

3.4.1 Theoretical analysis of the experimental set-up

As for the case shown in Sec. 3.2, the optical system affects the Stokes vector of the incident light following Eq. 3.1. However, in the Chenault–Chipman procedure the Mueller matrix for the system is written in the following way [44]:

$$
\begin{aligned}
M_{sys} &= M_{p2}\left(D_2\right) R(-\theta) M_R\left(\delta, D\right) R(\theta) M_{p1}\left(D_1\right) \\
&= A_2 \begin{pmatrix} 1 & D_2 & 0 & 0 \\ D_2 & 1 & 0 & 0 \\ 0 & 0 & \sqrt{1-D_2^2} & 0 \\ 0 & 0 & 0 & \sqrt{1-D_2^2} \end{pmatrix} \begin{pmatrix} 1 & 0 & 0 & 0 \\ 0 & \cos 2\theta & -\sin 2\theta & 0 \\ 0 & \sin 2\theta & \cos 2\theta & 0 \\ 0 & 0 & 0 & 1 \end{pmatrix} \\
&\quad \times A_s \begin{pmatrix} 1 & D & 0 & 0 \\ D & 1 & 0 & 0 \\ 0 & 0 & \sqrt{1-D^2}\cos 2\delta & \sqrt{1-D^2}\sin 2\delta \\ 0 & 0 & -\sqrt{1-D^2}\sin 2\delta & \sqrt{1-D^2}\cos 2\delta \end{pmatrix} \\
&\times \begin{pmatrix} 1 & 0 & 0 & 0 \\ 0 & \cos 2\theta & \sin 2\theta & 0 \\ 0 & -\sin 2\theta & \cos 2\theta & 0 \\ 0 & 0 & 0 & 1 \end{pmatrix} A_1 \begin{pmatrix} 1 & D_1 & 0 & 0 \\ D_1 & 1 & 0 & 0 \\ 0 & 0 & \sqrt{1-D_1^2} & 0 \\ 0 & 0 & 0 & \sqrt{1-D_1^2} \end{pmatrix},
\end{aligned} \tag{3.12}
$$

where $R(\theta)$ is the matrix for a rotational change of basis in the Mueller calculus [10], $M_{pi}\left(D_i\right)$ represents the ith horizontal linear polarizer with diattenuation D_i and average transmission A_i, and the term $M_R\left(\delta, D\right)$ represents the Mueller matrix of a retarder (LCVR) with retardance δ, diattenuation D, and average transmission A_s. The transmitted intensity is given by the first element of the transmitted Stokes vector (S^{out}), this is

$$
\begin{aligned}
I(\theta) = \kappa \big[& 1 + {}^1\!/_2 D_1 D_2 \left(1 + \sqrt{1-D^2}\cos\delta\right) \\
& + D\left(D_1 + D_2\right)\cos 2\theta \\
& + {}^1\!/_2 D_1 D_2 \left(1 - \sqrt{1-D^2}\cos\delta\right)\cos 4\theta \big] \\
= {} & a_0 + a_2 \cos 2\theta + a_4 \cos 4\theta,
\end{aligned} \tag{3.13}
$$

where κ is a normalization factor including the radiance of the source and the responsivity of the detector. Equation 3.13 is a Fourier series in θ with coefficients a_0, a_2, and a_4. These coefficients are as follow:

$$
a_0 = \kappa \left[1 + {}^1\!/_2 D_1 D_2 \left(1 + \sqrt{1-D^2}\cos\delta\right)\right], \tag{3.14}
$$

$$
a_2 = \kappa \left[D\left(D_1 + D_2\right)\right], \tag{3.15}
$$

$$
a_4 = \kappa \left[{}^1\!/_2 D_1 D_2 \left(1 - \sqrt{1-D^2}\cos\delta\right)\right]. \tag{3.16}
$$

The diattenuation D and retardance δ of the sample expressed in terms of the Fourier coefficients are [44]:

$$
D = \frac{a_2}{a_0 + a_4}\left(\frac{1 + D_1 D_2}{D_1 + D_2}\right), \tag{3.17}
$$

and

$$\delta = \cos^{-1}\left\{ \frac{a_0 - a_4\left(1 + \frac{2}{D_1 D_2}\right)}{\left[(a_0 + a_4)^2 - a_2\left(\frac{1+D_1D_2}{D_1+D_2}\right)^2\right]^{1/2}} \right\}. \tag{3.18}$$

The quantities a_0, a_2 and a_4; are determined experimentally by rotating the sample in increments of $\Delta\theta$ to produce a set of N angles $\theta_n = n\Delta\theta$, where n = 0, 1, 2,..., N - 1. The number of measurements is N and the increment $\Delta\theta$ is best chosen to satisfy $n\Delta\theta = 360^o$, where N > 8. N must be greater than 8 in order to determine the odd and even components of the four harmonics in the Fourier transform that are necessary for data reduction [44]. An intensity measurement is made at each θ_n. The phase of the fourth harmonic in Eq. 3.13 gives the orientation of the phase delay δ with respect to the x axis within an integer multiple of $\lambda/2$. The fast and slow axes of a device are not determined by this technique. Only the Fourier coefficients a_0, a_2, and a_4 are used to determine the diattenuation and retardance values. Other Fourier coefficients such as a_1, a_3, a_5, ...; must be zero in the absence of noise and systematic errors. However, beam-wander that arises from the rotation of a sample with non-plane parallel surfaces can affect, in particular, the harmonic a_1. A nonzero value for a_1 suggests the presence of beam-wander [44]. Since significant beam-wander also couples into a_2 and a_4, measurements on samples with non-plane-parallel surfaces have reduced accuracy. In the experimental results presented here, values of $a_1 > 0$ were found and, as can be seen in Table 3.4.1, the fitting of the detected signal to Eq. 3.13 without including a_1 is very poor at 1.5V, 5V and 5.5V. Hence, coefficient a_1 was taken into account in order to achieve a better fitting and, thus, to obtain coefficients a_0, a_2 and a_4 with a better accuracy. This is, the experimental intensity values were fitted to:

$$I(\theta) = a_0 + a_1 \cos\theta + a_2 \cos 2\theta + a_4 \cos 4\theta. \tag{3.19}$$

Using this fitting method, low noise measurements are obtained and experimental results are more stable than those from an FFT analysis as shown in the following section.

3.4.2 Experimental results

The LCVRs [24] used to perform this experiment are the same as those used in the previous cases and also to perform the polarimetric measurements presented in Chapters 4 and 5. The linear polarizers used to perform all the experiments for this Thesis were manufactured by Thorlabs [39], model: LPVISB050 (the data sheet of these devices is presented in Appendix B). The extinction ratio of these polarizers is $\varepsilon >$ 10,000:1. Hence, by using Eq. 2.6, from Chapter 2, the diattenuation for these polarizers is $D_{1,2} > 0.9998$. In order to simplify the calculations, the diattenuation value for the linear polarizers was approximated as $D_{1,2} = 1$.

Figure 3.4.1 shows the typical variation of the light intensity with the angle of rotation of the optical axes at different voltages applied to the LCVRs. In this case, the increments

of $\Delta\theta$ are 10. A set of 500 intensity measurements for each angular position was performed. The measurement time was 0.004 seconds. As can be seen, the intensity variation changes with the applied voltage. The highest variation is seen close to the retardance value of $\lambda/2$ (2.38V). In theory, for retardance values of 0λ (5.89V) and 1λ (1.53V) the detected intensity should be constant. However, a small intensity variation could be detected due to the beam-wander described above. Furthermore, light intensity in these cases could not have a perfectly harmonic variation due to the light source instability.

Diattenuation, retardance and the orientation of the sample's fast axis were obtained by making the intensity measurements as described above but at the applied voltage values shown in Table 3.4.1. Voltage was applied in steps of 0.5V, from 1.5V (1.01λ) to 5.5V (0.01λ), to cover one wavelength of retardance, which is the useful range of retardance in the devices employed to perform this experiment [24]. The data was reduced one voltage-value at a time. Examples of typical results for diattenuation, retardance and orientation of the fast axis as a function of the applied voltage are shown in Figs. 3.4.2, 3.4.3 and 3.4.4; respectively.

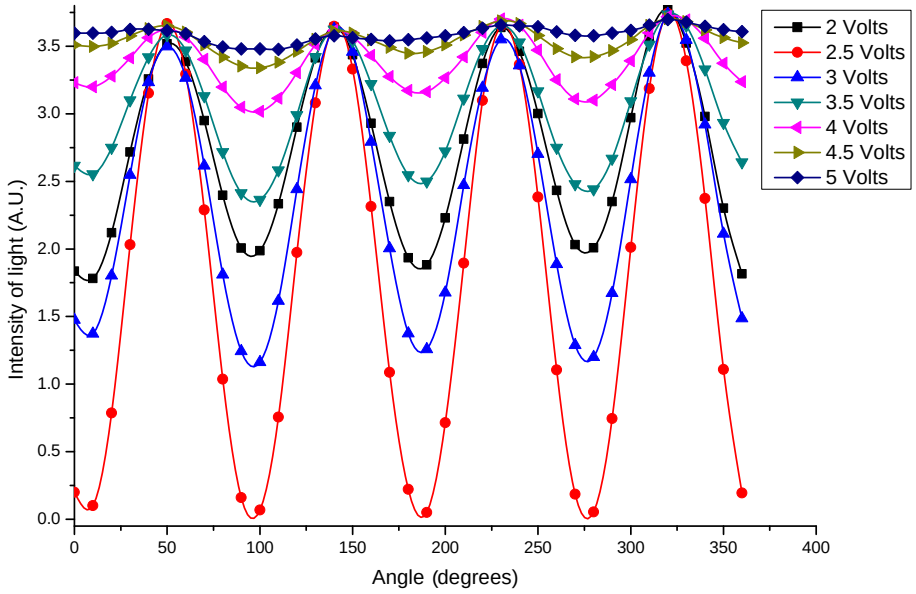

Figure 3.4.1: Typical variation of the light intensity with the angle of rotation (θ) of the optical axes at different voltages applied to the LCVRs.

Fit adjusted R^2	1.5V	2V	2.5V	3V	3.5V	4V	4.5V	5V	5.5V
Eq. 3.13	0.159	0.994	0.999	0.996	0.99	0.954	0.849	0.291	0.021
Eq. 3.19	0.88	0.997	0.999	0.999	0.998	0.994	0.992	0.97	0.937

Table 3.4.1: Fit adjusted R^2 values of the detected signal to Eq. 3.13 and Eq. 3.19.

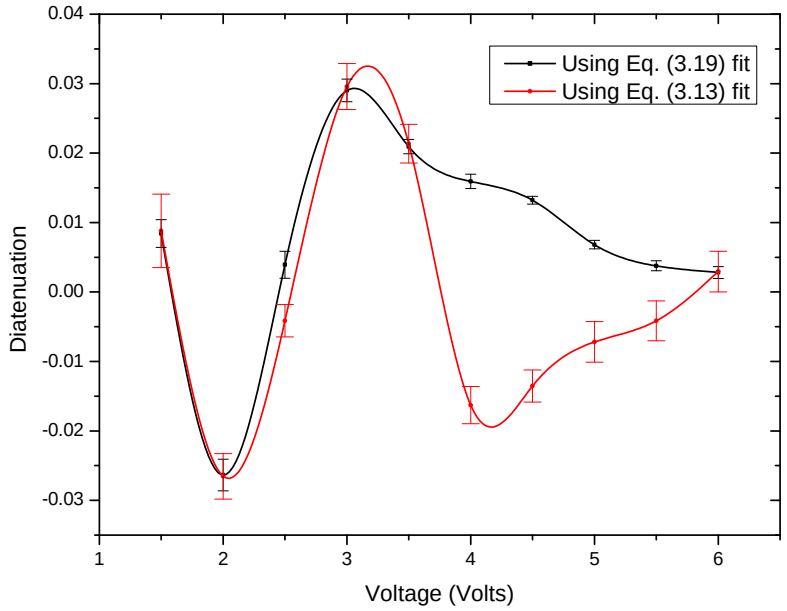

Figure 3.4.2: Diattenuation as a function of the applied voltage to an LCVR.

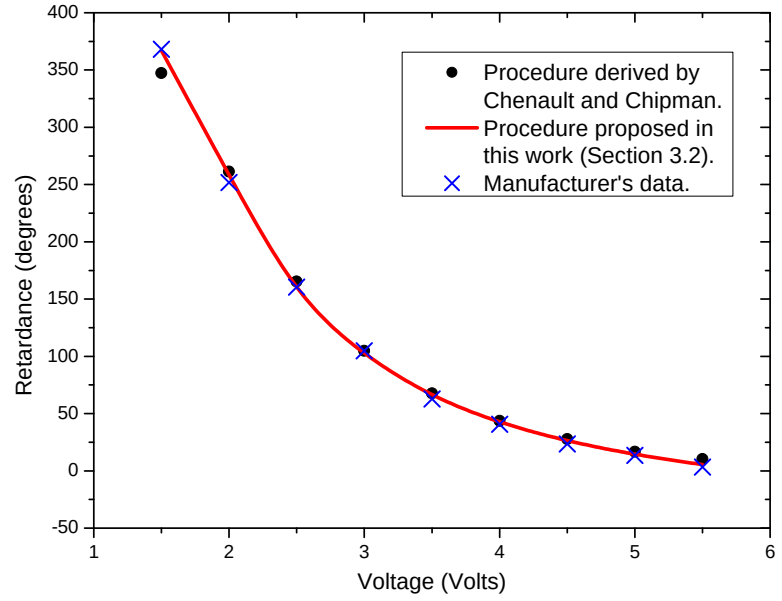

Figure 3.4.3: Comparison of experimental results for the retardance variation with the voltage as obtained with two methods and the manufacture's data. The resultant error bar for each measurement is smaller than its distinctive symbol.

As can be seen in Fig. 3.4.2, the LCVR's diattenuation changes with the voltage. In this experiment, the maximum value achieved for the diattenuation was around ± 0.027. Since this value induces only a small change in the polarization of light (see section 2.2), a negli-

gible effect on the experimental results from applications such as, for instance, polarimetric measurements is expected. Therefore, it is not necessary to take into account this parameter in the polarimetric measurement methods presented in this Thesis.

Figure 3.4.3 shows the experimental results for the retardance variation with the voltage as obtained with two methods: the procedure derived by Chenault and Chipman, presented in this section, and the procedure proposed in Sec. 3.2; compared with the data provided by the LCVR's manufacturer. As can be seen, the results of both methods match each other, except for the values close to 0º (*i.e.,* 0λ) and 360º (*i.e.,* 1λ) of retardance. In these two cases, the intensity measurements using the procedure described by Chenault and Chipman show a low contrast of the harmonic variation of light intensity. Thus, the fitting of Eq. 3.19 to the measurements is poor (see Table 3.4.1) and the experimental error increases. Therefore, the procedure described in Sec. 3.2 is more suitable for measuring the retardance of a variable retarder because it gives more stable and accurate results, particularly for retardance values near 0λ and 1λ. Furthermore, that method is simpler and easier to use.

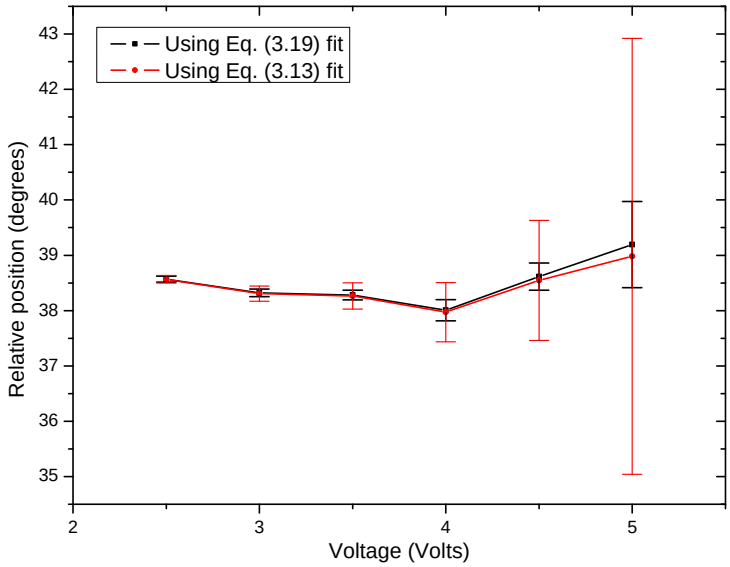

Figure 3.4.4: Retardation-axes position as a function of the applied voltage.

Finally, Fig. 3.4.4 shows the fast-axis orientation of the LCVR as a function of the voltage. In contrast to the experimental results shown in Sec. 3.3, the position of the axes has a variation of about 1º for a retardance range of almost half wavelength, from 0.45λ (2.5V) to 0.04λ (5V). The axes position for 1.5V (1.01λ), 2V (0.72λ), and 5.5V (0.01λ), goes off the scale of the figure because of the experimental error. Hence, these three measurements were discarded from the analysis. However, the experimental results obtained using the Chenault–Chipman procedure may be more accurate than those shown in Sec. 3.3 because this measurement method includes in its theoretical development all the optical properties

involved in the retarder operation and, thus, the effect of the retardation axes position can be analytically extracted. Furthermore, in general, there was also good agreement of results for the retardance measurement. The same experiment was performed on four retarders, from the same manufacturer [24], obtaining always the same results. The error bars in Figs. 3.4.2 and 3.4.3 were derived from the propagation of the standard error of coefficients a_0, a_2, and a_4 in Eqs. 3.17 and 3.18, using the *general method for uncertainty in functions* described in Ref. [45]. Moreover, the error bars in Fig. 3.4.4 represent the standard error of the calculation of the phase of the fourth harmonic in Eq. 3.19. The small change in the axes position measured in this work produces a negligible effect on the results of polarimetric measurements.

3.5 Measuring the depolarization of light in LCVRs

The depolarization effects of an LCVR on an incoming polarized light beam can be estimated from the calculation of the degree of polarization (p). In this case, measurements of the Stokes vector (defined in Eq. 2.1) of the light at both input and output optical aperture of the device are needed. The definition of p was presented in Sec. 2.1, Eq. 2.3.

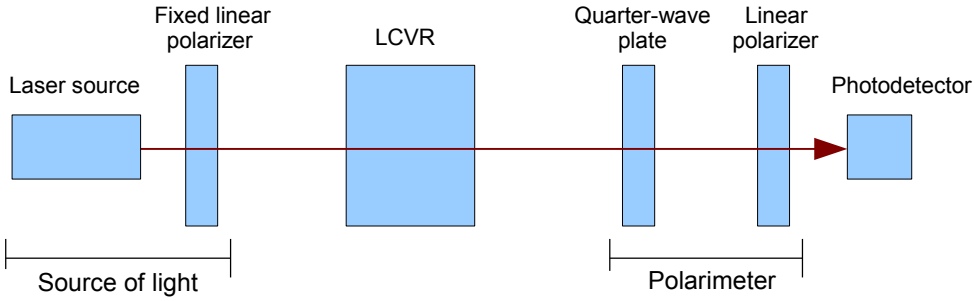

Figure 3.5.1: Block diagram for the experimental set-up used to measure the Stokes parameters to estimate the degree of polarization. The angles associated with each component refer to the relative angle of the optical axis of that component with respect to the horizontal plane.

The experimental set-up used to accomplish this task is shown in Fig. 3.5.1. The system consists of a polarized light source and a Stokes polarimeter, using a quarter-wave plate and a linear polarizer. The circular polarization values were measured with the axes of the quarter-wave plate at 45° with respect to the axis of the linear polarizer. The linear polarization values were measured with one of the axes of the retarder parallel to the axis of the polarizer, see section 2.1 for more information on the Stokes parameters measurement. The source of light includes an He-Ne laser at 633 nm and a fixed linear polarizer with its transmission axis at 45° with respect to the optical axes of the LCVR (see Appendix B for more details about these devices).

3.5.1 Experimental results using fixed voltage values

Linearly polarized light was applied to an LCVR with its fast axis at 45° with respect to the incoming polarization plane. This is the typical way to employ variable retarders to produce polarization changes in a light beam. The degree of polarization of the incident light was measured to be 0.998 ±0.001. Figure 3.5.2 shows the typical behavior of the measured Stokes parameters as a function of the voltage applied to an LCVR. Measurements of polarization states were made in steps of 0.2V, from 1V (1.09λ) to 6V (-0.003λ), to cover a range of retardance of one wavelength. A set of 500 intensity measurements for each applied voltage value was performed to measure each polarization state. The measurement time was 0.004 seconds. Therefore, the total measurement time for each polarization state was 2 seconds. The response time of the LCVR was taken into account before each measurement [24].

Figure 3.5.3 shows the degree of polarization of light as a function of the applied voltage. As can be seen, p at the output of an LCVR varies with the voltage and the lowest measured value of p is 0.973 ±0.003. This value corresponds to a degree of polarization reduction of $\sim 2.5\%$. The error associated to each measurement in Fig. 3.5.2 was derived from the propagation of the error (standard deviation) of the measurement of the polarization states to obtain the Stokes parameters. Hence, the error bars in Fig. 3.5.3 were derived from the propagation of the error of the Stokes parameters in Eq. 2.3 using the *general method for uncertainty in functions* described in Ref. [45].

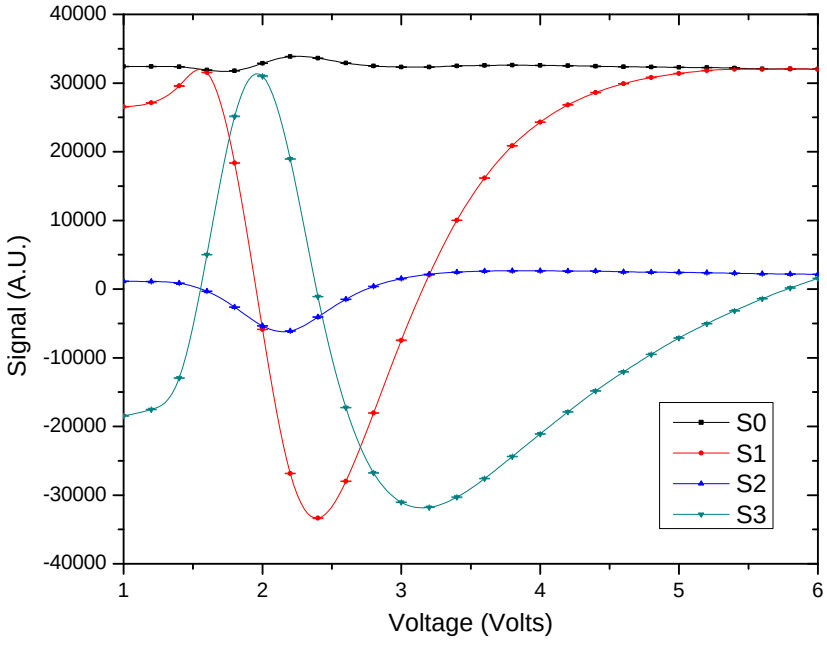

Figure 3.5.2: Typical behavior of the measured Stokes parameters as a function of the voltage applied to an LCVR using light at 633 nm. The resultant error bar for each measurement is smaller than its distinctive symbol.

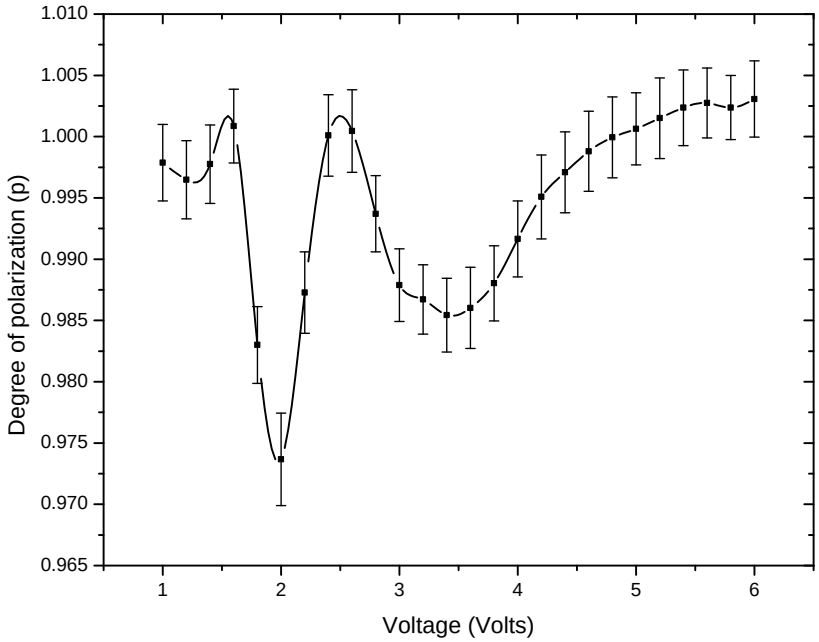

Figure 3.5.3: Degree of polarization of light (p) as a function of the voltage applied to an LCVR.

3.5.2 Experimental results using continuous voltage signals

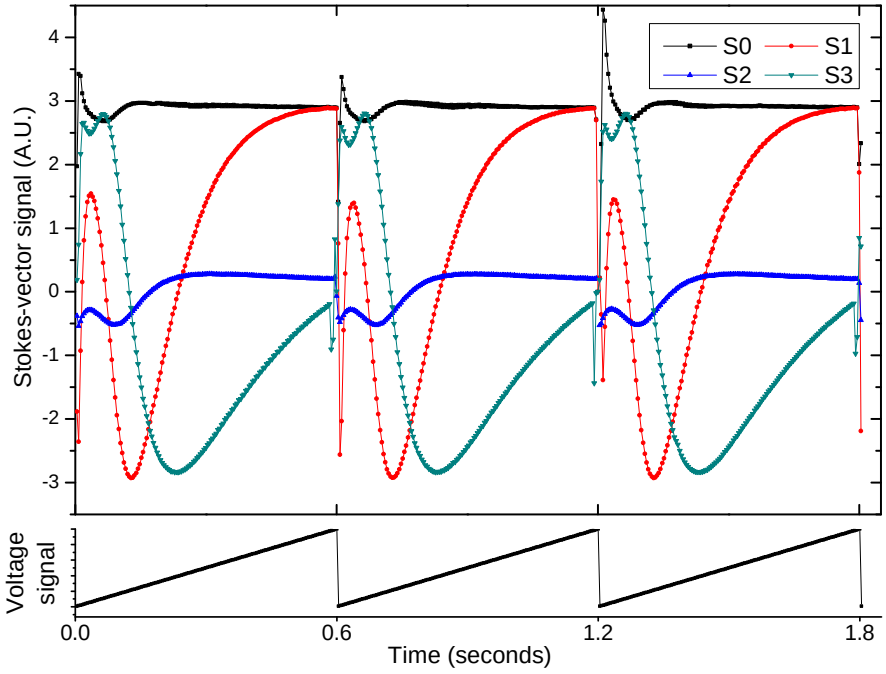

Figure 3.5.4: Stokes parameters behavior when a saw-tooth voltage signal is applied to an LCVR.

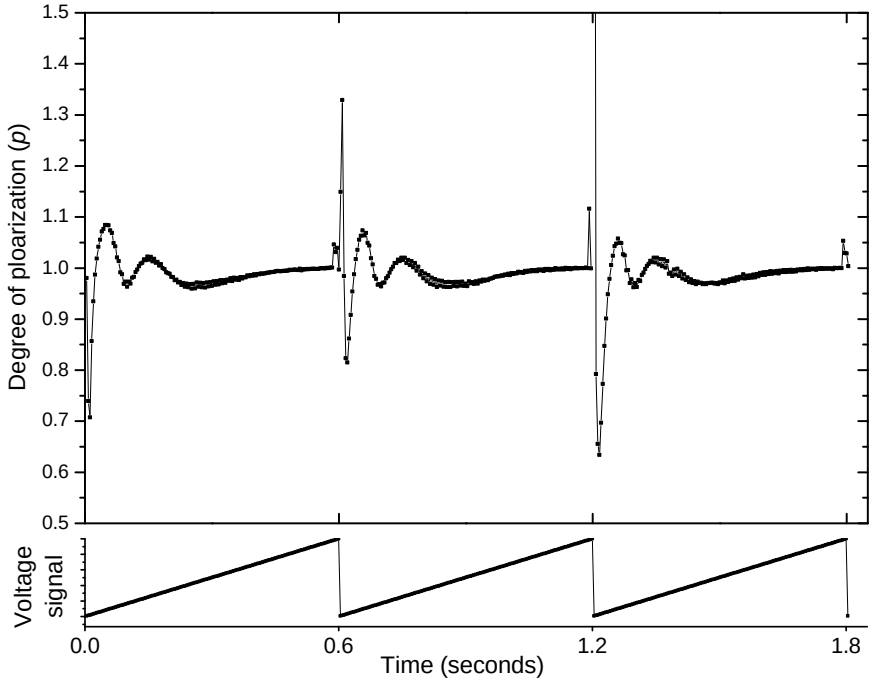

Figure 3.5.5: Degree of polarization when a saw-tooth voltage signal is applied to the LCVR.

As another example, Figs. 3.5.4 and 3.5.5 show the curves corresponding to the Stokes parameters behavior and the degree of polarization, respectively, when a continuous voltage signal that has the form of a linear ramp (sawtooth) is applied. The period of the signal is 0.6 seconds, and it covers a range from 1λ to 0λ that represents the typical values used in this Thesis to perform the polarization measurements with LCVRs. The peak-to-peak voltage values were obtained from the data shown in Fig. 3.2.5. In this case, the measurement time for each polarization state was 0.004 seconds. Values for p slightly higher than unity may be the result of inaccurate measurements of the Stokes parameters due to the short measurement time and the large gradient in the retardance values for these voltages.

It can be seen in this case that the behavior of the Stokes vector has some differences with respect to the previous case (Fig. 3.5.2) due to the sudden change in the retardance value at the end of each voltage cycle. This behavior induces atypical values for the degree of polarization of light in these points (Fig. 3.5.5). The lowest value for p is 0.63, at 1.22V. This result could be due to depolarization effects in the LCVR. However, this problem is diminished by applying a voltage signal that has a smooth form such as a sine-wave function, as shown in Figs. 3.5.6 and 3.5.7. Therefore, using a continually varying voltage could improve the LCVR function when this device is driven rapidly. The physical mechanism causing the depolarization effect shown in Fig. 3.5.5 is unknown. However this experiment could be useful to find errors sources and, hence, to improve the LCVR function when this device is driven rapidly.

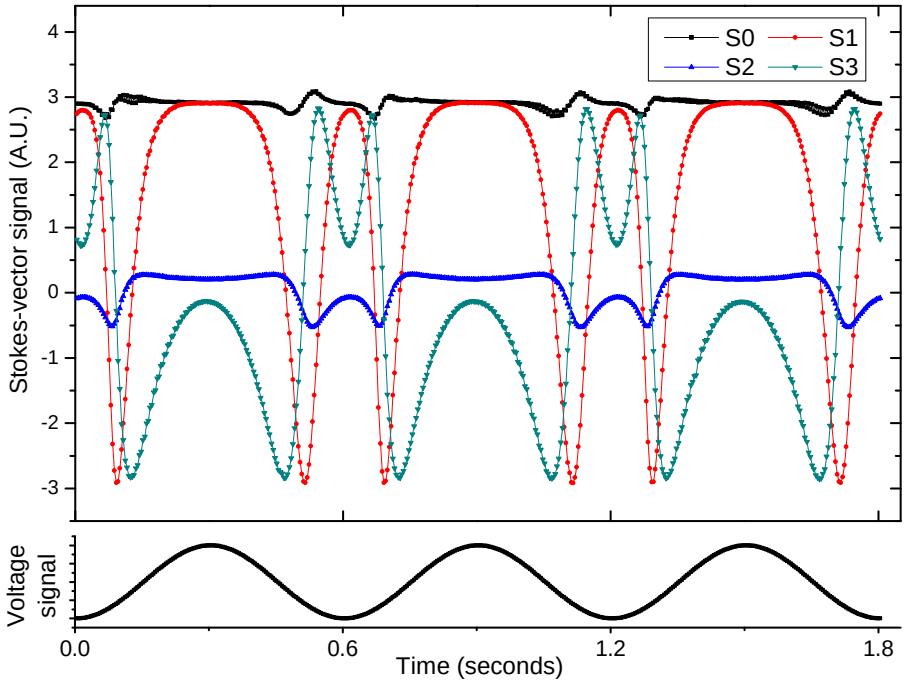

Figure 3.5.6: Stokes parameters behavior when a sine-wave voltage signal is applied to an LCVR.

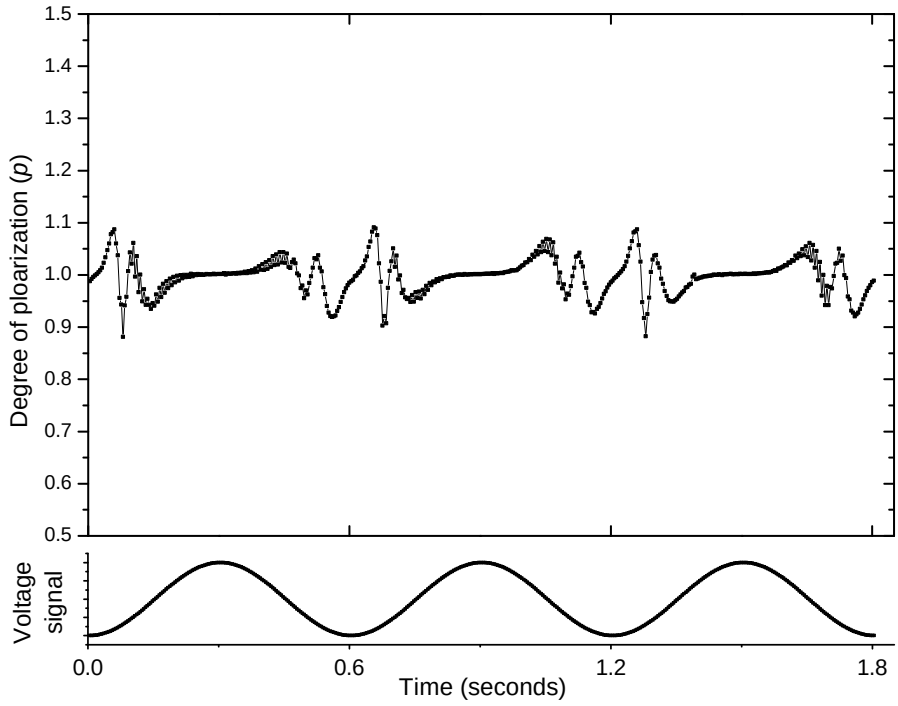

Figure 3.5.7: Degree of polarization when a sine-wave voltage signal is applied to an LCVR.

In contrast to the applied voltage signal, the resultant Stokes-vector signal in Fig. 3.5.6

does not have a perfectly symmetric behavior within each cycle because of the LCVR's response time, which depends on the retardance change sense (ascending or descending) [24].

3.6 Measuring the voltage dependence of the optical transmittance in LCVRs

The operational definition of the optical transmittance, as given by Hetch and Zajac [46], is

$$T = \frac{I_t}{I_i}, \tag{3.20}$$

where I_t is the irradiance transmitted by a sample (LCVR) and I_i is the incident irradiance on the sample. This definition is only valid for light at a normal incidence angle on the surface of a material. Hence, for a constant I_i, I_t was measured for the applied voltages values shown in Fig. 3.6.1. Measurements were performed using the entire optical window of these devices (about 1 cm diameter). In this case, the lowest measured value corresponds to a transmittance reduction of 3% and the maximum variation with the applied voltage represents a change of 1.14%. This variation should produce a negligible effect on the results of the polarimetric measurement methods proposed in Chapter 2. This procedure was repeated on four LCVRs obtaining always the same results.

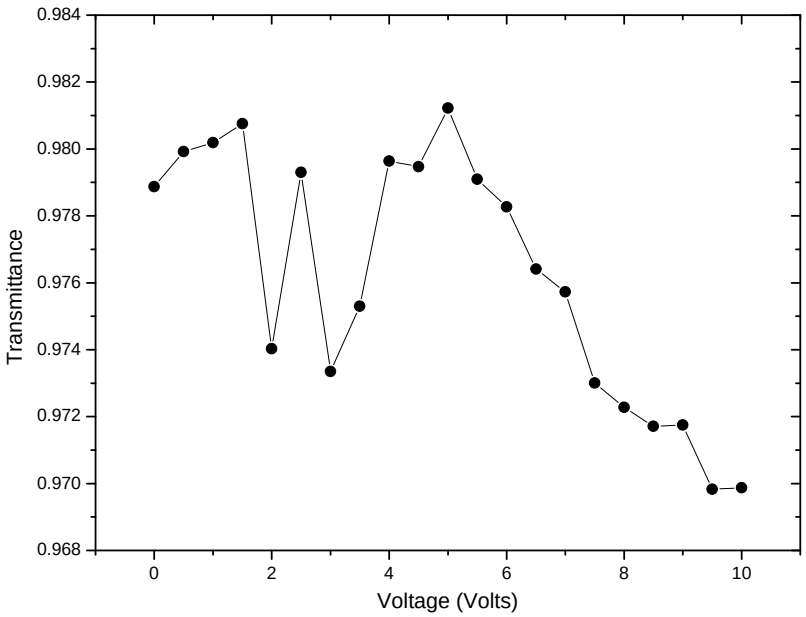

Figure 3.6.1: Voltage dependence of the optical transmittance in the LCVRs for a wavelength of 633 nm. The resultant error bar for each measurement is smaller than its distinctive symbol.

Chapter 4

Experimental results for the Stokes polarimeter

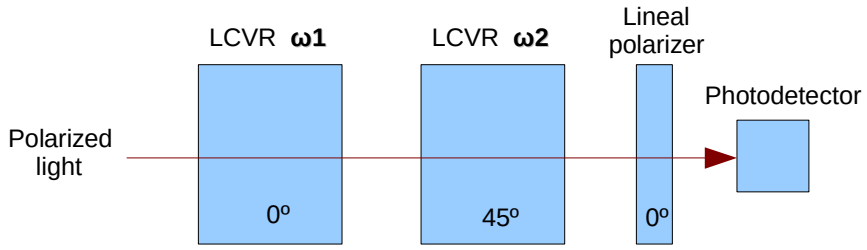

Figure 4.0.1: Block diagram of the experimental set-up used for the Stokes polarimeter. The angles associated with each component refer to the relative angle of the optical axis of that component with respect to the polarizer angle. ω1 and ω2 are the frequencies of the variations of the retardances.

In this chapter, experimental results of the Stokes-vector measurement methods shown in Chapter 2 are presented. Figure 4.0.1 shows the diagram of the experimental set-up for a Stokes polarimeter, the light to be analyzed passes through two liquid crystal variable retarders with their axes at 45º to each other and finally through a linear polarizer with its transmission axis parallel to the axis of the first retarder. Figure 4.0.2 shows a photograph of the Stokes polarimeter described here. Using the theoretical development derived in Sec. 2.3, the Stokes vector of light passing through a linear polarizer and a half-wave retarder, as the retarder is rotated, and also for a linear polarizer and a quarter-wave retarder, as the retarder is rotated, was measured. In the first case the polarization measured should shift between S1 (horizontal/ vertical linear polarization) and S2 ($+45^o/-45^o$ linear polarization), and in the second case the polarization should shift between linear and circular S3 polarization. Results of calculation, using Mathematica®, for these cases give the curves shown in Fig. 4.0.3. The experimental results for each case studied in Sec. 2.3 are shown in the next sections. The

data sheet of the wave plates used for the experiments presented in this work are presented in Appendix B.

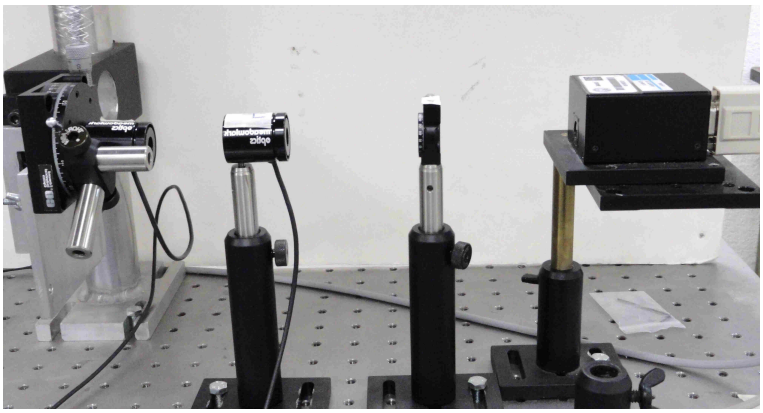

Figure 4.0.2: Stokes polarimeter.

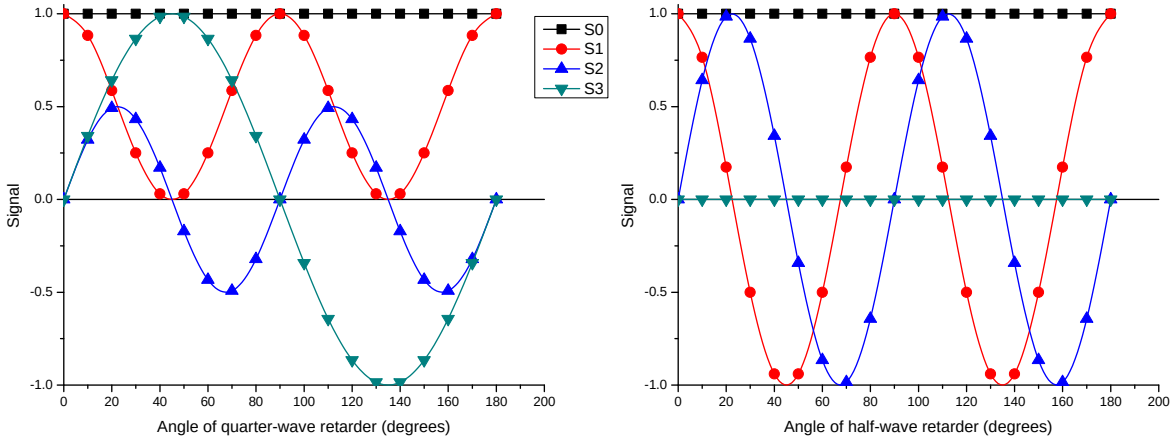

Figure 4.0.3: Simulation of the Stokes vector of light passing through a linear polarizer and a rotating quarter-wave plate (left) and also for a linear polarizer and a rotating half-wave plate (right).

For a rotating quarter-wave plate the resulting curves fit with the functions:

$$\begin{cases} S0 = A, \\ S1 = A\left(\cos^2 2\theta\right), \\ S2 = \frac{A}{2}\left(\sin 4\theta\right), \\ S3 = A\left(\sin 2\theta\right); \end{cases} \tag{4.1}$$

where A is a constant which depends on the S0 value (in Fig. 4.0.3, for instance, $A = 1$) and θ is the rotation angle of the wave-plate.

For the case of a rotating half-wave plate the resulting curves fit with the functions:

$$\begin{cases} S0 = A, \\ S1 = A\left(\cos 4\theta\right), \\ S2 = A\left(\sin 4\theta\right), \\ S3 = 0. \end{cases} \tag{4.2}$$

The above functions will be used for comparison with the experimental results presented in this Chapter, as an indication of the quality of the polarimeter.

All of the measurement methods for the Stokes vector presented here use the same experimental set-up (Fig. 4.0.1). Hence, the accuracy of the measurements is only related to the measurement method employed for each case. The measured parameter S0 is also a result relative to its measurement method. This is, the accuracy of that measurement is also affected by the experimental errors from each case. In order to compare the experimental results with the theory (Fig. 4.0.3), all of the measurements presented here are normalized with the average value of the resulting S0 curve from each case. Thus, the propagation of experimental errors in the calculus of the Stokes-vector parameters is avoided and the comparison of results with the theory for all the measured parameters, including S0, is more accurate.

4.1 Stokes polarimetry using Fourier analysis and nonlinear voltage-retardance function

For this measurement method, as was described in Sec. 2.3.2, a sinusoidal voltage signal was applied to the LCVRs to give a range of retardance from $\lambda/2$ to λ (the part of the voltage-retardance curve which is closest to linear, see Fig. 2.3.2); and the Stokes-vector elements are measured using Eq. 2.25 (see Sec. 2.3.2). Fig. 4.1.1 shows the experimental results using this method. Measurements were made in steps of 10º, from 0º to 180º, of the wave-plate angle position. The values employed for the frequencies of oscillation of the voltage applied to LCVR ω1 and LCVR ω2 were 5Hz and 2Hz, respectively. For this case, the measurement time for each Stokes vector was 2 seconds.

It can be seen that the behavior of the results is generally as expected but that there are asymmetries and discrepancies from the simulated results shown in Fig. 4.0.3. This may be caused by errors in optical alignment [47] or the effect of the non-linearity of the retardance variation. Figure 4.1.2 shows the experimental results only for the values: S0, S1(ω2), S2(2ω1), and S3(ω1); which were found to be the most stable values and those closest to the simulations. Variations between different solutions for the same Stokes term can be used as a measure of the reliability of the measurements. From this experiment, it has been found that measurements using the lowest index in the FFT analysis show a best fit with

the theory.

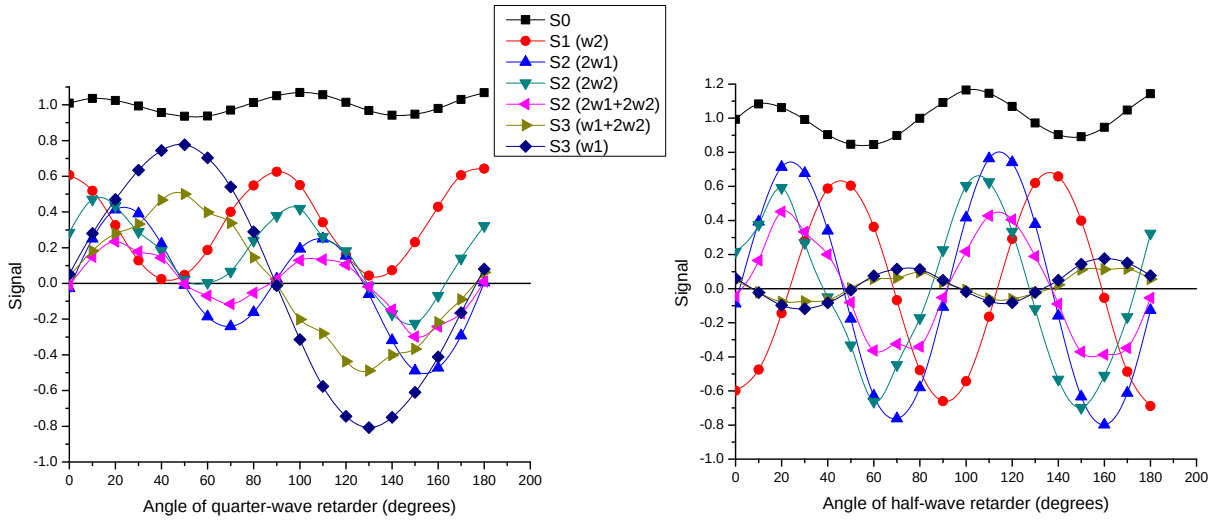

Figure 4.1.1: Experimental measurements of the Stokes vector of light using Fourier analysis and nonlinear voltage retardance function. The light is passing through a linear polarizer and a quarter-wave plate (left) and also for a linear polarizer and a half-wave plate (right). All of the measurements were normalized with the average value of the S0 curve.

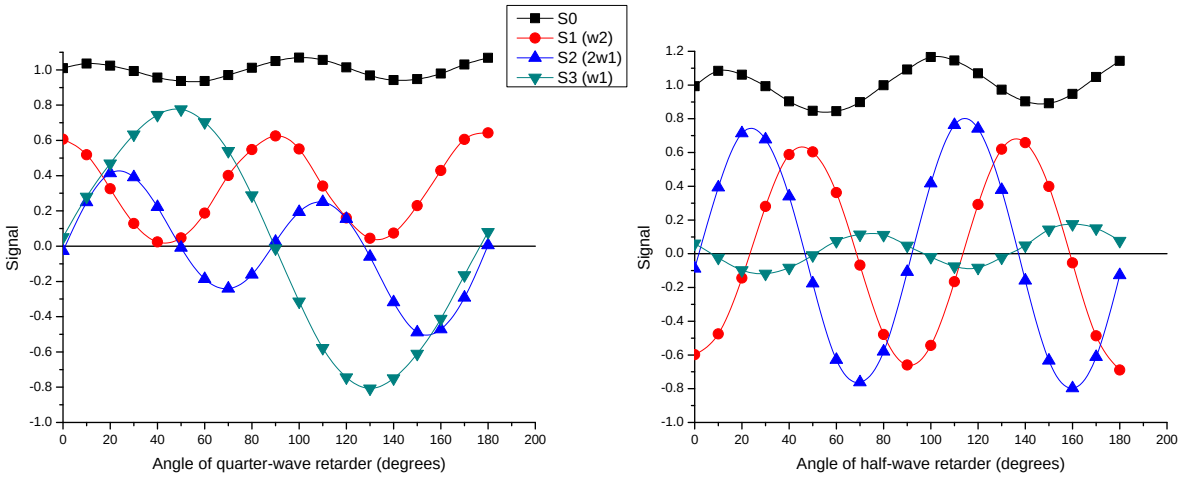

Figure 4.1.2: Experimental measurements for the values: S0, S1(ω2), S2(2ω1) and S3(ω1). In order to compare the experimental results with the theory, all of the measurements were normalized with the average value of the S0 curve.

As can be seen, there are some asymmetries in the nonlinear functions of the Stokes vector, and harmonic variations in the measurements for S0 is also evident. Using Eqs. 4.1 and 4.2, a fitting of the resulting curves shown in Fig. 4.1.2 to the theoretical curves (Fig. 4.0.3) was performed. Table 4.1.1 shows the coefficient of determination values (R^2) [48] for

the nonlinear functions and, also, the standard deviation (σ) [48] of the data for the constant functions.

Wave-plate	S0	S1	S2	S3
Quarter-wave	$\sigma = 0.045$	$R^2 = 0.162$	$R^2 = 0.683$	$R^2 = 0.913$
Half-wave	$\sigma = 0.102$	$R^2 = 0.718$	$R^2 = 0.92$	$\sigma = 0.092$

Table 4.1.1: Statistical parameters, R^2 and σ, for the fit of the resulting experimental curves to the theory.

Using these parameters, values for R^2 close to 1 and values close to zero for σ represent a good fit of the experimental results with the theory. As can be seen in the above table, in most of these cases, there is a poor fit of the measured Stokes parameters with the theoretical model.

4.2 Stokes polarimetry using Fourier analysis and linearized retardance

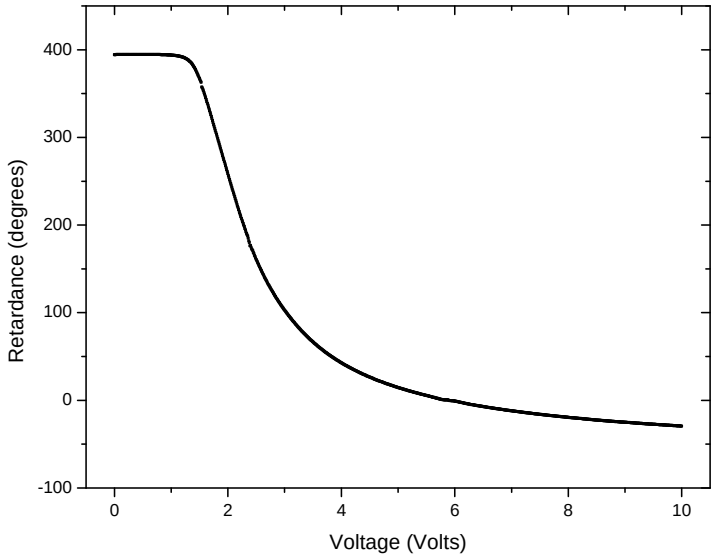

Figure 4.2.1: Voltage-retardance relation for an LCVR.

For this measurement method, the retardance variation of the LCVRs was linearized by using the results of the characterization of the voltage-retardance relationship, Fig. 4.2.1 (see Sec. 3.2). The procedure is as follows.

From the characterization previously performed on the LCVRs (see Chapter 3), the voltage-retardance relation in the range 0–10V is well known. The graph shown in Fig.

4.2.1 has a resolution of 0.01V. Hence, by using a LabVIEW® program, a linear fit between every consecutive pair of data values from the characterization was performed in order to interpolate values. Using this linear interpolation of data it is possible to find, with high precision, the appropriate voltage values to obtain any retardance variation required for the polarimetric measurements. In particular, the voltage values required to obtain a linear variation of retardance were calculated. Figure 4.2.2 shows the shape of the applied voltage with time and, also, the retardance variation obtained from the LCVRs.

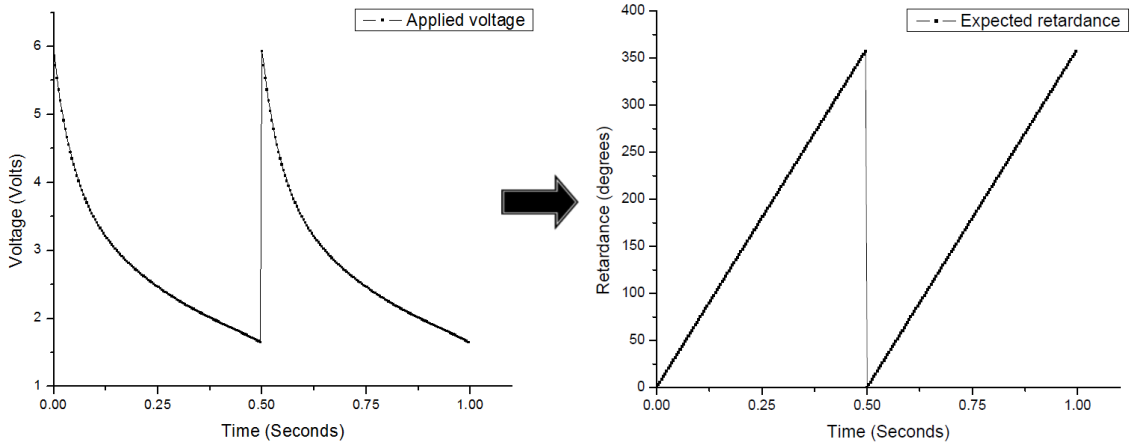

Figure 4.2.2: Shape of the applied voltage with time (left) and, also, the expected retardance variation from the LCVR (right). In this example, the applied voltage values were calculated to obtain a linear variation of retardance from 0º to 360º.

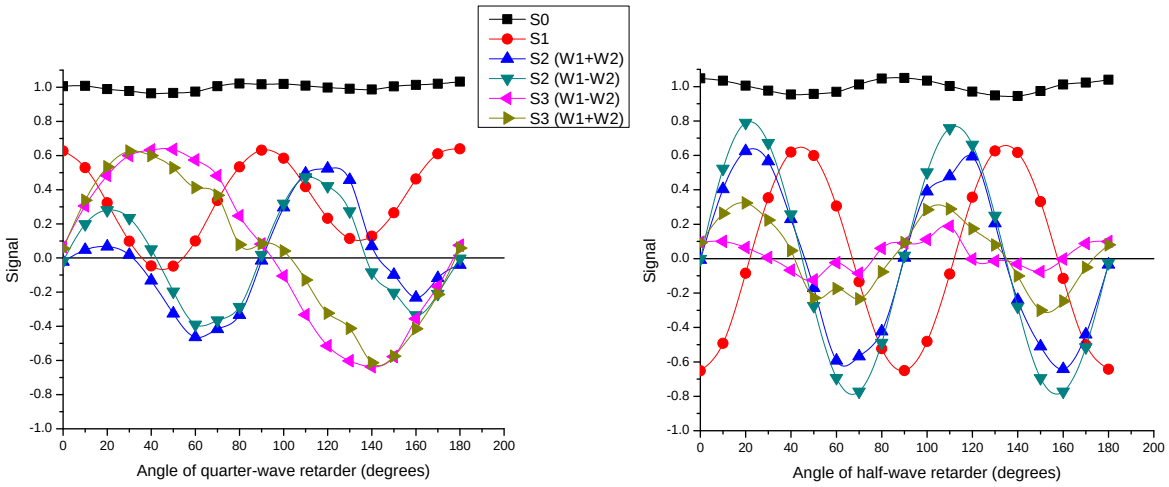

Figure 4.2.3: Experimental measurements of the Stokes vector of light using Fourier analysis and linearized retardance values. The light is passing through a linear polarizer and a quarter-wave plate (left) and also for a linear polarizer and a half-wave plate (right). All of the measurements were normalized with the average value of the S0 curve.

The Stokes-vector was measured using Eq. 2.33, derived in Sec. 2.3.3. Figure 4.2.3 shows the experimental results with this technique. Comparing these results with those given by the simulation, Fig. 4.0.3, it can be seen that the behavior of the results is, in general, as expected, although there are still some relatively small variations between different values for the same Stokes parameters, and there are still some asymmetries in the curves. In a similar way as the previous case, the values employed for the frequencies of oscillation of the voltage applied to LCVR ω1 and LCVR ω2 were 5Hz and 2Hz, respectively. The measurement time for each Stokes vector was 2 seconds.

Using this method, the statistical parameters for the fit of the resulting curves to the theoretical curves (Fig. 4.0.3) give the values shown in Table 4.2.1. As can be seen, this measurement method produced very similar results to those presented in the previous case. Possibly, the sudden change in the voltage values at the end of each variation cycle shown in Fig. 4.2.2 distorts the expected shape of retardance variation because of the response time of the LCVRs.

Wave-plate	S0	S1	S2 (ω1+ω2)	S2 (ω1-ω2)	S3 (ω1-ω2)	S3 (ω1+ω2)
Quarter-wave	$\sigma = 0.02$	$R^2 = 0.054$	$R^2 = 0.401$	$R^2 = 0.822$	$R^2 = 0.673$	$R^2 = 0.273$
Half-wave	$\sigma = 0.037$	$R^2 = 0.718$	$R^2 = 0.624$	$R^2 = 0.925$	$\sigma = 0.083$	$\sigma = 0.203$

Table 4.2.1: Statistical parameters, R^2 and σ, for the fit of the resulting experimental curves to the theory.

As was expected, the measurement of the Stokes parameters for S2 and S3 using the lowest frequencies in the FFT analysis show a best fit with the theory. Therefore, these results will be used for comparison with results from other measurement methods.

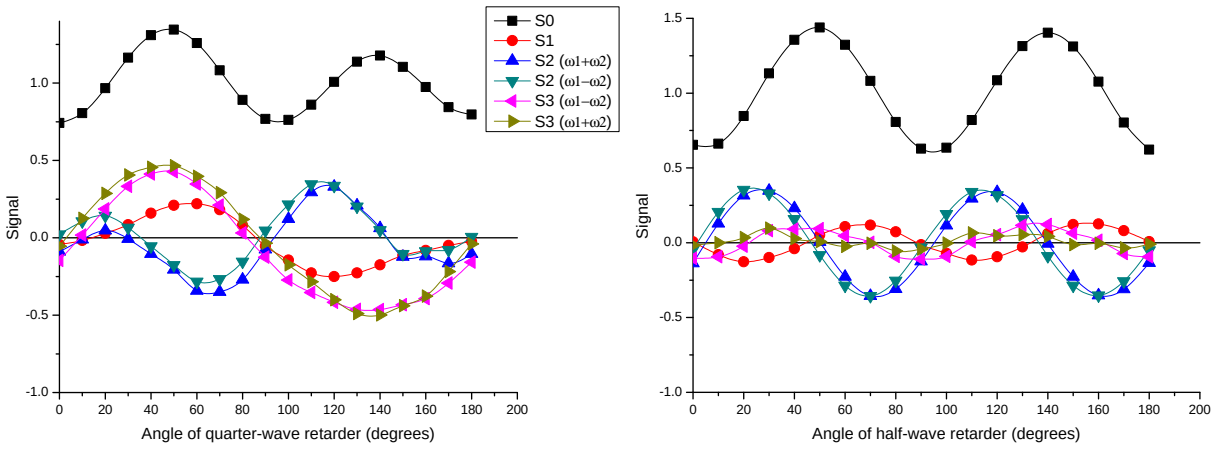

Figure 4.2.4: Experimental measurements of the Stokes vector of light using Fourier analysis and nonlinear retardance values.

In contrast, Fig. 4.2.4 shows results of applying the same method to the non-linearized retardance values with saw-tooth voltage oscillations. In this second case the results are very poor because of the nonlinear behavior of the retardance. The results in Fig. 4.2.3 show the improvement due to the use of a linear retardance variation.

4.3 Stokes polarimetry using a fitting procedure

This method uses Eqs. 2.36 and 2.37, derived in Sec. 2.3.4, to measure the Stokes parameters. In this case, a voltage signal which has the form of a linear ramp (sawtooth) was applied. From the characterization previously performed on the LCVRs, it is straightforward to know the retardance value for each value of voltage applied to the retarders. A linear interpolation of the values shown in Fig. 4.2.1 was used in order to obtain the values of the retardance for every value of voltage applied.

The experimental results are shown in Fig. 4.3.1. It can be seen that the behavior of the results is, in general, as expected, although there are some small asymmetries in the curves, and noise. The values employed for the frequencies of oscillation of the voltage applied to LCVR ω1 and LCVR ω2 were 3.33Hz and 1.11Hz, respectively. For this case, the measurement time for each Stokes vector was 1.8 seconds.

The statistical parameters for the fit of the resulting curves to the theoretical curves (Fig. 4.0.3) give the values shown in Table 4.3.1.

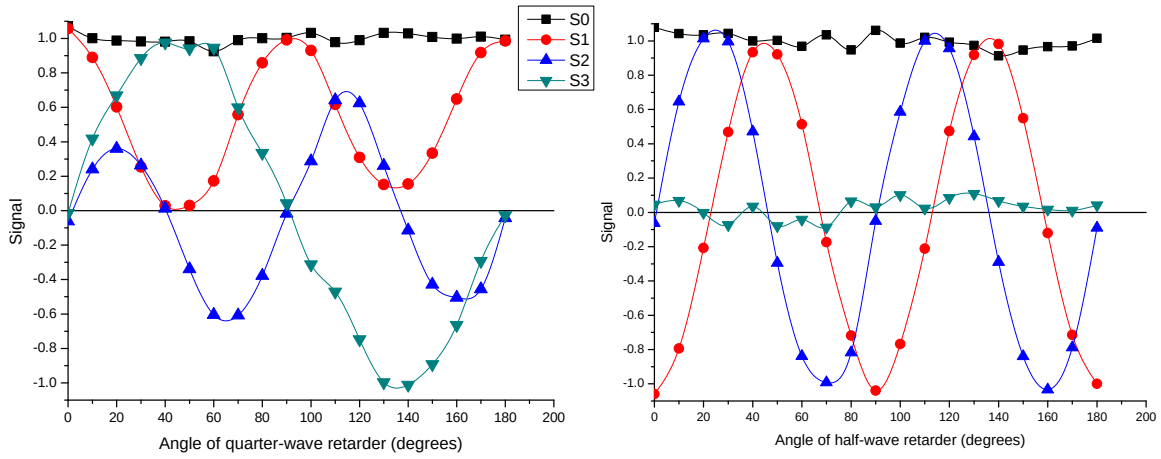

Figure 4.3.1: Experimental measurements of the Stokes vector of light using a fitting procedure. The light is passing through a linear polarizer and a quarter-wave plate (left) and also for a linear polarizer and a half-wave plate (right). All of the measurements were normalized with the average value of the S0 curve.

Wave-plate	S0	S1	S2	S3
Quarter-wave	$\sigma = 0.023$	$R^2 = 0.975$	$R^2 = 0.913$	$R^2 = 0.993$
Half-wave	$\sigma = 0.039$	$R^2 = 0.999$	$R^2 = 0.995$	$\sigma = 0.058$

Table 4.3.1: Statistical parameters, R^2 and σ, for the fit of the resulting experimental curves to the theory.

As can be seen in the above table, using this measurement method, there is a good fit of the measured Stokes parameters with the theoretical models shown in Fig. 4.0.3.

4.4 Comparison of experimental results

A comparison of the resulting statistical parameters from the three methods presented is shown in tables 4.4.1 and 4.4.2.

Measurement method	S0	S1	S2	S3
Fourier analysis	$\sigma = 0.045$	$R^2 = 0.162$	$R^2 = 0.683$	$R^2 = 0.913$
Fourier analysis and linearized retardance	$\sigma = 0.02$	$R^2 = 0.054$	$R^2 = 0.822$	$R^2 = 0.673$
Fitting method	$\sigma = 0.023$	$R^2 = 0.975$	$R^2 = 0.913$	$R^2 = 0.993$

Table 4.4.1: Comparison of the statistical parameter values, R^2 and σ, for the experimental results using a quarter-wave retarder.

Measurement method	S0	S1	S2	S3
Fourier analysis	$\sigma = 0.102$	$R^2 = 0.718$	$R^2 = 0.92$	$\sigma = 0.092$
Fourier analysis and linearized retardance	$\sigma = 0.037$	$R^2 = 0.718$	$R^2 = 0.925$	$\sigma = 0.083$
Fitting method	$\sigma = 0.039$	$R^2 = 0.999$	$R^2 = 0.995$	$\sigma = 0.058$

Table 4.4.2: Comparison of the statistical parameter values, R^2 and σ, for the experimental results using a half-wave retarder.

As can be seen, the measurement method using a fitting procedure shows the best correlation of the experimental results with the theory. Therefore, this method is more suitable for measuring the Stokes vector using continually varying voltage signals. Furthermore, this may be the best option to develop a method to measure the Mueller matrix of a general sample. Moreover, this method is the easiest to perform, of the three cases presented in this Thesis.

The results obtained with the fitting method show that there are no important effects of depolarization of the light on the measurements. The errors and discrepancies of values in the S0 curves in the other methods must be due to errors in each measurement method.

The measurement methods presented in this Chapter has been reported in an indexed journal: Reference [49].

Chapter 5

Experimental results for the Mueller polarimeter

The experimental results of the Mueller-matrix measurement methods shown in Chapter 2 are presented in this Chapter. Figure 5.0.1 shows the setup for the Mueller polarimeter using LCVRs. As can be seen, this device consists of two modules: a polarization state generator (PSG) and a polarization state analyzer (PSA). The sample under test is analyzed between those two modules. The PSG determines the polarization state of the incident light, whereas the PSA measures the change in this state after interaction with the sample. A photodetector measures the intensity of the light transmitted by the optical system. Figure 5.0.2 shows a photograph of the experimental set-up.

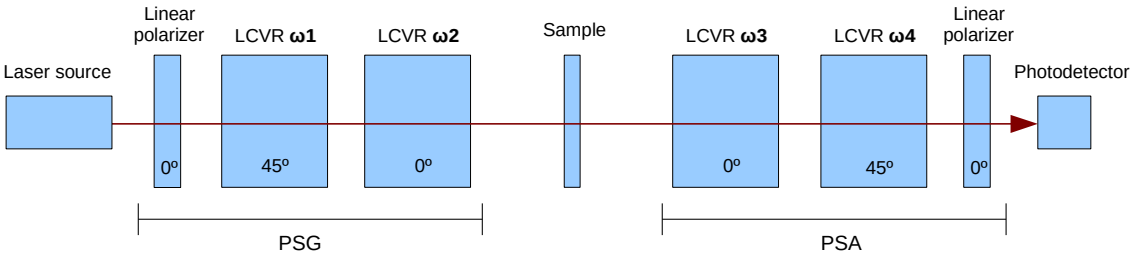

Figure 5.0.1: Block diagram of the experimental set-up used for the Mueller polarimeter. The angles associated with each component refer to the relative angle of the optical axis of that component with respect to the polarizer angle. The retarders are labelled as: $\omega 1$, $\omega 2$, $\omega 3$, and $\omega 4$; because of the frequencies of the variations of the retardances.

To perform this experiment, an He–Ne laser at 633 nm was used as a light source (see Appendix B). As in the previous experiments shown in this Thesis, the entire optical window of the LCVRs was used for the measurements.

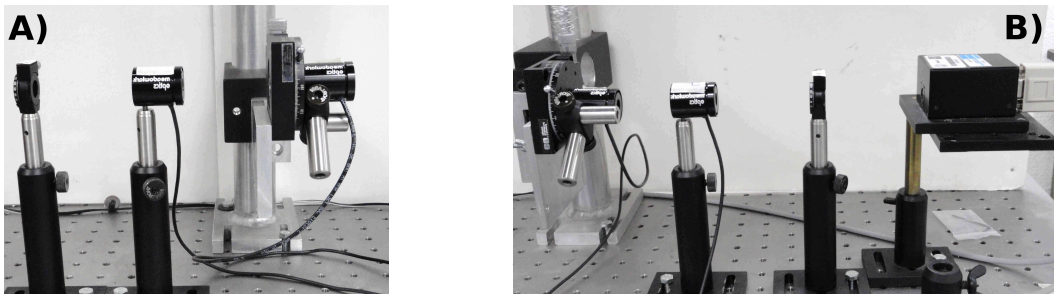

Figure 5.0.2: Photograph of the experimental setup for the Mueller polarimeter using LCVRs, showing the PSG (A) and the PSA (B).

5.1 Mueller polarimetry using a continually varying voltage

Analogously to the case of the Stokes-vector polarimeter shown in Sec. 4.3, a voltage signal which has the form of a linear ramp (sawtooth) was applied and the retardance values involved in each measurement were obtained from the characterization previously performed on the LCVRs (Chapter 3, Sec. 3.2). The Mueller matrix was measured following the method described in Sec. 2.4.2. The 4×4 identity matrix is the Mueller matrix of the air. An example of experimental values obtained for this Mueller matrix is:

$$M_{Air} = \begin{pmatrix} 1 & -0.054 & 0.052 & 0.021 \\ -0.029 & 0.986 & -0.031 & 0.083 \\ -0.014 & -0.037 & 0.955 & 0.046 \\ -0.039 & -0.001 & -0.051 & 0.897 \end{pmatrix}. \tag{5.1}$$

The Mueller elements are all normalized by the first entry, M_{11}. In the example shown in Eq. 5.1, the Mueller matrix was obtained with an accuracy error estimated at 1–10%, depending on the Mueller-matrix element. The measurement error of each matrix element is ± 0.005. Experimental results for a rotating linear polarizer are shown in Fig. 5.1.1. Measurements were made in steps of 10°, from 0° to 180°. It can be seen that the behavior of the results is, in general, as expected. A Glan-Thompson prism polarizer was used as study sample in this work, the data sheet of this device is presented in Appendix B.

Measurements and calculations were performed in LabVIEW®. The measurement time for each complete Mueller matrix was 1.8 seconds. Different values of frequencies for each retarder are required to differentiate each term of the linear combination shown in Eq. 2.48 (see Sec. 2.4.2) and so, by fitting a polynomial to the detected signal, all of the Mueller matrix elements can be calculated. In this case, the values employed for the frequencies of oscillation of the applied voltage to LCVRs were $\nu 1$=1.11 Hz, for LCVR $\omega 1$; $\nu 2$=5 Hz, for LCVR $\omega 2$; $\nu 3$=3.33 Hz, for LCVR $\omega 3$; and $\nu 4$=1.66 Hz, for LCVR $\omega 4$. These frequencies

correspond to time periods of $\tau 1$=0.9 seconds, $\tau 2$=0.2 seconds, $\tau 3$=0.3 seconds and $\tau 4$=0.6 seconds; respectively. Each period value is an integer multiple of the total measurement time because of programming requirements. Using this criterion, and taking into account the response time of the LCVRs [24], some tests were performed to choose time period (frequency) values that allowed fast measurements with good quality. An advantage of the measurement method proposed here is that the operation of the polarimeter is easier than methods of measurement using Fourier analysis [1, 3, 6, 23] or a step-voltage method, as it is shown in the next section.

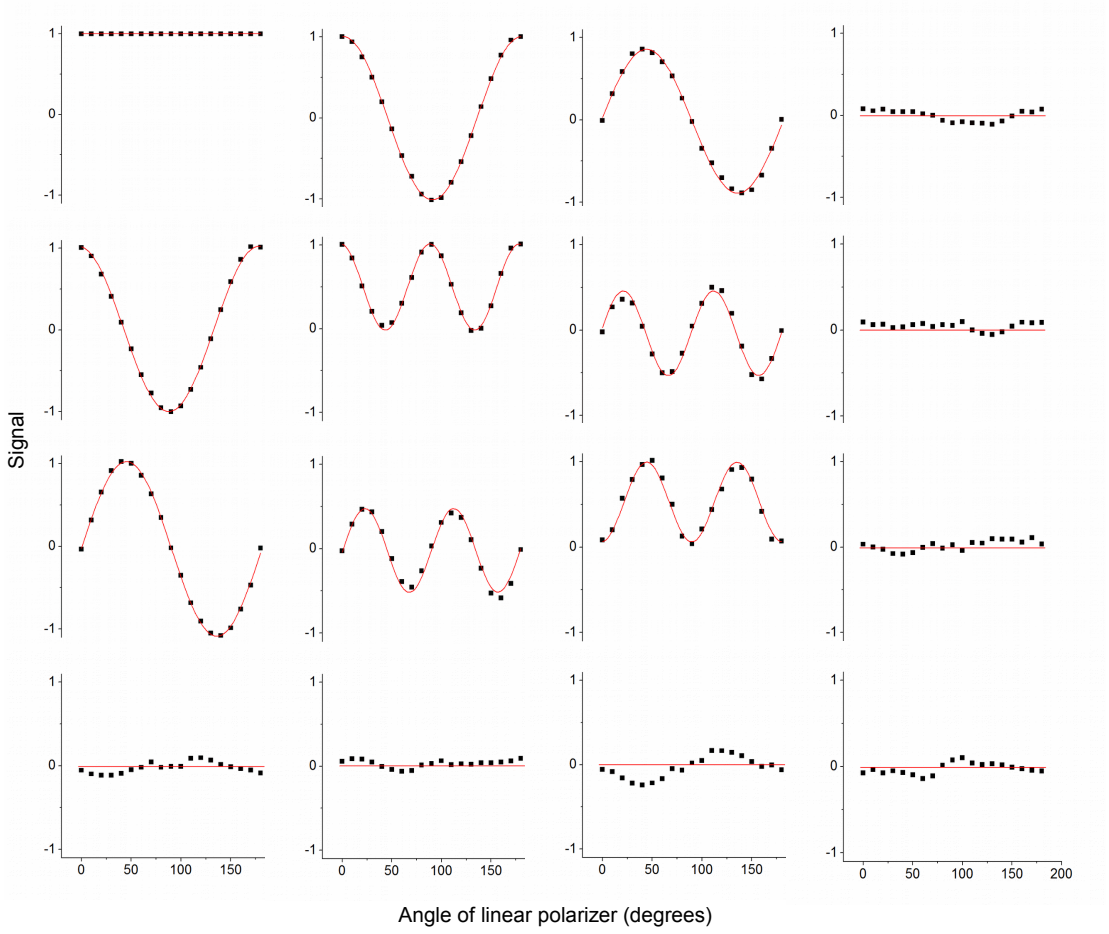

Figure 5.1.1: Sixteen Mueller-matrix elements (classified as they appear in the matrix) of a Glan–Thompson prism polarizer drawn as a function of its optical angle (in degrees), obtained using a continually varying voltage method of measurement. The dots are the experimental results including device and sample imperfections; the solid curves are the fitted theoretical curves of an ideal polarizer. The Mueller elements are all normalized by the first entry, M_{11}.

For comparison of results with the theory, in a similar way as the case of the Stokes polarimeters presented in Chapter 4, measurements from each component of the Mueller matrix shown in Fig. 5.1.1 were fitted to the expected theoretical curves for the Mueller

matrix of a rotating linear polarizer (see Chapter 2). The matrix 5.2, named as SP (statistical parameters), shows the resultant R^2 coefficient for the nonlinear functions and also the standard deviation (σ) of the data for the constant functions. As can be seen, there is a good agreement of the measurements with the theory.

$$SP = \begin{pmatrix} \sigma = 0 & R^2 = 0.999 & R^2 = 0.976 & \sigma = 0.068 \\ R^2 = 0.999 & R^2 = 0.996 & R^2 = 0.966 & \sigma = 0.045 \\ R^2 = 0.994 & R^2 = 0.975 & R^2 = 0.962 & \sigma = 0.06 \\ \sigma = 0.065 & \sigma = 0.044 & \sigma = 0.128 & \sigma = 0.064 \end{pmatrix}. \tag{5.2}$$

5.2 Mueller polarimetry using a step-voltage method

In contrast with the previous case, this method analyzes the optical signal resulting from the application of a few specific retardation values, for each retarder, which are changing in time. Nevertheless, the experimental set-up used is the same as that in the previous case (Fig. 5.0.1). The Mueller matrix of a general sample is measured following the theory developed by Bickel and Bailey [36] described in Sec 2.4.3. The voltage values needed for the measurements were obtained using the characterization performed on the LCVRs (Chapter 3, Sec. 3.2) and the linear interpolating procedure of data describe in Sec. 4.2. To improve results, both the voltages and the rotation angles of the retarders were adjusted manually to get the precise retardance values required in each measurement step. This issue could be due to the effects of the fast-axis rotation with the applied voltage [7]. The variation of other optical parameters, reported in Chapter 3, such as diattenuation, transmittance and depolarization of light could also be involved in the mentioned problem. This issue makes the set-up of the polarimeter difficult using this measurement method, which represents a disadvantage with respect to the measurement method shown in the previous section. The response time to reach the programmed retardance in these devices has been reported as 5-20 ms [24] depending on the retardance change sense (ascending or descending). For this measurement method, we have considered this time of transition before each measurement.

An example of experimental values obtained, using this method, for the Mueller matrix for a gap of air is:

$$M_{Air} = \begin{pmatrix} 1 & -0.003 & 0.017 & 0.013 \\ -0.013 & 0.975 & -0.021 & -0.011 \\ -0.021 & -0.011 & 0.971 & -0.011 \\ 0.019 & 0.012 & 0.023 & 1.026 \end{pmatrix}. \tag{5.3}$$

In this case, the Mueller matrix was obtained with an accuracy error estimated at 1–3%, depending on the Mueller-matrix element. In a similar way as the previous case, the measurement error of each matrix element is ± 0.005. Figure 5.2.1 shows the experimental results

for a rotating linear polarizer, using this technique. As in the case described above, measurements were made in steps of 10º, from 0º to 180º. Measurements and calculations were performed in LabVIEW®. The measurement time for each complete Mueller matrix was 2 seconds.

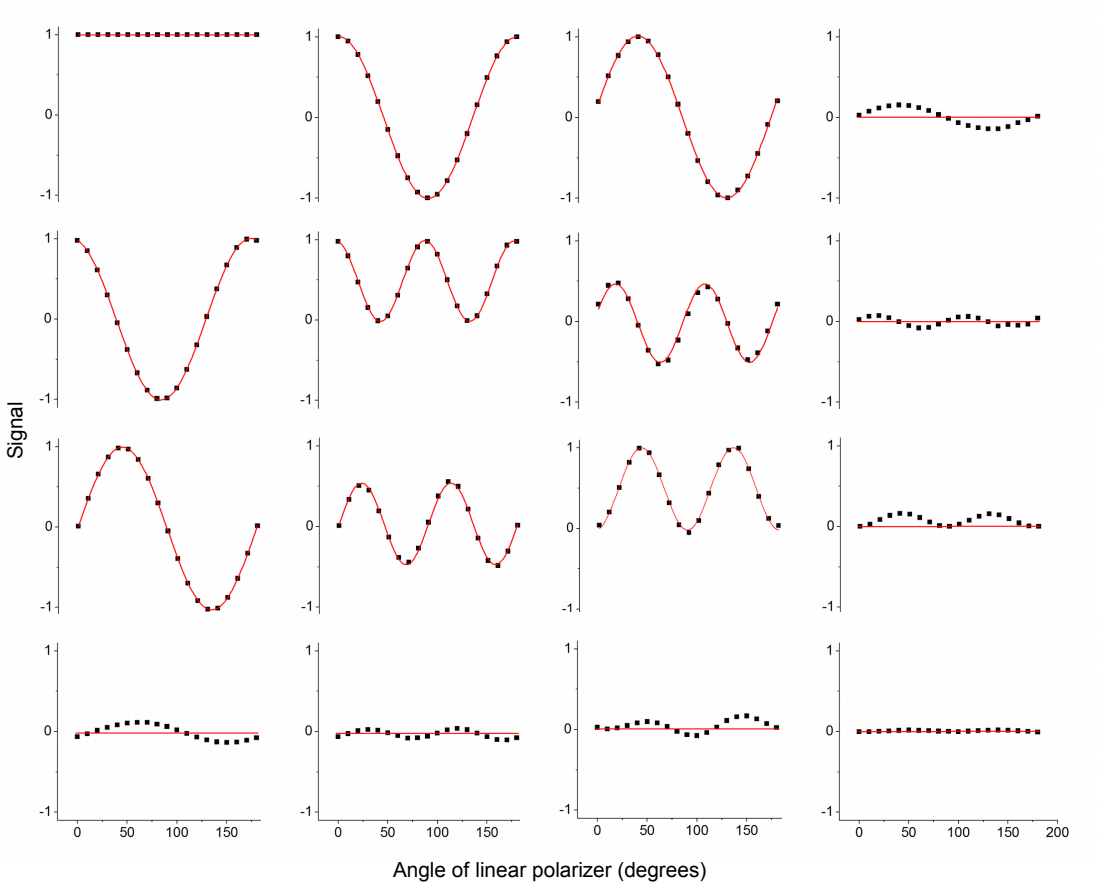

Figure 5.2.1: Sixteen Mueller-matrix elements (classified as they appear in the matrix) of a Glan–Thompson prism polarizer drawn as a function of its optical angle (in degrees), obtained using a step-voltage method of measurement. The dots are the experimental results including device and sample imperfections; the solid curves are the fitted theoretical curves of an ideal polarizer. The Mueller elements are all normalized by the first entry, M_{11}.

$$SP = \begin{pmatrix} \sigma = 0 & R^2 = 0.999 & R^2 = 0.999 & \sigma = 0.105 \\ R^2 = 0.999 & R^2 = 0.998 & R^2 = 0.983 & \sigma = 0.051 \\ R^2 = 0.999 & R^2 = 0.988 & R^2 = 0.99 & \sigma = 0.06 \\ \sigma = 0.091 & \sigma = 0.046 & \sigma = 0.07 & \sigma = 0.008 \end{pmatrix}. \tag{5.4}$$

Eq. 5.4 shows the statistical parameters for the measurements presented in Fig. 5.2.1. Comparing Eqs. 5.2 and 5.4 it can be seen that the measurements obtained with both

methods are very similar. Moreover, the experimental results reported here have similar quality to those obtained with other methods reported by other authors [6, 20, 22, 23, 35].

By using the theory described in this section, it is possible to use an alternative 36 measurements method (generation and analysis of six independent polarization states), instead of the 16 measurements method, to measure the Mueller matrix of a general sample. Possibly, that method could provide more accurate results, but it would require a longer time of measurement (approximately double the time). Furthermore, the operation of the polarimeter would be more complicated than in the case described in this section.

The experimental results presented here, particularly in the measured Mueller matrix for air, show that the accuracy of results for the step-voltage method is slightly better than those for the measurement method proposed here. It is possible that the polarimeter operation is better using the step-voltage method because, in this case, both the voltages and the rotation angles of the retarders are adjusted manually to get the required retardance values. In this way, the inaccuracy in the applied voltage values is avoided and the effect of the fast-axis rotation with the voltage, discussed in Chapter 3, is automatically taken into account. However, in the current conditions, both methods meet the needed requirements (speed and accuracy of measurement) for the application cited in Chapter 1 [16, 17]. Furthermore, it has been found that the experimental set-up of the polarimeter operation was much easier using the new method proposed here. This advantage makes this method more suitable for use in the cited application compared to the step-voltage method. The slight differences between results may be due to the residual nonlinearity in the retardance still present in the fitting method because of the effect of the variation with the voltage of the optical-axes position and other properties of the LCVRs discussed in Chapter 3 and, also, because of the response time of the LCVRs.

In work not reported in this Thesis, we have tested methods to measure the complete Mueller matrix using continually varying voltage and Fourier analysis of the detected signal, following a theoretical development derived in a similar way to those described in Chapter 4. In these cases, the results obtained were rather poor [50], most probably due to the propagation of measurement errors in the calculations of the Mueller matrix elements, because, in this case, the optical system and the mathematical calculations required become more complex.

The measurement methods presented in this Chapter has been reported in an indexed journal: Reference [51].

Chapter 6

Conclusions

Details of the analysis and experimental implementation of a set of polarimetric techniques using liquid crystal variable retarders (LCVRs) have been presented. The novel polarimetric methods proposed in this work were developed using analysis of the nonlinear voltage-retardance relationship for the LCVRs. Usually, the LCVRs are employed with fixed retardance values due to the nonlinear voltage–retardance behavior that they show. However, for the measurement methods presented here, the nonlinear voltage–retardance relationship is first measured, and then a linear fit of the known retardance terms to the detected signal is performed. In order to ensure the quality of the polarimetric measurements, a set of experimental procedures to characterize optical polarization properties as a function of the applied voltage for LCVRs have been employed to estimate possible error sources.

In this Chapter, a summary of the tasks accomplished and some final remarks about the results obtained during this work are presented. At the end, topics derived from this work that remained without investigation, or are currently being investigated, will be described as a proposal for future research. Furthermore, a new research project for application of the Mueller polarimeter developed in this work is described. In addition, early work and the current status of that project are shown.

6.1 Summary and conclusions

6.1.1 Characterization of optical polarization properties for LCVRs

The study of optical properties can be useful to improve results, or estimate errors, in applications using these devices. In this work, a set of experimental procedures to measure optical properties as a function of the voltage applied to the LCVRs used in this Thesis have been proposed. The measured properties were: retardance, diattenuation, transmittance, optical axes position, and output depolarization effects. These properties are involved in the operation of the LCVRs and are the most significant for optical applications such as

polarimetry. The presented techniques have good accuracy, and show good agreement with the expected results. Results and technical issues from all the methods were discussed and the most appropriate procedures to accomplish the proposed study were found.

The obtained results of the retardance measurements using the procedure proposed in this Thesis (Sec. 3.2) match with the data provided by the manufacturer, within the accuracy of the measurements presented here.

In Sec. 3.3 it is shown a simple method to locate the optical axes position by rotating the LCVR to obtain the maximum light intensity transmitted after transmission in a fixed linear polarizer. In this case, a wide range of variation of the axes position was found along the entire operation voltage range. This result is similar to that obtained by other authors, by using a different measurement method [7]. However, this method is very imprecise when the retarder is driven at voltages giving values of retardances close to 0λ and 1λ. This is only a phenomenological experiment and the physical mechanism that produces the behavior of the results presented here is unknown. It is possible that the result obtained here does not only represent the effect of the axes position. This result could be due to a combination of many different optical effects not exclusively related to the retardance. Therefore, this method may not be appropriate for this task.

An analytical procedure developed by Chenault and Chipman [44] to measure diattenuation, retardance, and retardation axes position was also performed (Sec. 3.4). The maximum diattenuation value given by this experiment for the LCVRs used in this work was around ± 0.027. Although this value induces a small change in the polarization state, this effect must be investigated and considered as a possible issue for any practical application given to these devices. In this case, the results of the measured retardance, as a function of the voltage applied to the LCVR, match with the results obtained using the procedure described in Sec. 3.2, and also with the data provided by the manufacturer, except for the values close to 0λ and 1λ due to the beam-wander effect. Therefore, it has been found that the procedure described in Sec. 3.2 is more suitable for measuring the retardance of a variable retarder because it gives more stable and accurate results, particularly for these retardance values. Furthermore, this method is simpler and easier to implement with respect to that proposed by Chenault and Chipman.

In contrast to the experimental results shown in Sec. 3.3, the Chenault–Chipman procedure shows that the position of the axes has a variation of about 1° for a retardance range of one wavelength. The experimental results obtained using this procedure may be more accurate than those shown in Sec. 3.3 because this measurement method includes in its theoretical development all of the optical properties involved in the retarder operation. Thus, the effect of the retardation axes position can be analytically extracted.

The main experimental error source for the Chenault–Chipman procedure is the beam wander effect, due to a deficient set-up alignment. This issue reduces the accuracy of the results [44]. Nevertheless, including beam wander, this method yields results in good agree-

ment with the results for the retardance measurement obtained with the method discussed in Sec. 3.2.

Furthermore, a straightforward method to estimate the depolarization of light in this kind of optical devices using the measured Stokes parameters was discussed in Sec. 3.5. It has be found a degree of polarization reduction of $\sim 2.5\%$ and this should not be an important effect for applications such as polarimetric measurements. However, this topic must be investigated in order to evaluate its real impact on the results from each technical application.

Atypical values for both the measured Stokes parameters and the degree of polarization have been found using a fast continuous voltage signal that has the form of a sawtooth function to drive the retarder. However, these problems are reduced by applying a voltage signal that has a smooth form such as a sine-wave function, which avoids sudden changes of retardance values. Therefore, taking this into account the LCVR performance could be improved when driven using a smooth continually varying voltage.

In addition, intensity measurements shown in this work (Fig. 3.2.2) do not show evidence of optical activity effects. Hence, this topic was not studied in this work.

Finally, the voltage dependence of the optical transmission in the LCVRs was measured (Sec. 3.6) and a negligible effect was found. Thus, this is not an issue for the polarimetry of light using this type of retarders.

It is known that there is a temperature dependence of the optical retardance of LCVRs [52], especially, at low voltages. Measurements presented in this Thesis were made at room temperature (21°C, approximately) and were repeated on different days and climate conditions, always obtaining the same results. It is possible that small changes in the room temperature have a negligible impact on the results of measurement methods using a continually variable voltage compared to methods using a few specific retardation values (step-voltage methods).

The results obtained with the experiments presented in this Chapter show good accuracy and good agreement with the expected results. Hence, these procedures can be considered as an alternative to the use of other known techniques [52, 53] for characterizing variable retarders.

6.1.2 Stokes-vector polarimetry

Experimental results from three different methods to measure the Stokes parameters of a light beam using LCVRs have been presented. The first two methods are Fourier analyses of the detected signal, whereas the third method proposed here is a linear fit using the known retardance values.

The first method uses a Fourier analysis with a sine-wave retardance variation over the "most linear" part of the nonlinear voltage-retardance curve for the LCVRs. The retardance variation in this case was in the range $\lambda/2$ to λ. The obtained results showed a poor fit of

the measured Stokes parameters with the theoretical models.

In the second method proposed here, the interpolated voltages are applied to the retarders to obtain the correct sawtooth retardance variation with time. In this case the retardance range was 0 to λ. The signal was then analyzed with a Fourier method to find the required Stokes vector. This measurement method produced very similar results to those presented in the previous case. Possibly, the sudden change in the voltage values at the end of each cycle distorts the expected shape of retardance variation (a sawtooth function) because of the response time of the LCVRs. Analogously to the case described in Sec. 3.5, a voltage signal that has a smooth form such as, for instance, a sine-wave function could improve results of this measurement method.

In the third method proposed in this work, using a fitting procedure, the voltages were applied to the retarders in the form of a saw-tooth waveform and the nonlinearities were included in the functions used to fit the measured signal as a linear sum of terms proportional to the elements of the required Stokes vector. It is important to emphasize that the fit is linear in the Stokes vector components. This method produced the best results, with smaller asymmetries and a smaller error in the S0 curve (which is the total intensity in the beam and should touch each other elements of the Stokes vector when it is the only other non-zero element). The results obtained with this method show that there are no important effects of depolarization of the light on the measurements. The errors and discrepancies of values in the S0 curves in the other methods must be due to errors in each measurement method.

A comparison of the resulting statistical parameters from the three methods shows that the measurement method using a fitting procedure has the best correlation of the experimental results with the theory. Therefore, this method is more suitable for measuring the Stokes vector using continually varying voltage signals and, also, this may be the best option to develop a method to measure the Mueller matrix of a general sample. Furthermore, this method is the easiest to perform, of the three cases presented in Chapter 4.

6.1.3 Mueller-matrix polarimetry

Two methods to measure the complete Mueller matrix using LCVRs have been presented. The first one is a fitting procedure analogous to that for measuring the Stokes parameters presented in Chapter 4, whereas the second one is a typical step-voltage method presented here to compare between results obtained with the use of fixed retardance values and those obtained using a continually varying voltage. It has been found that there are no significant differences between the results obtained in the new method proposed here with those obtained with a method using a few specific retardation values (step-voltage methods), with similar measuring times. Moreover, the experimental results reported in this work have similar quality to those obtained with other measurement methods and reported by other authors [6, 20, 22, 23, 35]. Both methods presented here meet the needed requirements (speed and

accuracy of measurement) for the application cited in Chapter 1, and proposed as future work in Sec. 6.2.2, but the operation of the polarimeter is much easier using the new method proposed here. Hence, this method is more suitable for this application. The slight differences between results may be due to the residual nonlinearity in the retardance still present in the fitting method because of the effect of the variation with the voltage of the optical-axes position and other properties of the LCVRs discussed in Chapter 3 and, also, because of the response time of the LCVRs.

Currently, new developments in optical instrumentation require new measurement techniques. This work has shown that polarimetric techniques using LCVRs give results with quality comparable to those obtained with measurement methods using other kind of retarders such as, for instance, photoelastic modulators (PEMs) [6, 22] or Pockels cells [20]. For this kind of applications, the main disadvantage of LCVRs with respect to other devices is the non-linearity of the voltage-retardance variation. Moreover, it has been found that the variation with the applied voltage of other optical characteristics should be taken into account for the development of optical applications. Nevertheless, the set of experimental techniques proposed in this work facilitates the use of LCVRs for new applications. In particular, liquid-crystals based retarders are opening up new applications for the measurement of polarization of light due to features such as small size, low weight, a low voltage requirement, and low cost; with respect to electro-optic retarders.

6.2 Proposal for future research

6.2.1 Improving polarimetric measurements

- The study presented in Chapter 3 shows that, besides retardance, there are more polarization properties of the LCVRs depending on the voltage variation that should be taken into account in applications using these devices. From the results obtained in this study, the variation of these properties with the applied voltage is not considered as an important issue for the polarimetric measurements. However, an accurate analysis of the experimental errors induced by this effect should be useful to evaluate its real impact. Furthermore, this effect could be taken into account in the development of polarimetric methods in order to improve results. The same idea can be used to improve results of the method for measuring the retardance-voltage relationship presented in Sec. 3.2.

- Results of the experiments presented in Secs. 3.5, 4.2, and 5.1 suggest the use of voltage signals having a smooth form (for example, a sine-wave function) to drive the LCVRs in order to improve the results of the measurements methods. Work is continuing to develop polarimetric techniques taking into account this idea.

- In work not reported in this Thesis, a calibration method for polarimeters using eigenvalues developed by Compain *et al.* [54] was used with negligible effect on preliminary qualitative results. The experimental setup configuration presented in this work does not use mirrors or refractive elements that could induce alterations of the polarization state of the light and, hence, on the measurements. However, work is continuing to obtain quantitative results in order to evaluate the real impact of this calibration method on the polarimeter.

- A new calibration method for polarimeters using analysis of the detected signal is being investigated [55, 56]. This procedure will be useful to avoid experimental errors related to instrumentation issues.

- In this work, intensity measurements averaged over a solid angle (using a photodetector) were obtained; a detection system able to spatially resolve the polarization behavior requires that the LCVR's windows be characterized using a CMOS or a CCD camera.

6.2.2 Scanning Polarimetric Scatterometer for Two-Dimensional Rough Surfaces

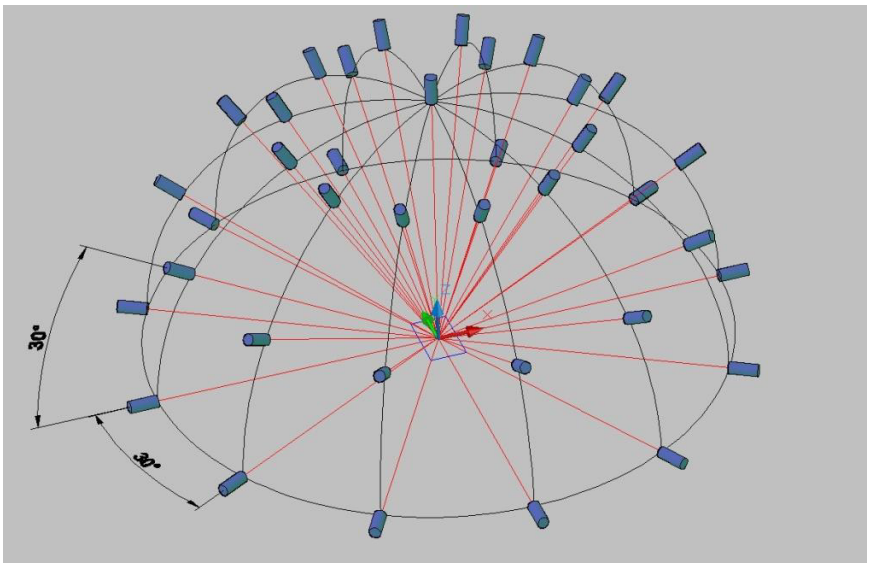

Figure 6.2.1: Measuring the light scattered by a 2D rough surface. Cylinders represent the possible location of both PSG and PSA modules of a Mueller-matrix polarimeter. Drawing courtesy of R. Nava-Sandoval from CCADET-UNAM. [60]

As was mentioned in the introduction, the original motivation for this work is a project to build a polarimetric scatterometer to study 2D rough surfaces. Rough surface scattering has applications in a wide range of scientific and technological areas such as the interpretation

of remote sensing images [57], the security validation of documents and packages [58] or in the testing and imaging of printed circuits [59]. However, the recent theoretical, numerical and experimental advances in this area have used one-dimensional (1D) surface structure, for example lines on a flat substrate. Many applications involve scattering from surfaces with two-dimensional (2D) surface roughness. This type of surface has proved to be more difficult to analyze theoretically and more difficult to measure experimentally. However, recent advances in the theoretical and numerical aspects of scattering of vector-electromagnetic waves in rough surfaces have opened up the possibility of studying the 2D roughness problem. To verify the validity of the numerical models developed for these cases it is important that experimental results be obtained to compare with the numerical results. For a 2D rough surface this involves measuring the scattered light in the full hemisphere above the rough surface as shown in Fig 6.2.1. In comparison, for 1D rough surfaces, the measurements are performed in a single plane.

To measure the polarization of the scattered light, a scanning scatterometer is under development at the Centro de Ciencias Aplicadas y Desarrollo Tecnológico, UNAM. This device uses two rotational movements to scan a detector over the hemisphere of interest (See Fig. 6.2.2). The optical instrumentation includes a complete Mueller-matrix polarimeter based on LCVRs (Fig 6.2.3). More details about this project can be found in Refs. [16, 17, 60, 61].

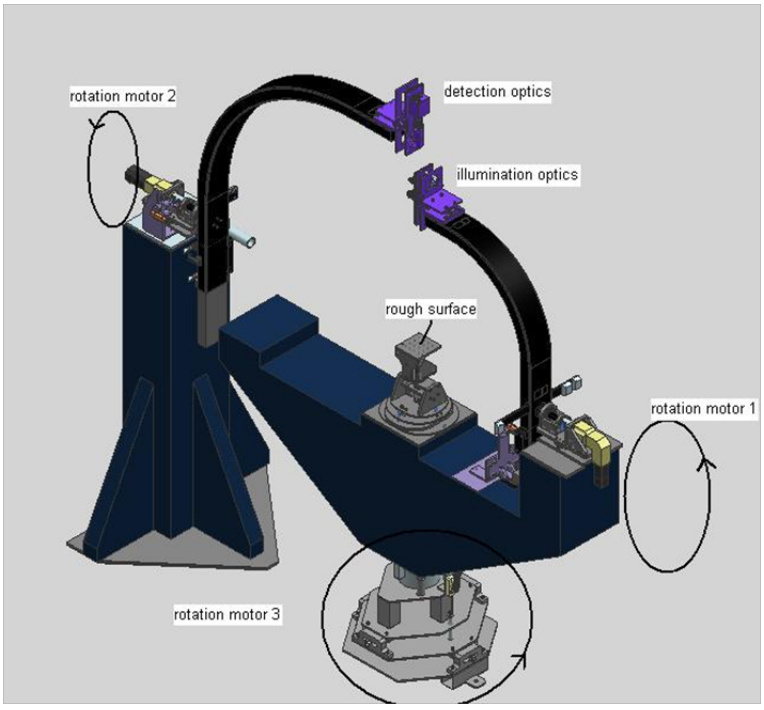

Figure 6.2.2: Scanning scatterometer for 2D rough surfaces [16].

Current status

The scanning scatterometer is currently under development. The mechanical system is almost completed (See Fig. 6.2.4). Electrical components have been integrated to the system. A LabVIEW® program for the automated operation of the system is also under development. Adjustments and calibration of the system are currently being performed in order to ensure measurements with the expected quality and precision [60].

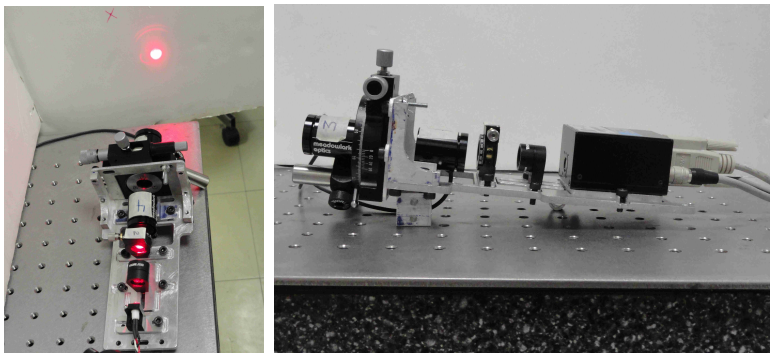

Figure 6.2.3: Set-up for the PSG (left) and PSA (right) using LCVRs.

Figure 6.2.4: Current status of the mechanical system.

Bibliography

[1] D. Goldstein. *Polarized Light*, 2nd edition, Marcel Dekker, New York, 2003.

[2] R. M. A. Azzam, "Oscillating-analyzer ellipsometer," Rev. Sci. Instrum. 47, 624–628 (1976).

[3] R. M. A. Azzam, "Photopolarimetric measurement of the Mueller matrix by Fourier analysis of a single detected signal," Opt. Lett. 2, 148–150 (1978).

[4] D. H. Goldstein, "Mueller matrix dual-rotating-retarder polarimeter," Appl. Opt. 31, 6676–6683 (1992).

[5] J. S. Tyo, Z. Wang, S. J. Johnson, and B. G. Hoover, "Design and optimization of partial Mueller matrix polarimeters," Appl. Opt. 49, 2326–2333 (2010).

[6] G. Martínez-Ponce, C. Solano, and C. Pérez-Barrios, "Hybrid complete Mueller polarimeter based on phase modulators," Opt. Lasers Eng. 49, 723–728 (2011).

[7] P. Terrier, J. M. Charbois, and V. Devlaminck, "Fast-axis orientation dependence on driving voltage for a Stokes polarimeter based on concrete liquid-crystal variable retarders," Appl. Opt. 49(22), 4278–4283 (2010).

[8] T. Scharf, *Polarized light in liquid crystal and polimers*, John Wiley & Sons, New Jersey, 2007.

[9] C. Brosseau, *Fundamentals of Polarized Light*, Wiley, New York, 1998.

[10] R. M. A. Azzam and N. M. Bashara. *Ellipsometry and polarized light*. Elsevier, Amsterdam, 2003.

[11] T. Kihara, "Measurement of Stokes parameters by quarter-wave plate and polarizer," Appl. Mech. Mater. 3–4, 235–242 (2005).

[12] O. G. Rodrguez-Herrera. *Far-field method for the characterisation of three-dimensional fields: vectorial polarimetry*. PhD thesis, National University of Ireland, Galway, 2009.

[13] D. Lara-Saucedo. *Three-dimensional Complete Polarisation Sensitive Imaging using a Confocal Mueller Matrix Polarimeter*. PhD thesis, Imperial College, London, 2005.

[14] S. L. Jacques, J. C. Ramella-Roman, and K. Lee, "Imaging skin pathology with polarized light," J. Biomed. Opt. 7, 329–340 (2002).

[15] I. S. Nerbo, S. LeRoy, M. Foldyna, M. Kildemo, and E. Sondergard, "Characterization of inclined GaSb nanopillars by Mueller matrix ellipsometry," J. Appl. Phys. 108, 014307 (2010).

[16] N. C. Bruce, A. Dominguez-Báez, T. Santana-Sánchez, X. Téllez-Díaz, A. Nogueira-Jiménez, and R. Nava-Sandoval, "Design of a scanning polarimetric scatterometer for rough surface scattering measurements," J. Phys. Conf. Ser. 274, 012135 (2011).

[17] R. Nava-Sandoval, N. C. Bruce-Davidson, T. Santana-Sánchez, "Desarrollo de un esparcímetro goniométrico para medición polarimétrica de luz esparcida en superficies rugosas," B.C.T. INIMET No. 1, (enero-junio), 10-16 (2011).

[18] D. Lara and C. Dainty, "Axially resolved complete Mueller matrix confocal microscopy," Appl. Opt. 45, 1917–1930 (2006).

[19] O. G. Rodríguez-Herrera, D. Lara, and C. Dainty, "Far-field polarization-based sensitivity to sub-resolution displacements of a sub-resolution scatterer in tightly focused fields," Opt. Express 18, 5609–5628 (2010).

[20] F. Delplancke, "Automated high-speed Mueller matrix scatterometer," Appl. Opt. 36, 5388-5395 (1997).

[21] F. Delplancke, "Investigation of rough surfaces and transparent birefringent samples with Mueller-matrix scatterometry," Appl. Opt. 36, 7621–7628 (1997).

[22] Randall C. Thompson, Jerold R. Bottiger, and Edward S. Fry, "Measurement of polarized light interactions via the Mueller matrix," Appl. Opt. 19, 1323-1332 (1980)

[23] A. De Martino, Y. K. Kim, E. Garcia-Caurel, B. Laude, and B. Drévillon, "Optimized Mueller polarimeter with liquid crystals," Opt. Lett. 28, 616–618 (2003).

[24] See <www.meadowlark.com/> for more information on the fabrication and operation of the Liquid-Crystal Variable Retarders used in this Thesis.

[25] W. Weller and H. Winkler, *Elektrodynamik*, Teubner, Leipzig, 1979.

[26] J. R. Reitz, F. S. Milford & R. W. Christy, *Fundamentos de la Teroría Electromagnética*, Addison- Wesley, Iberoamericana, 1986.

[27] J. D. Jackson, *Classical Electrodynamics,* John Wiley & Sons Ltd. 1962

[28] M. Born and E. Wolf, *Principles of Optics*, 6th edn, Pergamon, New York, 1993.

[29] J. W. Goodmann, *Statistical Optics*, Wiley, New York, 2000.

[30] R. A. Chipman. Polarimetry. In M. Bass, editor, *Handbook of Optics*, volume 2, chapter 22, pages 22.1–22.37. McGraw-Hill, 1995.

[31] L. Mandel and E. Wolf. *Optical Coherence and Quantum Optics*. Cambridge University Press, New York, 1st edition.

[32] W. A. Shurcliff and S. S. Ballard. *Polarized Light*. D. Van Nostrand Company, Inc., 1964.

[33] P. S. Hauge, R. H. Mueller, and C. G. Smith. Conventions and formulas for using the Mueller-Stokes calculus in ellipsometry. *Surface Science*, 96:81–107, 1980.

[34] R. A. Chipman. Polarization analysis of optical systems. *Opt. Eng.*, 28:90-99, 1989.

[35] M. Mujat and A. Dogariu, "Real-time measurement of the polarization transfer function," Appl. Opt. 40, 34–44 (2001).

[36] W. S. Bickel and W. M. Bailey, "Stokes vectors, Mueller matrices and polarized scattered light," Am. J. Phys. 53, 468–478 (1985).

[37] J. Delgado-Aguillon, J. Garduño-Mejía, J. M. Lopez-Tellez, N. C. Bruce, M. Rosete-Aguilar, C. J. Roman-Moreno, and R. Ortega-Martınez, "Direct inversion methods for spectral amplitude modulation of femtosecond pulses," Rev. Sci. Instrum. 85(4), 043105 (2014).

[38] A. Peinado, A. Lizana, J. Vidal, C. Iemmi, and J. Campos, "Optimization and performance criteria of a Stokes polarimeter based on two variable retarders," Opt. Express 18, 9815 (2010).

[39] See <https://www.thorlabs.com/> for more information on the technical specifications of the linear polarizers used in this Thesis.

[40] D. C. Ghiglia and M. D. Pritt, *Two-Dimensional Phase Unwrapping: Theory, Algorithms, and Software*, John Wiley & Sons, New York, 1998.

[41] M. A. Schofield and Y. Zhu, "Fast phase unwrapping algorithm for interferometric applications," Opt Lett. 28(14), 1194–1196 (2003).

[42] J. M. López-Téllez, N. C. Bruce and O. G. Rodríguez-Herrera, "Characterization of optical polarization properties for liquid-crystal based retarders," paper in preparation.

[43] J. M. López-Téllez, N. C. Bruce, J. Delgado-Aguillón, J. Garduño-Mejía and M. Avendaño-Alejo, "Experimental method to characterize the retardance function of optical variable retarders," Am. J. Phys. 83(2), 143 (2015).

[44] D. B. Chenault and R. A. Chipman, "Measurements of linear diattenuation and linear retardance spectra with a rotating sample spectropolarimeter," Appl. Opt. 32, 3513–3519 (1993).

[45] D. C. Baird, *Experimentation: An Introduction to Measurement Theory and Experiment Design*, 2nd edition, Prentice Hall, January 1988.

[46] E. Hecht and A. Zajac, *Optics*, Addison-Wesley, Reading, Massachusetts, 1974.

[47] J. M. López-Téllez and N. C. Bruce, "The effect of alignment errors in polarimetry of light using liquid-crystal variable retarders," Proc. SPIE 8011, 801107 (2011).

[48] M. R. Spiegel, *Schaum's Outline of Theory and problems of Statistics*, Third Edition, McGraw-Hill, U.S.A.,1999.

[49] J. M. López-Téllez and N. C. Bruce, "Stokes polarimetry using analysis of the nonlinear voltage-retardance relationship for liquid-crystal variable retarders," Rev. Sci. Instrum. 85(3), 033104 (2014).

[50] J. M. López-Téllez. *Desarrollo de un polarímetro de Mueller con retardadores variables de cristal líquido*. Master's thesis, UNAM, Mexico, 2011.

[51] J. M. López-Téllez and N. C. Bruce, "Mueller-matrix polarimeter using analysis of the nonlinear voltage-retardance relationship for liquid-crystal variable retarders," App. Opt., 53(24), 5359 (2014).

[52] R. L. Heredero, N. Uribe-Patarroyo, T. Belenguer, G. Ramos, A. Sánchez, M. Reina, V. Martínez Pillet, and A. Álvarez-Herrero, "Liquid-crystal variable retarders for aerospace polarimetry applications," App. Opt., 46, 689-698 (2007).

[53] P. Zhang, Y. Tan, W. Liu, and W. Chen, "Methods for optical phase retardation measurement: a review," Sci. China Tech. Sci., 56, 1155–1163 (2013).

[54] E. Compain, S. Poirier, and B. Drevillon, "General and selfconsistent method for the calibration of polarization modulators, polarimeters, and Mueller-matrix ellipsometers," Appl. Opt. 38, 3490–3502 (1999).

[55] C. F. LaCasse, R. A. Chipman, and J. S. Tyo, "Band limited data reconstruction in modulated polarimeters," Opt. Express 19, 14976-14989 (2011).

[56] C. F. LaCasse, O. G. Rodríguez-Herrera, R. A. Chipman, and J.S. Tyo, "Spectral density response functions for modulated polarimeters," Appl. Opt. 54, 9490-9499 (2015)

[57] J. A. Ogilvy, *Theory of Wave Scattering from Random Rough Surfaces*, IOP Publishing, Bristol, 1991.

[58] J. D. R. Buchanan, R. P. Cowburn, A. V. Jausovec, D. Petit, P. Seem, G. Xiong, D. Atkinson, K. Fenton, D. A. Allwood and M. T. Bryan, "Fingerprinting documents and packaging," Nature 436, 475 (2005).

[59] J. C. Stover, *Optical Scattering: Measurement and Analysis,* 3rd ed. (SPIE press, 2012).

[60] R. Nava-Sandoval, N. C. Bruce-Davidson, J. M. López-Téllez, "Ajustes Previos a la calibración de un Esparcímetro Goniométrico para medición polarimétrica de la luz esparcida en superficies rugosas," B.C.T. INIMET No. 1, (enero-junio), 9-22 (2014).

[61] J. M. López-Téllez, N. C. Bruce, and R. Nava-Sandoval, "Scanning Polarimetric Scatterometer for Two-Dimensional Rough Surfaces," in Frontiers in Optics 2015 OSA Technical Digest (online) (Optical Society of America, 2015), paper JTu4A.35.

Appendix A

Publications

The experimental techniques developed in this Thesis and its main results have been reported in a series of indexed publications from prestigious journals and conference proceedings. The first page from each paper is presented in this appendix.

Journal papers

Characterization of optical polarization properties for liquid-crystal based retarders

JUAN M. LÓPEZ-TÉLLEZ*, NEIL C. BRUCE, AND OSCAR G. RODRÍGUEZ-HERRERA.

Centro de Ciencias Aplicadas y Desarrollo Tecnológico, Universidad Nacional Autónoma de México, Mexico City, 04510.
**Corresponding author: jm.lopeztellez@gmail.com*

Received XX Month XXXX; revised XX Month, XXXX; accepted XX Month XXXX; posted XX Month XXXX (Doc. ID XXXXX); published XX Month XXXX

We present the analysis and implementation of a set of experimental procedures to characterize optical polarization properties as a function of the applied voltage for liquid-crystal variable retarders (LCVRs), in transmission mode. The studied properties are those involved in the operation of the LCVRs and, generally, are the most significant for optical applications: retardance, diattenuation, optical axes position, and output depolarization effects. The correct characterization of these polarization properties can be useful to improve results, or estimate errors, in applications using these devices. The results obtained show good accuracy and good agreement with the expected results.

OCIS codes: *(120.0120) Instrumentation, measurement, and metrology; (230.3720) Liquid-crystal devices; (160.4760) Optical properties; (230.5440) Polarization-selective devices; (120.5410) Polarimetry.*

http://dx.doi.org/10.1364/AO.99.099999

1. INTRODUCTION

Nowadays, liquid crystal cells, which have a birefringence that depends on an applied voltage, are finding increased use in research labs as modulators or retarders [1-3]. Modern methods of polarization measurement use variable retarders such as electro-optics or liquid-crystal variable retarders (LCVRs) [4-6]. To obtain the best results using these devices, accurate knowledge of the polarization properties is required. For instance, it is important to characterize the relationship between the observed retardance and the applied voltage in order to verify the manufacturer's characterization and to be able to produce a set of polarization states with high precision. The most significant properties involved in the operation of the LCVRs for optical applications are: retardance, diattenuation, degree of polarization of light at the output of the device (depolarization effects), and the optical axes position. In this work, a set of experimental procedures to characterize these properties as a function of the applied voltage for liquid-crystal retarders, in transmission mode, is proposed.

In previous papers we presented the development of a method for measuring the retardance-voltage relationship for liquid-crystal devices [7, 8]. This procedure was successfully employed to characterize devices for optical applications such as polarimetry [8, 9] and modulators for reconfiguration of ultra short pulses [1]. Due to the great utility of this method, and also for comparison of results with another procedure presented in this work, this method is described in Sec. 2. In Sec. 3 a simple method to locate the optical-axes position of an LCVR is proposed. Then, the details of a slightly modified version for the procedure developed by Chenault and Chipman [10] to measure diattenuation, retardance and the optical axes position are presented in Sec. 4. In Sec. 5, we show a procedure to study the depolarization of the light at the output of the liquid-crystal devices from the analysis of the measured Stokes vectors. Finally, in Sec. 6, we discuss the results and present our conclusions.

In our research experience, we found that the measurement methods proposed in this paper are the most accurate, simple, and easy to use for characterizing our LCVR. We present these procedures as an alternative to the use of other known techniques for accomplishing this task.

A. Description of the LCVRs used in this work

For this work, we have employed a set of nematic liquid-crystal variable retarders manufactured by Meadowlark Optics [11]. These devices work in transmission mode. Figure 1 shows a schematic model for the LCVRs construction. These devices are constructed using optically flat fused silica windows coated with transparent conductive indium tin oxide (ITO). Two windows are aligned and spaced a few microns apart and the cavity is filled with birefringent nematic liquid crystal material. Electrical contacts are attached and the device is environmentally sealed. Anisotropic nematic liquid crystal molecules form uniaxial birefringent layers in the liquid crystal cell. On average, molecules are aligned with their long axes parallel, but with their centers randomly distributed, as shown in Fig. 1. With no voltage applied, the liquid crystal molecules lie parallel to the glass substrates and maximum retardation is achieved. When voltage is applied, liquid crystal molecules begin to tip perpendicular to the fused silica windows. As voltage increases, molecules tip further causing a reduction in the effective birefringence and hence, retardance. The response time to reach the programmed retardance in these devices has been reported as 5–20 ms [11] depending on the retardance change sense (ascending or descending). For our experiments, this time of transition was taken into account. More details on the

Experimental method to characterize the retardance function of optical variable retarders

Juan M. López-Téllez,[a] Neil C. Bruce,[b] Jesús Delgado-Aguillón, Jesús Garduño-Mejía, and Maximino Avendaño-Alejo
Centro de Ciencias Aplicadas y Desarrollo Tecnológico, Universidad Nacional Autónoma de México, México D.F. 04510

(Received 20 February 2014; accepted 6 September 2014)

In this work, we present an experimental method to characterize variable optical retarders, which can have linear or non-linear behavior of the retardance variation. A theoretical analysis of such is presented using a combination of Stokes vectors and Mueller matrixes for three different optical retarders. A straightforward method for phase unwrapping, or reconstructing the original phase from the measured retardance, is proposed that yields high-accuracy results. This work can be used in an undergraduate optics lab to help students understand the concepts of retardance and its control and also how variable retardance devices work.
[http://dx.doi.org/10.1119/1.4896078]

I. INTRODUCTION

In undergraduate optics courses, polarization is an important topic and is usually studied by the investigation of the Fresnel coefficients or by simple natural effects such as optical activity or transmission in calcite crystals.[1–6] Retardance can also be taught through the use of fixed quarter-wave or half-wave retarders to produce different polarization states of light. However, modern methods of polarization measurement use variable retarders such as electro-optics or liquid crystal cells.[6–12] In particular, liquid crystal cells, which have a retardance that depends on an applied voltage, are finding increased use in research labs as modulators or retarders.[9–13] When using these devices, it is important to characterize the relationship between the observed retardance and the applied voltage in order to verify the manufacturer's characterization and to be able to produce given polarization states with high precision. We have also found that the process of retarder characterization is useful for allowing undergraduate students to better understand the concept of retardance and its control and also how these devices work. The applied-voltage-to-retardance relation for liquid crystal cells is nonlinear, and there is no simple theory to explain it. To this end, we suggest that such devices be characterized with a parallel experiment dealing with the production of specific polarization states, to check the validity of the characterization. With this idea, we have characterized a Soleil-Babinet compensator, which has a straightforward theoretical treatment. Our technique is used to calculate the wedge angle of the prisms in the compensator, a specification typically not provided by the manufacturers.

The experimental procedure described here generates data in the range between 0° and 180°. Because of the trigonometric functions that are used in the analysis procedure, an analysis known as "phase unwrapping" must be performed on the experimental data to indirectly obtain the original, continuous function of the applied-voltage-to-retardance relationship by removing discontinuities known as "phase jumps" (see Appendix). This problem can be solved for low-noise data by integrating the wrapped phase over the full domain of voltage values.[14] The final result is a continuous curve that shows the full range of variation of the optical retardance with voltage applied, which usually spans more than a wavelength (0°–360°).

The process of phase unwrapping refers to a set of techniques that are used to reconstruct (optical) signals in a large number of application areas, such as interferometry,[14,15] magnetic resonance imaging (MRI),[16] and holography.[17] This technique has been a major topic of research for over two decades, to such an extent that there are numerous papers[18–21] and a book dedicated to this topic.[22] In this work, we address this problem and present a straightforward phase unwrapping method that yields high-accuracy results. The problem described here corresponds to the simplest case of one-dimensional phase unwrapping, so this work can be used to introduce this topic to undergraduate students.

In Sec. II, we present information on the fabrication and operation of the variable retarders that we characterized with the technique described here. We used three different types of variable retarders with the characterization technique: A Soleil-Babinet Compensator (SBC), and two retarders based on liquid crystals, a Nematic Liquid Crystal Variable Retarder (LCVR), and a pixilated Amplitude Spatial-Light-Modulator (SLM-A). These retarders were used because they were already available in our laboratory. In Sec. III, we describe the theory underlying the experiment, and in Sec. IV the experimental results are presented. Finally, in Sec. V, we discuss the results and present our conclusions. We include an appendix to present the phase unwrapping algorithm used to complete the characterization.

II. THE VARIABLE RETARDERS USED

A. Nematic liquid crystal variable retarder

Nematic Liquid Crystal Variable Retarders (LCVR's)[23] are constructed using optically flat fused silica windows coated with transparent conductive indium tin oxide (ITO). Two windows are aligned and spaced a few microns apart, and the cavity is filled with birefringent nematic liquid crystal material. Electrical contacts are attached, and the device is environmentally sealed. Anisotropic nematic liquid crystal molecules form uniaxial birefringent layers in the liquid crystal cell. On average, the molecules are aligned with their long axes parallel, but with their centers randomly distributed, as shown in Fig. 1. With no voltage applied, the liquid crystal molecules lie parallel to the glass substrates and maximum retardation is achieved. When voltage is applied, the

Mueller-matrix polarimeter using analysis of the nonlinear voltage–retardance relationship for liquid-crystal variable retarders

J. M. López-Téllez* and N. C. Bruce

Centro de Ciencias Aplicadas y Desarrollo Tecnológico, Universidad Nacional Autónoma de México, Circuito Exterior S/N, Ciudad Universitaria, Apdo. Postal 70-186, México D.F. 04510, Mexico

*Corresponding author: jmlopez@comunidad.unam.mx

Received 12 May 2014; revised 7 July 2014; accepted 14 July 2014; posted 15 July 2014 (Doc. ID 211924); published 13 August 2014

A method for using liquid-crystal variable retarders (LCVRs) with continually varying voltage to measure the complete Mueller matrix of a general sample is presented. The LCVRs are usually employed with fixed retardance values due to the nonlinear voltage–retardance behavior that they show. For the measurement method presented here, the nonlinear voltage–retardance relationship is first measured, and then a linear fit of the known retardance terms to the detected signal is performed. For a gap of air, the measurement error in the Mueller-matrix polarimeter is estimated at 1%–10%, depending on the Mueller-matrix element. Also, we present experimental results for a Glan–Thompson prism polarizer as a test sample, and we use the measured Mueller parameters as functions of the orientation of the optical axes of the polarizer as an indication of the quality of the polarimeter. In addition, results are compared to a typical step-voltage method to measure the Mueller matrix. Both methods give good results.

OCIS codes: (120.0120) Instrumentation, measurement, and metrology; (120.4640) Optical instruments; (120.5410) Polarimetry; (230.3720) Liquid-crystal devices; (230.5440) Polarization-selective devices.

http://dx.doi.org/10.1364/AO.53.005359

1. Introduction

Mueller polarimetry is well established [1–5], and it has applications in many scientific and technological areas. Techniques that involve the determination of optical properties through the measurement of the polarization of light scattered by rough surfaces are found in applications such as biological tissue analysis [6] and optical characterization of advanced materials [7], among many others. A project to build a goniometric scatterometer in our laboratory to characterize materials with 2D surface roughness [8,9] has motivated the development of a Mueller-matrix polarimeter, which must meet some specific requirements, such as high-speed measurements, low-weight components, and no moving parts, in order to avoid mechanical vibrations that could affect the accuracy of the measurements. The most frequent techniques found in the literature and used to measure the Mueller matrix are based on fixed linear polarizers and rotating retarders [1–5]. They normally use a Fourier analysis of the detected signal to obtain the Mueller-matrix components. However, modern methods of polarimetric measurement use variable retarders such as electro-optics or liquid-crystal cells [10–15], which have a retardance that depends on the voltage applied. We have implemented a Mueller-matrix polarimeter using a liquid-crystal system manufactured by Meadowlark Optics, because these devices meet the requirements described above and, furthermore, they are cheaper

1559-128X/14/245359-08$15.00/0

Direct inversion methods for spectral amplitude modulation of femtosecond pulses

Jesús Delgado-Aguillón, Jesús Garduño-Mejía,[a] Juan Manuel López-Téllez, Neil C. Bruce, Martha Rosete-Aguilar, Carlos Jesús Román-Moreno, and Roberto Ortega-Martínez
Centro de Ciencias Aplicadas y Desarrollo Tecnológico, Universidad Nacional Autónoma de México, A. P. 70-186, C.U., México City, D.F., 04510, Mexico

(Received 21 October 2013; accepted 21 March 2014; published online 9 April 2014)

In the present work, we applied an amplitude-spatial light modulator to shape the spectral amplitude of femtosecond pulses in a single step, without an iterative algorithm, by using an inversion method defined as the generalized retardance function. Additionally, we also present a single step method to shape the intensity profile defined as the influence matrix. Numerical and experimental results are presented for both methods. © *2014 AIP Publishing LLC*. [http://dx.doi.org/10.1063/1.4870282]

I. INTRODUCTION

Femtosecond pulse shaping is typically achieved by different techniques which involve phase modulation with Spatial Light Modulators (SLM) based on liquid-crystal display (LCD) arrays,[1–4] acousto-optic programmable dispersive filters (AOPDF),[5] and micro-machined deformable membrane mirrors (MMDM),[6,7] each of them with its advantages and disadvantages, depending on the particular application.[8–10] Although accurate modulation can be achieved, a main limitation is related to the convergence speed of the pulse shaping controlled typically with iterative algorithms. Actual convergence time could take up to several minutes. For this work, we have applied an amplitude SLM (SLM-A) consisting of a linear LC array of 128 independent pixels (model SLM-128-A-VN, CRi-Inc., Figure 1) and present two simple and straightforward methods: for intensity profile modulation at a single wavelength and for spectral amplitude modulation of femtosecond pulses. In both cases, desired modulated profile can be achieved in a single step without an evolutionary process.

II. RETARDANCE CHARACTERIZATION

As a first step, for the intensity profile or spectral modulation process, it is necessary to characterize the actual retardance generated by the SLM-A as a function of the applied voltage and wavelength. In this section, we describe the SLM-A operational principle and the retardance characterization method that we have applied.[11] To produce the amplitude modulation, the fast axis of the SLM is tilted at 45° with respect to *p*-polarization of the input beam and polarizers are placed at the entrance and the exit (Figure 1). A change of index of refraction Δn involves phase retardance in one of the optical axes and then a birefringence change in each LCD-pixel. In this way, the local phase change is a function of the applied voltage V, the input local light frequency ω, and the actual pixel thickness d, according to the following equation:[12]

$$\Gamma(\omega, V) = \frac{\omega \Delta n(\omega, V) d}{c}. \tag{1}$$

For the SLM characterization (Figure 2), uniform illumination was applied by reducing the input intensity with a filter (f), expanding the beam with a telescope, which includes a focusing cylindrical lens (C), microscope objective (MO), and a lens (L) which selects and collimates only the central and homogeneous intensity region of the expanded laser beam line. Modulated intensity was generated with the SLM combined with the pair of linear polarizers (P_1 and P_2) and was measured with a linear array CCD (ALPHALAS-CCD-3600-D).

To measure the retardance function (Γ), the Müeller matrix of each pixel of the SLM was calculated by measuring the local transmitted intensity of each pixel as a function of the digital applied voltage. In combination with the Stokes vector (S_0), constructed with the maximum illumination intensity at the CCD (I_0), and the Müeller matrix of the entire system (M_s), the actual retardance can be retrieved according to the following equations:[13,14]

$$S = M_S S_0, \tag{2}$$

$$S_0 = I_0 = \begin{pmatrix} 1 \\ 0 \\ 0 \\ 0 \end{pmatrix}, \tag{3}$$

$$M_s = M_p(\theta_p) M_r(\Gamma, \theta_r) M_p(\theta_p), \tag{4}$$

where M_p are the Müeller matrices of the linear polarizers at angle θ_p and $M_r(\Gamma, \theta)$ is the Müeller matrix of a wave plate of retardance Γ at angle θ_r. For our characterization settings $\theta_p = 0$ and $\theta_r = 45°$. With this we calculate the Stokes vector according to Eq. (2). The retardance can then be calculated from the first element (the total intensity) of the measured Stokes vector

$$S_{(1)} = I = A(1 + \cos(\Gamma)) \tag{5}$$

[a]jesus.garduno@ccadet.unam.mx

Stokes polarimetry using analysis of the nonlinear voltage-retardance relationship for liquid-crystal variable retarders

J. M. López-Téllez[a] and N. C. Bruce
Centro de Ciencias Aplicadas y Desarrollo Tecnológico, Universidad Nacional Autónoma de México, Circuito Exterior S/N, Ciudad Universitaria, Apdo. Postal 70-186, México D.F., 04510, Mexico

(Received 29 November 2013; accepted 20 February 2014; published online 12 March 2014)

We present a method for using liquid-crystal variable retarders (LCVR's) with continually varying voltage to measure the Stokes vector of a light beam. The LCVR's are usually employed with fixed retardance values due to the nonlinear voltage-retardance behavior that they show. The nonlinear voltage-retardance relationship is first measured and then a linear fit of the known retardance terms to the detected signal is performed. We use known waveplates (half-wave and quarter-wave) as devices to provide controlled polarization states to the Stokes polarimeter and we use the measured Stokes parameters as functions of the orientation of the axes of the waveplates as an indication of the quality of the polarimeter. Results are compared to a Fourier analysis method that does not take into account the nonlinear voltage-retardance relationship and also to a Fourier analysis method that uses experimental voltage values to give a linear retardance function with time. Also, we present results of simulations for comparison. © *2014 AIP Publishing LLC*. [http://dx.doi.org/10.1063/1.4867458]

I. INTRODUCTION

The measurement of the polarization of light is well established.[1–13] Recently, more use has been made of variable retarders, for example, liquid crystal retarders or electro-optic cells which have changes of the retardance depending on the voltage applied to the system. Typically, the use of this type of systems involves the application of harmonic variations of voltage to give harmonic variations of the retardance, and thus harmonic variations of the signal detected after transmission in a linear polarizer. However, liquid crystal variable retarders (LCVR's) have a nonlinear voltage-retardance relationship which distorts the retardances if a harmonic voltage is applied, complicating the interpretation of the detected signals, so that a step-voltage method is generally used with this type of device.[2,3] However, this method is more sensitive to noise than methods using a continually variable voltage, particularly for low light intensities, because the results depend on the measurement of a few values; whereas methods using a continually variable voltage, such as those proposed here, integrate noise over many measurements so, its effect on the final results is reduced.

In this paper we present the experimental characterization of LCVR's and the use of this characterization to numerically generate a linearized retardance which is corrected to follow a saw-tooth function, thus eliminating the distortions in the detected signal caused by the nonlinearity. Using this method, we have implemented a Stokes polarimeter using a liquid crystal system manufactured by Meadowlark Optics®. Details on the fabrication and operation of the LCVR's can be found in Ref. 14.

In Sec. II we present the characterization of the LCVR's, and an example of the typical results obtained, compared to the manufacturer-provided data. In Sec. III we present details of the three methods considered to analyze the measured signal to obtain the Stokes vector of light and results are presented for each case. First we present a method using the direct nonlinear relationship between voltage and retardance. In this case a sinusoidal voltage was applied over a range giving retardance from $\lambda/2$ to λ. This range was chosen as it is the part of the voltage-retardance curve which is closest to linear and it was also found that a larger range of retardance gave extremely poor results. This case is included to show the effect of the nonlinearity on the measured Stokes vector parameters. We also give details of two linearized methods. First when a saw-tooth retardance is obtained by applying the correct voltage signal to the retarders. In this case the full 0 to λ retardance range is used and the signal is analyzed by Fourier analysis. Second, we propose a fitting algorithm where the fitting functions take into account the nonlinear voltage-retardance relationship. This method uses a saw-tooth voltage oscillation giving a range of retardance from 0 to λ. Finally in Sec. 5 we discuss the results and present our conclusions.

II. CHARACTERIZATION OF AN LCVR

Figure 1 shows the set-up used to characterize our LCVR's. A photodetector measures the intensity of the light transmitted by the optical system. The detected light intensity depends on the retardance which, also, depends on the voltage applied to the LCVR. Figure 2 shows the light intensity variation with the voltage applied, for a wavelength of 633 nm.

The optical system affects the Stokes vector of the light following the relation,

$$S = M_s S_i, \tag{1}$$

where S_i is the Stokes vector of the light coming from the source and S is the Stokes vector of the light at the detector. The term M_s is the Mueller matrix of the system and can be analyzed in terms of the Mueller matrices of the components,

[a]jmlopez@comunidad.unam.mx

Conference proceedings

Scanning Polarimetric Scatterometer for Two-Dimensional Rough Surfaces

Juan Manuel López-Téllez[1]*, Neil C. Bruce[1] and Rigoberto Nava-Sandoval[1]
[1] *Centro de Ciencias Aplicadas y Desarrollo Tecnológico, Universidad Nacional Autónoma de México, Circuito Exterior S/N, Ciudad Universitaria, Apdo. Postal 70-186, México D.F., 04510, México.*
* *jm.lopeztellez@gmail.com*

Abstract: We present the mechanical design and polarization optics of a goniometric scatterometer for studying the polarized light scattering from 2D rough surfaces. The optical instrumentation includes a Mueller polarimeter based on liquid-crystal retarders.
OCIS codes: (120.4640) Optical instruments; (290.5820) Scattering measurements; (120.5410) Polarimetry; (230.3720) Liquid-crystal devices.

1. Introduction.

Rough surface scattering has applications in a wide range of scientific and technological areas, for example, in the security validation of documents and packages [1] or in the testing and imaging of printed circuits [2]. However, the recent theoretical, numerical and experimental advances in this area have used one-dimensional (1D) surface structure, for example lines on a flat substrate. Many applications involve scattering from surfaces with two-dimensional (2D) surface roughness. This type of surface has proved to be more difficult to analyze theoretically and more difficult to measure experimentally. However, recent advances in the theoretical and numerical aspects of scattering of vector-electromagnetic waves in rough surfaces have opened up the possibility of studying the 2D roughness problem. To verify the validity of the numerical models developed for these cases is important that experimental results be obtained to compare with the numerical results. For a 2D rough surface this involves measuring the scattered light in the full hemisphere above the rough surface. This compares to the measurement in a single plane for 1D rough surfaces.

To measure the polarization of the scattered light we have chosen to build a scanning scatterometer which uses two rotational movements to scan a detector over the hemisphere of interest (See Fig. 1). The optical instrumentation includes a complete Mueller-matrix polarimeter based on liquid crystal variable retarders (LCVR's) [3].

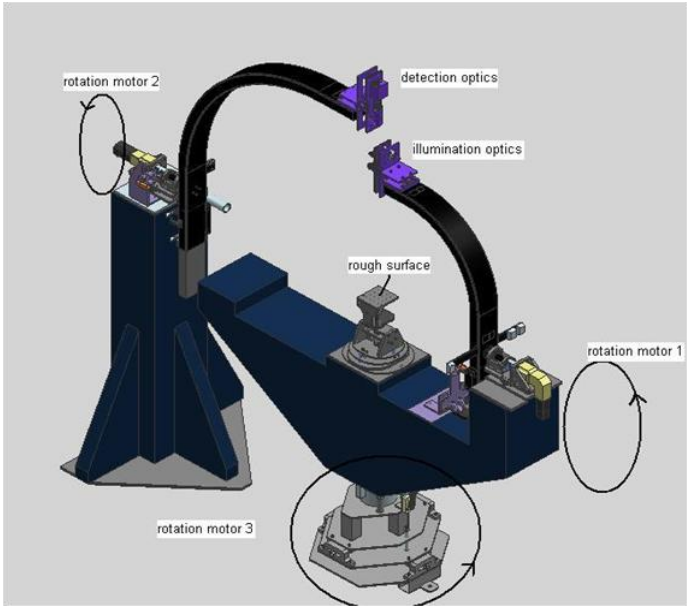

Fig. 1. Scatterometer model.

2. Mechanical design.

Figure 2 shows a diagram of the design of the scatterometer. The position of the rough surface is indicated in the figure and can be adjusted in height to account for different types and thicknesses of substrates. The illumination optics consists of a laser diode with a wavelength of 635nm, a collimating lens and a polarization-state generator

Polarimetry of light using analysis of the nonlinear voltage-retardance relationship for liquid-crystal variable retarders

Juan Manuel Lopez-Tellez[1,*] and Neil C. Bruce[1]
[1] *Centro de Ciencias Aplicadas y Desarrollo Tecnológico, Universidad Nacional Autónoma de México, Circuito Exterior S/N, Ciudad Universitaria, Apdo. Postal 70-186, México D.F., 04510, México.*
* *jmlopez@comunidad.unam.mx*

Abstract: We present a method for using liquid-crystal variable retarders (LCVRs) with continually varying voltage to measure, both, the Stokes vector of a light beam and the complete Mueller matrix of a general sample.
OCIS codes: (120.0120) Instrumentation, measurement, and metrology; (120.4640) Optical instruments; (120.5410) Polarimetry; (230.3720) Liquid-crystal devices; (230.5440) Polarization-selective devices.

1. Introduction

The measurement of the polarization of light is well established [1-3]. Recently, more use has been made of variable retarders, for example, liquid crystal retarders or electro-optic cells which have changes of the retardance depending on the voltage applied to the system. The LCVRs are usually employed with fixed retardance values due to the nonlinear voltage-retardance behavior that they show. For the measurement method presented here, the nonlinear voltage-retardance relationship is first measured and then a linear fit of the known retardance terms to the detected signal is performed. We use known waveplates (half-wave and quarter-wave) as devices to provide controlled polarization states to the Stokes polarimeter, and we use the measured Stokes parameters as functions of the orientation of the axes of the waveplates as an indication of the quality of the polarimeter. In addition, we present results of simulations for comparison. Also, we have used this technique to measure the complete Mueller matrix of a general sample. For a gap of air, the measurement error in the Mueller-matrix polarimeter is estimated at 1–10%, depending on the Mueller-matrix element. For this case, we present experimental results for a Glan–Thompson prism polarizer as a test sample, and we use the measured Mueller parameters as functions of the orientation of the optical axes of the polarizer as an indication of the quality of the polarimeter.

2. Stokes polarimeter

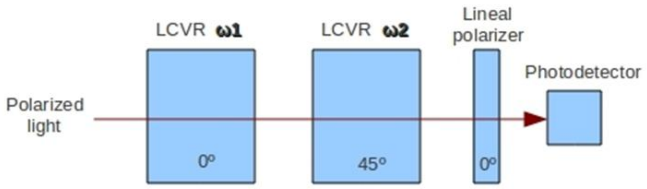

Fig. 1. The set-up for a Stokes polarimeter. The angles associated with each component refer to the relative angle of the optical axis of that component. **ω1** and **ω2** are the frequencies of the variations of the retardances.

Figure 1 shows the set-up used for the Stokes polarimeter. The light to be analyzed passes through two liquid crystal variable retarders with their axes at 45° to each other and finally through a linear polarizer with its transmission axis parallel to the axis of the first retarder. The idea of this method is to adjust the detected intensity, *I*, to a linear combination

$$I = A + B\cos(\delta_2) + C\sin(\delta_1)\sin(\delta_2) + D\cos(\delta_1)\sin(\delta_2). \quad (1)$$

So, we have

$$A = \frac{1}{2}S_{i0}, \quad B = -\frac{1}{2}S_{i1}, \quad C = -\frac{1}{2}S_{i2}, \quad D = \frac{1}{2}S_{i3}; \quad (2)$$

where S_{i0}, S_{i1}, S_{i2} and S_{i3}; are the components of the Stokes vector of the incident light beam, S_i. The development of the above equations and, also, details on the experimental set-up for the Stokes polarimeter are shown in Ref. [4].

In this case, we have applied a voltage signal which has the form of a linear ramp (saw tooth), this is

$$V = V_{\min} + (V_{\max} - V_{\min})\mathrm{mod}\left(\frac{t}{t_i}\right), \quad (3)$$

and the retardance, δ, is given by the nonlinear relationship of figure 2.

Ajustes Previos a la calibración de un Esparcímetro Goniométrico para medición polarimétrica de la luz esparcida en superficies rugosas

Autores: M. en I. Rigoberto Nava-Sandoval *
Dr. Neil Charles Bruce-Davidson**
M. en I. Juan Manuel López-Téllez **

***Coordinador de Sección de Desarrollo de Prototipos.**
****Grupo de Óptica Aplicada**
Centro de Ciencias Aplicadas y Desarrollo Tecnológico de la Universidad Nacional Autónoma de México, Ciudad de México, México.

Correo-e:rigoberto.nava@ccadet.unam.mx

Resumen

En este trabajo se presenta el procedimiento de medición de parámetros geométricoscomo paralelismo, perpendicularidad y coaxialidad entre otros, así como los ajustesmecánicos a los que debe someterse un esparcímetro de resolución angular, el cual es utilizado para estudiar el esparcimiento de la luz en superficies rugosas bidimensionales. También se mencionan los instrumentos de medición empleados para alinear sus ejes. El procedimiento descrito en este documento le permite al instrumento estar en condiciones adecuadas para realizar dichas mediciones con la calidad y precisión que este estudio requiere.

Palabras clave: instrumentos ópticos, esparcimiento de la luz; medición y ajuste.

Abstract.

A method to measure geometric parameters such as parallelism, perpendicularity and coaxiality, among others, as well as the mechanical adjustments to be made on a goniometric scatterometer for the study the light spreading on two-dimensional rough surfaces is presented. The measuring instruments used to align the axes of the scatterometer are also mentioned. The procedure described makes the instrument fit to carry out the said measurements with the expected quality and precision.

Experimental method to characterize a liquid-crystal variable retarder and its application in a Stokes polarimeter

J.M. López-Téllez and N.C. Bruce.
Centro de Ciencias Aplicadas y Desarrollo Tecnológico, Universidad Nacional Autónoma de México, México, D.F. 04510

ABSTRACT

We present an experimental method to characterize a liquid-crystal variable retarder (LCVR). In addition, experimental results using LCVR's to measure the four Stokes parameters of a light beam simultaneously are presented. We use known waveplates (half-wave and quarter-wave) as devices to provide controlled polarization states to the Stokes polarimeter, and we use the measured Stokes parameters as functions of the orientation of the axes of the waveplates as an indication of the quality of the polarimeter. Also, we present results of simulations for comparison.

Keywords: Polarization of light, Stokes parameters, Liquid-crystal variable retarder, Optical retardance, Polarimetry, Stokes polarimeter.

1. INTRODUCTION

The measurement of the polarization of light is well established [1-10]. Recently, more use has been made of variable retarders, for example, liquid crystal retarders which have changes of the retardance depending on the voltage applied to the liquid crystal system. The use of this type of systems involves the application of harmonic variations of voltage to give harmonic variations of the retardance, and thus harmonic variations of the signal detected after transmission in a linear polarizer. We have acquired a liquid crystal system manufactured by Meadowlark Optics® and we have implemented a Stokes polarimeter.

Nematic Liquid Crystal Variable Retarders (LCVR's), by Meadowlark Optics®, are constructed using optically flat fused silica windows coated with transparent conductive indium tin oxide (ITO). Two windows are aligned and spaced a few microns apart and the cavity is filled with birefringent nematic liquid crystal material. Electrical contacts are attached and the device is environmentally sealed. Anisotropic nematic liquid crystal molecules form uniaxial birefringent layers in the liquid crystal cell. On average, molecules are aligned with their long axes parallel, but with their centers randomly distributed, as shown in Figure 1. With no voltage applied, the liquid crystal molecules lie parallel to the glass substrates and maximum retardation is achieved. When voltage is applied, liquid crystal molecules begin to tip perpendicular to the fused silica windows. As voltage increases, molecules tip further causing a reduction in the effective birefringence and hence, retardance [9].

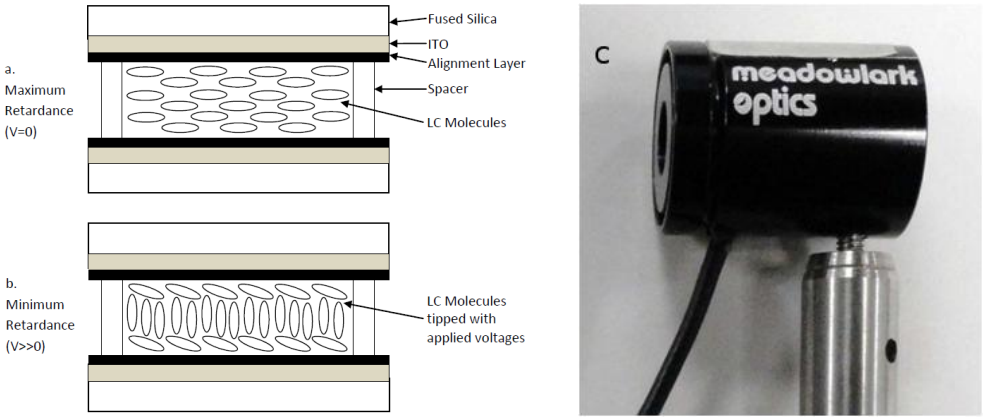

Figure 1: LCVR construction showing molecular alignment (a) without and (b) with applied voltage (drawing not to scale [9]). Also, LCVR photo (c).

8th Iberoamerican Optics Meeting and 11th Latin American Meeting on Optics, Lasers, and Applications, edited by Manuel Filipe P. C. Martins Costa, Proc. of SPIE Vol. 8785, 87852J

The effect of alignment errors in polarimetry of light using liquid-crystal variable retarders.

J.M. López-Téllez and N.C. Bruce.
Centro de Ciencias Aplicadas y Desarrollo Tecnológico, Universidad Nacional Autónoma de México, México, D.F. 04510

ABSTRACT

Experimental results using Liquid-Crystal Variable Retarders (LCVRs) to measure the four Stokes parameters of a light beam simultaneously are presented. We use known waveplates (half-wave and quarter-wave) as known sources to provide controlled polarization states to the Stokes polarimeter, and we use the measured Stokes parameters as functions of the orientation of the axes of the waveplates as an indication of the quality of the polarimeter. The effects of errors in optical alignment and nonlinearity of the retardance variation on the results are presented and discussed. We also present results of simulations for comparison. Finally, we present the advances obtained in the development of a Mueller matrix polarimeter for use in a goniometric scatterometer.

Keywords: polarization, Stokes vector, Mueller matrix, surface scattering, scatterometer.

1. INTRODUCTION

The measurement of the polarization (Stokes vector or Mueller matrix) of light is well established[1-8]. Recently, more use has been made of variable retarders, for example, liquid crystal retarders which have changes of the retardance depending on the voltage applied to the liquid crystal system. The use of this type of systems involves the application of sinusoidal variations of voltage to give sinusoidal variations of the retardance, and thus harmonic variations of the signal detected after transmission in a linear polarizer. We have acquired a liquid crystal system manufactured by *Meadowlark Optics*™ and we have implemented a Stokes polarimeter as an intermediate step to producing a Mueller matrix polarimeter. However, because of linearity considerations for the retardance variation, we have had to modify the equations relating the detected signal to the Stokes parameters measured.

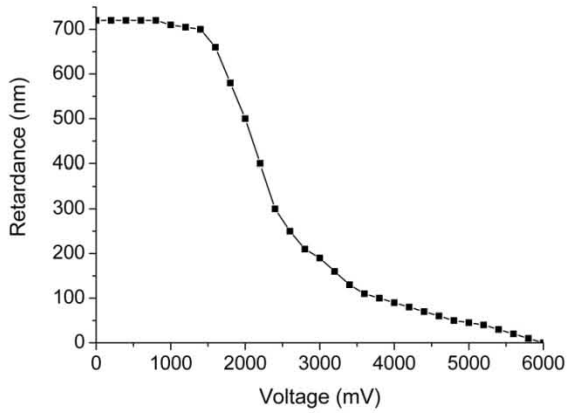

Figure 1: Retardance vs voltage for a typical liquid crystal retarder for a wavelength of 633nm.

Figure 1 shows the typical variation of the retardance with the voltage applied. It can be seen that the curve is not linear, especially for higher values of the voltage which give lower values of retardance. If the retardance does not depend linearly on the voltage then the voltage variations (which are usually sinusoidal) cannot be related directly to the retardance variations, and the analysis of the signals becomes very complicated. To avoid these problems we use the

22nd Congress of the International Commission for Optics: Light for the Development of the World, edited by Ramón Rodríguez-Vera, Rufino Díaz-Uribe, Proc. of SPIE Vol. 8011, 801107
2011 SPIE · CCC code: 0277-786X/11/$18 · doi: 10.1117/12.901214

Stokes polarimetry using liquid-crystal variable retarders and non-linear voltage-retardance function

C.A. Velázquez Olivera, J.M. López Tellez and N.C. Bruce
Centro de Ciencias Aplicadas y Desarrollo Tecnológico,
Universidad Nacional Autónoma de México, México, D.F. 04510

ABSTRACT

Stokes polarimetry using variable retardance elements such as Pockel´s cells and liquid crystals is a well-developed technique. There are two standard methods of analysis to extract the Stokes vector from the data using only one detector. One is to use only certain values of the retardances to obtain data for a number of fixed polarization combinations. The other is to use all the polarization combinations of the retardances for an oscillating voltage applied to the cells, and perform a Fourier analysis on the time varying signal. This method requires a linear relationship between the applied voltage and the obtained retardance. However, in general, for liquid-crystal variable retarders, this relationship is not linear. We present an analysis of a proposed method to use a nonlinear voltage-retardance relation to extract the Stokes parameters of a light beam. The method assumes a known nonlinear function relating the voltage and the retardance and uses a least-squares fit of the measured data to the calculated Mueller matrix of the polarimeter.

Stokes polarimeter, variable retardance

1. INTRODUCTION

Variable-retardance elements such as Pockel´s cells or liquid crystals are routinely used in polarimeters to measure the Stokes vector of a light beam or the Mueller matrix of a system [1-7]. In the literature, two methods have been proposed and implemented to extract the useful information from measured data with only one detector. One method is to use a limited number of fixed retardances, determined by the voltages applied to the elements, and use the known polarization states generated to calculate the Stokes vector or Mueller matrix required. The second method requires the use of an oscillating voltage giving an oscillating retardance. The detected signal is then Fourier transformed to detect the principle frequency contributions and these Fourier coefficients can be related to the components of the Stokes vector or Mueller matrix to be measured. This second method requires a linear relationship between the applied voltage and the retardance generated in the variable-retardance element, so that the relationship between the Fourier coefficients of the signal and the required parameters can be found.

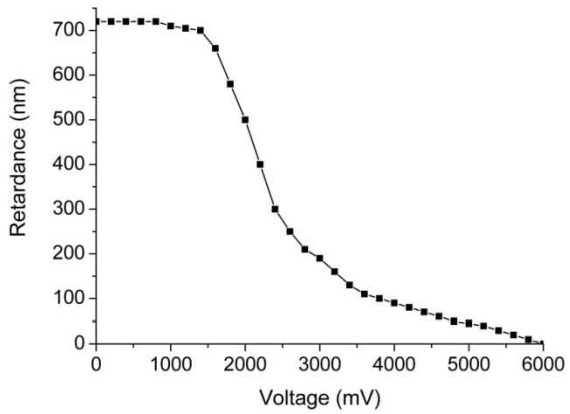

Figure 1. Retardance vs voltage for a typical liquid crystal retarder for a wavelength of 633nm

22nd Congress of the International Commission for Optics: Light for the Development of the World,
edited by Ramón Rodríguez-Vera, Rufino Díaz-Uribe, Proc. of SPIE Vol. 8011, 80110C
2011 SPIE · CCC code: 0277-786X/11/$18 · doi: 10.1117/12.901661

Science popularization

ACADEMIA MEXICANA DE ÓPTICA, A.C.

INTERNATIONAL YEAR OF LIGHT 2015

Explorando en la Óptica, ACADEMIA MEXICANA DE ÓPTICA, A.C.

Edición especial celebrando el 2015 Año Internacional de la Luz.

Medición de la polarización de la luz

Neil C. Bruce y Juan Manuel López Téllez

neil.bruce@ccadet.unam.mx, jml.56@hotmail.com

Centro de Ciencias Aplicadas y Desarrollo Tecnológico (CCADET), Universidad Nacional Autónoma de México (UNAM).

Resumen: La polarización de la luz es un campo de estudio muy desarrollado. Sin embargo, los nuevos avances en la tecnología de la instrumentación óptica requieren de nuevas técnicas de medición. En particular, los dispositivos basados en cristales líquidos están abriendo nuevas aplicaciones para la medición de la polarización.

Introducción

La luz es una onda vectorial electromagnética, con una amplitud y una dirección de un campo eléctrico y un campo magnético en cada punto del espacio [1]. Las ecuaciones de Maxwell relacionan los campos eléctricos y magnéticos; con ellas conoceremos la dirección y amplitud del campo magnético si sabemos la amplitud y dirección del campo eléctrico. Al comportamiento de la dirección y amplitud del campo eléctrico con la propagación de la onda se le conoce como *polarización* de la luz [2]. Algunos ejemplos de polarización son (ver la Figura 1): polarización lineal, en donde el vector de campo eléctrico oscila siempre en el mismo plano; polarización circular, en donde el vector de campo eléctrico gira alrededor de un eje paralelo al vector de onda, que indica la dirección de propagación del haz, realizando un giro completo en la distancia de la longitud de

Appendix B

Data sheet of optical components

Data sheets containing the most relevant technical information about the main optical components used in this work are presented in this appendix.

Liquid Crystal Variable Retarders

Liquid crystal devices should be electrically driven with an AC waveform with no DC component to prevent ionic buildup which can damage the liquid crystal layer. We require a 2 kHz square wave of adjustable amplitude for controlling our Liquid Crystal Variable Retarders (LCVR). Our Basic Controller and Four Channel Interface described on pages 59-61 ensure these drive requirements are met. A temperature sensing and control option can be added to our LCVRs for accurate controlling of the operating temperature. The sensor is attached directly to the LCVR substrate, outside its clear aperture. Without this option, retardance decreases by approximately 0.2% to 0.3% per °C increase in temperature.

Key Benefits

- **Computer control capability**
- **Temperature control options**
- **Usable from 450 to 1800 nm**
- **Precision non-mechanical retardation control**

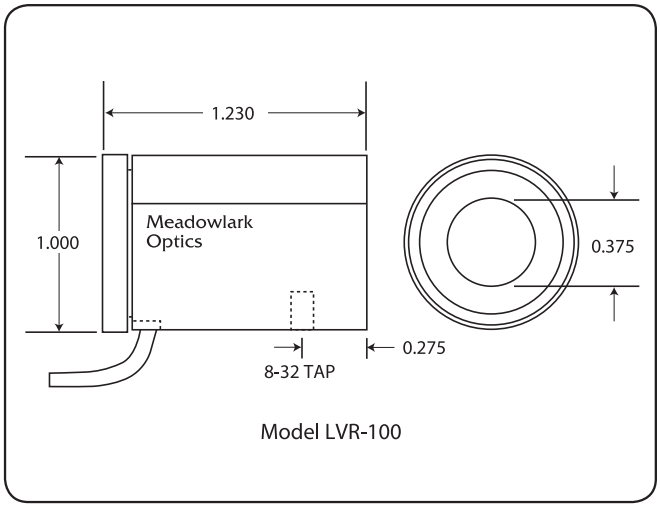

Fig. 4-9 Model LVR-100 dimensions
All dimensions in inches

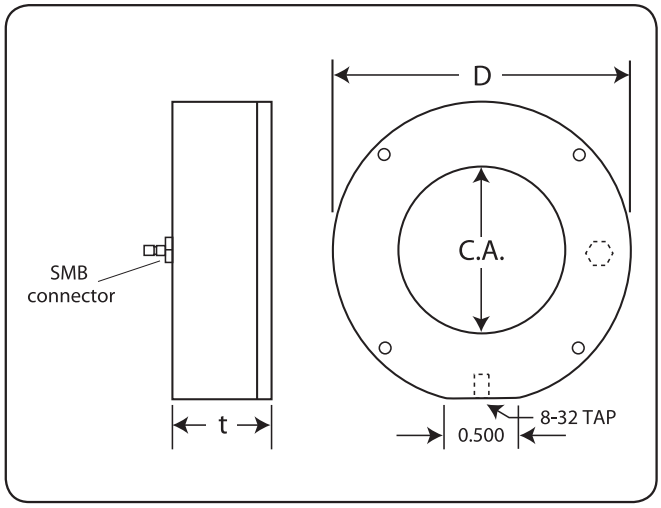

Fig. 4-10 Models LVR-200 and LVR-300 dimensions
All dimensions in inches

SPECIFICATIONS	
Retarder Material	Nematic liquid crystal
Substrate Material	Optical quality synthetic fused silica
Wavelength Range	450-1800 nm (specify)
Retardance Range	
Without compensator With compensator	~30 nm to λ/2 0 to λ/2 custom ranges are available
Transmitted Wavefront Distortion (at 632.8 nm)	≤ λ/4
Surface Quality	40-20 scratch and dig
Beam Deviation	≤ 2 arc min
Reflectance (per surface)	≤ 0.5% at normal incidence
Diameter Tolerance	± 0.005 in.
Temperature Range	0° C to 50°C
Recommended Safe Operating Limit	500 W/cm², CW 300 mJ/cm², 10 ns, visible

ORDERING INFORMATION			
Diameter, D (in.)	*Clear Aperture, CA (in.)*	*Thickness t (in.)*	*Part Number*
Without Attached Compensator (30 nm to λ/2)			
1.00	0.37	1.23	LVR - 100
2.00	0.70	0.75	LVR - 200
3.00	1.60	1.00	LVR - 300
With Attached Compensator (0 nm to λ/2)			
1.00	0.37	1.23	LRC - 100
2.00	0.70	0.75	LRC - 200
3.00	1.60	1.00	LRC - 300

We offer standard liquid crystal variable retarders to cover four spectral regions:

VIS: 450 - 700 nm IR 1: 650 - 950 nm
IR 2: 900 - 1250 nm IR 3: 1200 - 1700 nm

Please specify spectral region when placing your order.
For temperature control option, append-TSC to part number .

Metal Package PMT with Internal Charge Amp+ADC Type

Photosensor Modules H7468 Series

The H7468 series are photosensor modules assembled with a photomultiplier tube, an AD converter circuit and a microcontroller. These photosensor modules operate from a single +5 V supply and convert the photomultiplier tube analog signals into 12-bit digital data which can be sent to a PC (personal computer) through the RS-232C interface. The photomultiplier tube supply voltage and measurement start/stop can also be controlled from the PC.

Product Variations

Type No.	Spectral Response	Features
H7468	300 nm to 650 nm	For visible range
H7468-01	300 nm to 850 nm	For visible to near IR range
H7468-03	185 nm to 650 nm	For UV to visible range
H7468-20	300 nm to 900 nm	High sensitivity in near IR range

Specifications

Parameter			H7468				Unit
Suffix			None	-01	-03	-20	—
Input Voltage (Vcc)			+4.75 to +5.25				V
Max. Input Voltage			+6				V
Max. Input Current			35				mA
Effective Area			ϕ8				mm
Digital Output: Maximum Output Current			25				mA
Digital Output: Maximum Sink Current			25				mA
Voltage between Digital Input and GND			-0.3 to Vcc +0.3				V
Peak Sensitivity Wavelength			420	400	420	630	nm
Cathode Sensitivity	Luminous Sensitivity	Min.	40	80	40	350	A/lm
		Typ.	70	150	70	500	
	Blue Sensitivity Index (CS 5-58)		8.0	—	8.0	—	—
	Red/White Ratio		—	0.2	—	0.45	—
	Radiant Sensitivity *1		62	60	62	78	mA/W
Gain *2		Typ.	7.0×10^5	5.0×10^5	7.0×10^5	5.0×10^5	—
Anode Dark Current *2, *3		Typ.	0.2	0.4	0.2	2	nA
		Max.	2	4	2	20	
Integration Capacitance			1000				pF
AD Converter Resolution			12				bit
Integration Time			0.04 to 500 (0.01 step)				ms
Dead Time			0.01 to 500 (0.01 step)				ms
Sampling Time	Continuous Reading		4 to 1000				ms
	Fixed Set Reading		0.05 to 1000				ms
Measurement Count (fixed set reading)			1 to 127				—
PMT Supply Voltage			0 to 1000				V
Digital High-Level Input Voltage		Min.	4				V
Digital Low-Level Input Voltage		Max.	1				V
Digital High-Level Output Voltage		Min.	Vcc -0.7				V
Digital Low-Level Output Voltage		Max.	0.6				V
RS-232C Interface Setting			RS-232C, 9600 baud, Parity none, 8 data bits, 1 stop bit				—
Operating Ambient Temperature			+5 to +50				°C
Storage Temperature			-20 to +50				°C
Weight			105				g

*1: Measured at the peak sensitivity wavelength *2: PMT supply voltage: 800 V
*3: After 30 minute storage in darkness

Characteristics (Cathode radiant sensitivity, PMT gain)

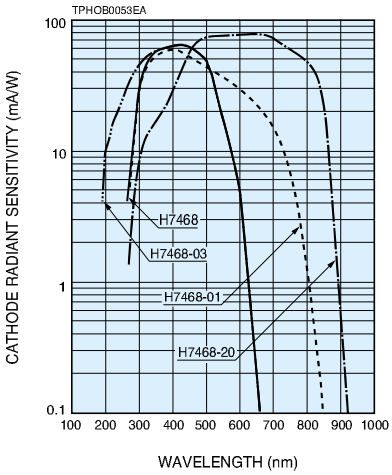

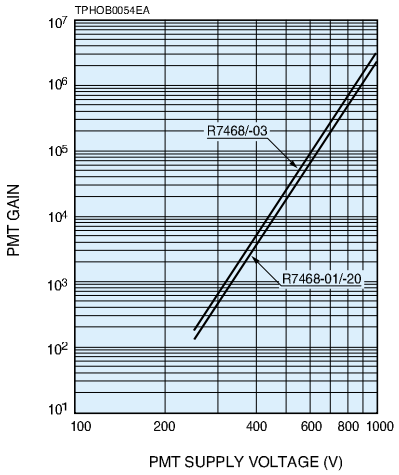

Connection Diagram

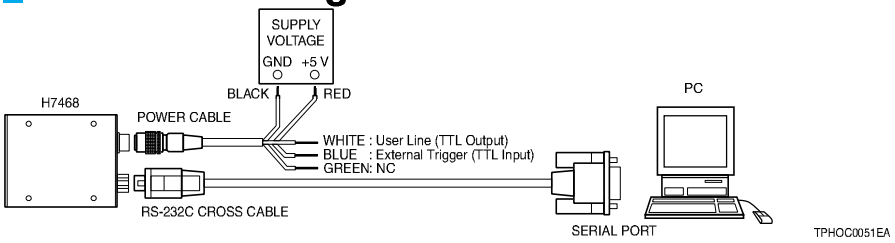

Block Diagram

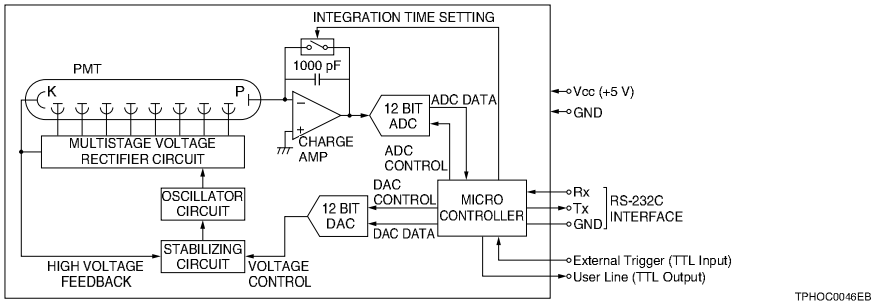

Dimensional Outlines (Unit: mm)

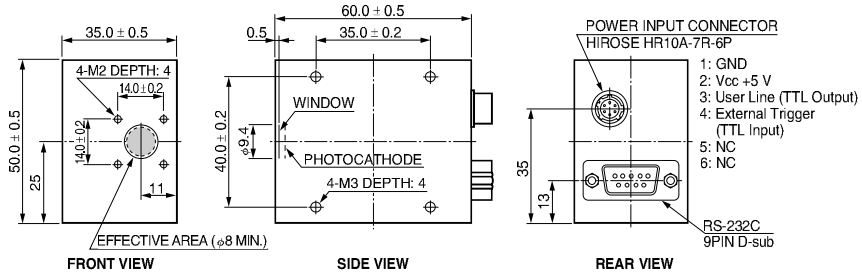

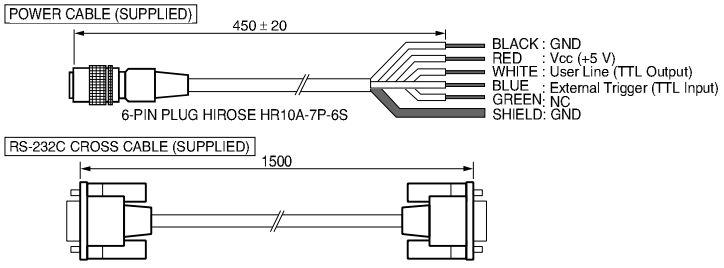

Option

(Optical Fiber Adapter) (Unit: mm)

E5776 (FC Type)

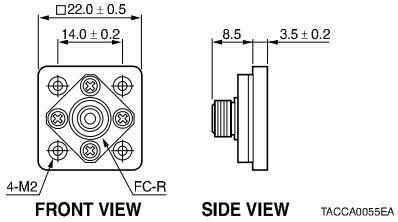

E5776-51 (SMA Type)

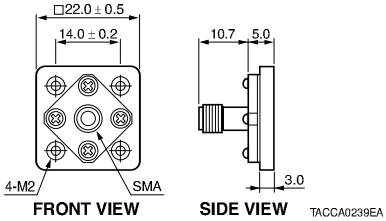

Model 1137P, 7mW Linear Polarization, JDSU HeNe Laser

Stock No. #62-725

Availability: IN STOCK

$1030.00

1 or more for $1030.00.

Specifications

Model Number	1137P
Minimum Output Power, $TEM_{0\,0}$ (mW)	7.0
Laser Class - CDRH	IIIb
Beam Diameter (mm)	0.81
Beam Diameter Tolerance (%)	±3
Beam Divergence (mrad)	1.00
Beam Divergence Tolerance (%)	±3
Polarization	500:1
Longitudinal Mode Spacing, Nominal (MHz)	435
RMS Noise	30 Hz - 10 MHz: 0.2%
Wavelength (nm)	632.8
Spatial Mode	$TEM_{0\,0}$
Mode Quality, M^2	>95%
Maximum Drift	Mean Power over 8 hrs: ±2.5
Warm-Up Time (minutes)	10
Pointing Stability (mrad/°C)	From Cold Start, 25°: <0.1
Pointing Stability after Warm Up (mrad/°C)	After 15 min: <0.02
Static Alignment	Centered to Outer Cylinder: ±0.01" Parallel to Outer Cylinder: ±1.0 mrad
Diameter of Laser Head (inches)	1.74
Length of Laser Head (inches)	15.79
Weight (lbs)	1.3
Operating Temperature (°C)	-40 to +70
Storage Temperature (°C)	-40 to +150
Operating Humidity	0 to 100%, non-condensing
110V Power Supply	#62-734
220V Power Supply	#62-740
Output Power (mW)	7
Output Type	Free Space

Type of Laser	HeNe
Color	Red
Manufacturer	JDSU
CE Certified	Yes
RoHS	N

Technical Information

Beam Expander Mounting Configurations

Click on an item below to be brought to that item's product page.

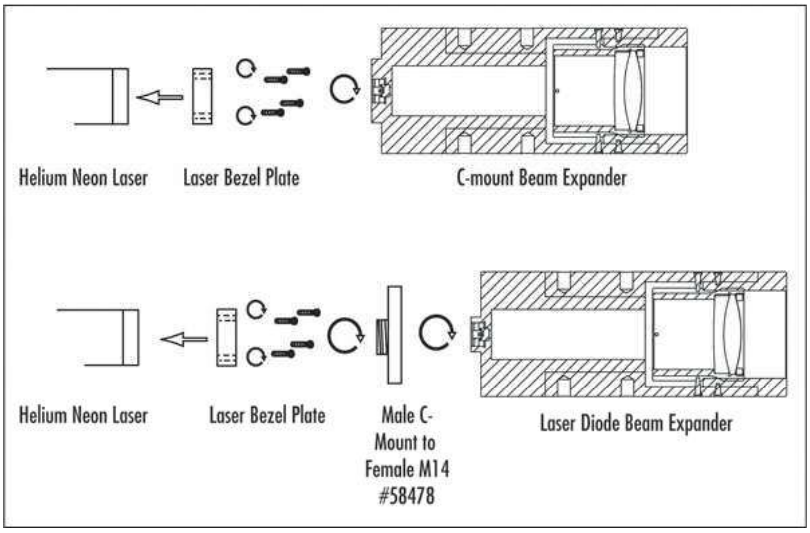

REV. #	DESCRIPTION:	NAME/DATE:
A	INITIAL RELEASE	Hit. 07/24/08

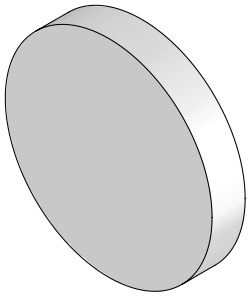

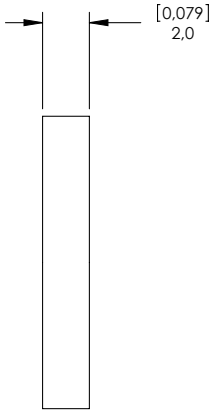

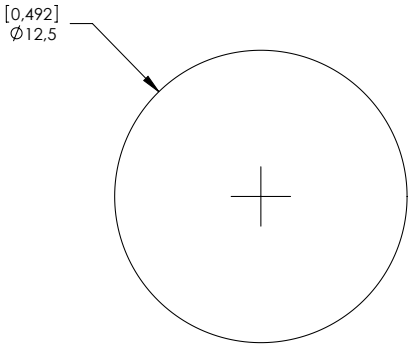

SPECIFICATIONS:
WAVELENGTH RANGE: 500 TO 720nm
EXTINCTION RATIO:
>10,000:1 @ 500 to 720nm
CLEAR APERTURE: 90% OF SURFACE DIMENSION
WAVEFRONT DISTORSION: < λ/4 @ 633nm
ACCEPTANCE ANGLE: ±20°
LASER DAMAGE THRESHOLD:
CONTINUOUS BLOCK: 1W/cm²
CONTINUOUS PASS: 5W/cm²
OPERATING TEMPERATURE: -20°C TO +120°C

NOTE:
FOR INFORMATION ONLY.
NOT FOR MANUFACTURING

TOLERANCES
UNLESS OTHERWISE SPECIFIED:
DIMENSIONS ARE IN MILLIMETERS AND INCHES
LINEAR TOLERANCES:
ONE PLACE DECIMAL: ±0.2
TWO PLACE DECIMAL: ±0.04
ANGULAR: ±30'

	NAME	DATE
DRAWN	Hit.	07/24/08
ENG APPR.	Hit.	07/24/08
MFG APPR.	XX	XX/XX/XX

THORLABS INC. PO BOX 366 NEWTON NJ

TITLE: Ø12.5mm VIS LINEAR POLARIZER

MATERIAL:	SIZE	REV.
SCHOTT GLASS B270	A	A

SCALE: 4:1	SHEET 1 OF 1

DWG. NO.	PART NO.
18161-E0W	LPVISB050

5 4 3 2 1

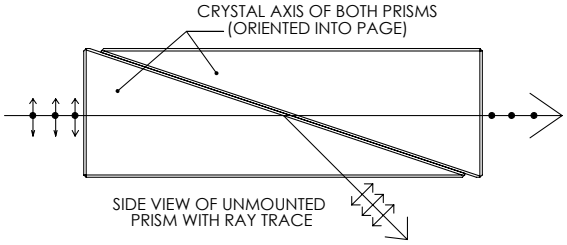

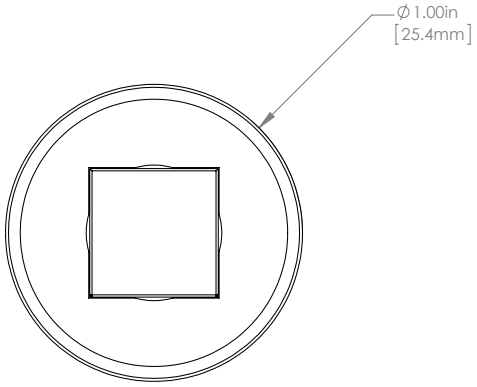

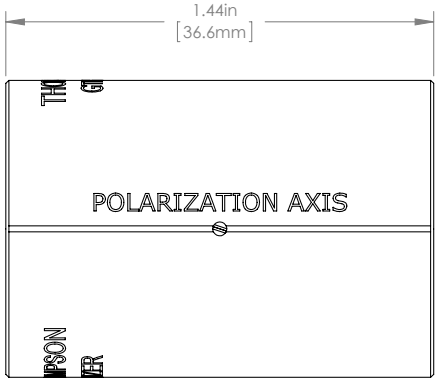

NOTES/SPECIFICATIONS:
1. EXTINCTION RATIO: 100,000:1
2. WAVEFRONT DISTORTION: ≤ λ/4 @ 632.8nm
3. CLEAR APERTURE: 10.0mm x 10.0mm
4. SURFACE QUALITY (INPUT & OUTPUT FACES): 20-10 SCRATCH-DIG
5. COATED SURFACES: ENTRANCE AND EXIT WINDOWS
6. MATERIAL:
   1. OPTICS: OPTICAL GRADE CALCITE
   2. HOUSING: BLACK ANODIZED 6061-T6 ALIMUNIUM

FOR INFORMATION ONLY
NOT FOR MANUFACTURING PURPOSES

DRAWING PROJECTION		
	NAME	DATE
DRAWN	SS	06/SEP/2011
APPROVAL	MG	20/SEP/11

VALUES IN PARENTHESIS ARE CALCULATED AND MAY CONTAIN ROUNDOFF ERRORS

THORLABS
www.thorlabs.com

GLAN THOMPSON POLARIZER

MATERIAL	REV
SEE NOTES	B

ITEM #	APPROX WEIGHT
GTH10M	0.15 kg

ORDER OF ASSEMBLY		
ORDER	ITEM NUMBER	MATERIAL
1	ENGRAVED HOUSING	ALUMINUM
2	O-RING	NEOPRENE
3	633nm WAVEPLATE	CRYSTAL QUARTZ
4	SM05RR	ALUMINUM

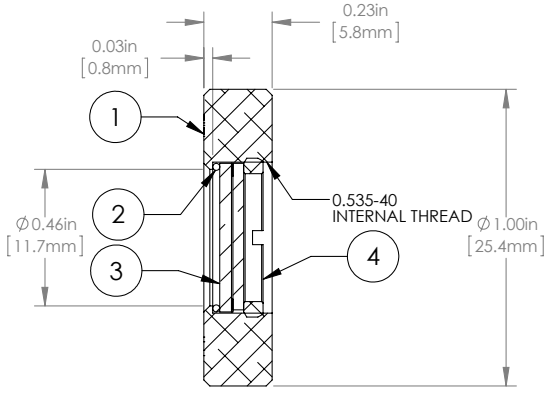

SECTION A-A

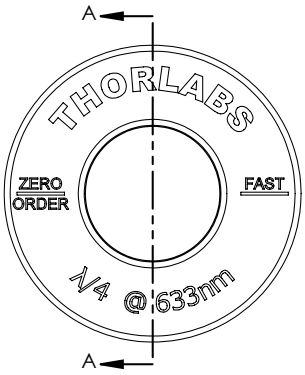

NOTES/SPECIFICATIONS:

1. UNMOUNTED DIAMETER: 0.50" ±0.004 (12.7mm ±0.1)
2. BEAM DEVIATION: <10 arcsec
3. RETARDANCE ACCURACY (TYP): <λ/300
4. TRANSMITTED WAVEFRONT ERROR: λ/8 AT 633nm
5. SURFACE QUALITY: 20-10 SCRATCH-DIG
6. CLEAR APERTURE: ∅0.39" (∅10.0mm)
7. COATING: VAR AT 633nm, R<0.25%, 0° AOI/PER SURFACE

FOR INFORMATION ONLY
NOT FOR MANUFACTURING PURPOSES

DRAWING PROJECTION		
	NAME	DATE
DRAWN	EMT	23/JAN/13
APPROVAL	MG	12/FEB/13

VALUES IN PARENTHESIS ARE CALCULATED AND MAY CONTAIN ROUNDOFF ERRORS

THORLABS
www.thorlabs.com

MOUNTED ZERO-ORDER QUARTER WAVEPLATE AT 633nm

MATERIAL	REV
SEE TABLE	D

ITEM #	APPROX WEIGHT
WPQ05M-633	4.0 g

ORDER OF ASSEMBLY		
ORDER	ITEM NUMBER	MATERIAL
1	ENGRAVED HOUSING	ALUMINUM
2	O-RING	NEOPRENE
3	633nm WAVEPLATE	CRYSTAL QUARTZ
4	SM05RR	ALUMINUM

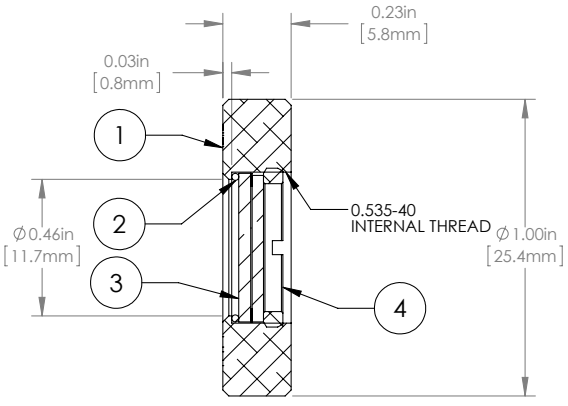

SECTION A-A

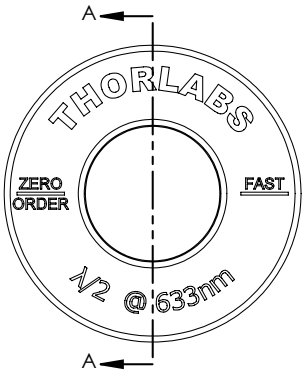

NOTES/SPECIFICATIONS:

1. UNMOUNTED DIAMETER: 0.50" ±0.004 (12.7mm ±0.1)
2. BEAM DEVIATION: <10 arcsec
3. RETARDANCE ACCURACY (TYP): <λ/300
4. TRANSMITTED WAVEFRONT ERROR: λ/8 AT 633nm
5. SURFACE QUALITY: 20-10 SCRATCH-DIG
6. CLEAR APERTURE: Ø0.39" (Ø10.0mm)
7. COATING: VAR AT 633nm, R<0.25%, 0° AOI/PER SURFACE

FOR INFORMATION ONLY
NOT FOR MANUFACTURING PURPOSES

DRAWING PROJECTION		
	NAME	DATE
DRAWN	EMT	23/JAN/13
APPROVAL	MG	12/FEB/13

VALUES IN PARENTHESIS ARE CALCULATED AND MAY CONTAIN ROUNDOFF ERRORS

THORLABS
www.thorlabs.com

MOUNTED ZERO-ORDER HALF WAVEPLATE AT 633nm

MATERIAL	REV
SEE TABLE	D

ITEM #	APPROX WEIGHT
WPH05M-633	4.0 g